KINEMATICS OF DUMMIES DURING CRASH USING FINITE ELEMENTS AND MULTIBODY DYNAMICS

by

Sertan Aşkan

B.S., Mechanical Engineering, Boğaziçi University, 1998

Submitted to the Institute for Graduate Studies in
Science and Engineering in partial fulfillment of
the requirements for the degree of
Master of Science

Graduate Program in Mechanical Engineering
Boğaziçi University

2006

KINEMATICS OF DUMMIES DURING CRASH
USING FINITE ELEMENTS AND MULTIBODY DYNAMICS

APPROVED BY:

Prof. Günay Anlaş (Thesis Supervisor)	.....
Assoc. Prof. Hasan Bedir	.....
Prof. Gökmen Ergün	.....

DATE OF APPROVAL: 16.June.2006

ACKNOWLEDGEMENTS

This research has been conducted with the collaboration of the Mechanical Engineering Department of Boğaziçi University and the Product Development Department of Ford Otosan A.Ş. In this regard, I would like to express my gratitudes to my thesis supervisor, Professor Günay Anlaş and to Ford Otosan Safety Team Leader, Dr. Mustafa Erdener for their advices, encouragements and guidings during the research. I am thankful to Mr. Barış Şenyener, Ford Otosan Vehicle Engineering Department Manager and to Dr. Ali Çınar, Ford Otosan Structural Integrity Team Supervisor for granting me the chance to engage in the study of such an interesting subject. I also wish to extend my sincere thanks to Cem Sakaryalı and Michel Paas, Research Engineers at Ford of Europe Product Development Department for their help and for sharing their experience in model building. I would also like to thank Professors Gökmen Ergün and Hasan Bedir for their review of my thesis and their kind advices.

ABSTRACT

KINEMATICS OF DUMMIES DURING CRASH USING FINITE ELEMENTS AND MULTIBODY DYNAMICS

First, multibody dynamics model of the occupant compartment is built using a commercial software, *Madymo*. Occupant results from *Madymo* model are compared to sled test results and *Madymo* model is calibrated to better simulate the sled test, by modifying the coefficients and functions in *Madymo* model. Second, vehicle finite element model is built using finite element software, *Radioss* and vehicle structure deformation results from *Radioss* are compared to real crash test results to validate the finite element model. As a last step, results from *Radioss* are integrated into *Madymo* model to simulate a vehicle crash test, offset front impact into a deformable barrier at 56 km/h. Predefined injury criteria parameters, which are measured in a crash test and calculated by *Madymo* are compared. It is shown that, in case the *Madymo* model is initially calibrated with sled test data and in the existence of a validated finite element model with crash test, integrating both techniques is a very quick, reliable and efficient way to model occupant kinematics during crash.

ÖZET

SONLU ELEMANLAR VE ÇOKLU KÜTLE DİNAMİĞİ İLE ÇARPIŞMA ANINDA TEST MANKENİNİN HAREKETİNİN İNCELENMESİ

Bu çalışmada, ilk önce yolcu yaşam alanının dinamik modeli Madymo ticari yazılımı ile hazırlanmıştır. Madymo modelinden elde edilen yolcu değerleri kızak testi sonuçları ile karşılaştırılarak, Madymo modelindeki katsayılar ve fonksiyonlar kızak testini daha iyi simule edecek şekilde değiştirilmiştir. İkinci aşamada, aracın sonlu elemanlar modeli Radioss yazılımı ile kurulup, sonlu elemanlar analizinden elde edilen sonuçlar gerçek test sonuçları ile karşılaştırılıp, modelin güvenirliliği doğrulanmıştır. Son olarak, Radioss modelinin çıktıları Madymo modeline girilip gerçek testin, 56 km/s saat hızda deforme olabilen engele aracın belli bir oranda çarpması, simulayonu yapılmıştır. Test sırasında ölçülen yaralanma değerleri ile Madymo tarafından hesaplanan yaralanma değerlerini karşılaştırılmıştır. Katsayıları ve fonksiyonları kalibre edilmiş bir Madymo modeli ile testle doğrulanmış bir sonlu elemanlar modelinin olması durumunda her iki tekniğin birleştirilmesinin test mankeninin hareketinin incelenmesi için güvenilir ve hızlı bir metod olduğu gösterilmiştir.

TABLE OF CONTENTS

LIST OF FIGURES

LIST OF TABLES

LIST OF SYMBOLS/ABREVIATIONS

a. b. c	hyperellipsoid semi-axes [m]
C	ramp function
C_d	damping coeeficient [kN.s/m]
F_d, F_e, F_f	damping, elastic and friction forces [kN]
F_Z	compressive axial force [kN]
i, j	integers
n	hyperellipsoid degree
P	point of application of forces
P_i	point on i^{th} surface
t	time [ms, s]
v	relative velocity between interacting contact surfaces [m/s]
x, y, z	coordinates at global coordinate system [m]
$x_{e,m}$, $x_{e,s}$	penetration into master and slave surfaces [m]

CCB	Cross Car Beam
ECE	Economic Commission of Europe
EU	European Union
FE	Finite Elements
HIC	Head Injury Criteria
IP	Instrument Panel
NIC	Neck Injury Criteria
TCFC	Tibia Compressive Force Criteria
TI	Tibia Index
VC	Viscous Criteria

1. OBJECTIVE

This study is aimed at developing a low cost, quick and reliable method to understand occupant kinematics during vehicle crash. Understanding occupant kinematics is essential for a proper vehicle interior compartment and restraint system design. Crash tests, simulating different crash modes are performed to set the design parameters; however, performing a crash test is expensive in nature, and requires time to evaluate different design proposals. As a result, computer aided engineering programs are widely used to simulate crash tests. Currently, two approaches are widely used in automotive industry in simulating crash tests: Finite element and multi-body dynamics. Finite element approach is reliable and has proven itself in modeling vehicle structure deformation but not as reliable in simulating occupant behavior. On the other hand, multi-body dynamics approach has proven itself in simulating occupant behavior but it is not as good in modeling vehicle structure deformation. To benefit from successful sides of both approaches, an integrated model is built, that uses both approaches.

First, a multibody dynamics model of the driver compartment is built using multibody dynamic simulation solver, *Madymo.* Model parameters are calibrated using sled test results of Ford Motor Company's Dunton Safety Laboratory in United Kingdom. Sled test is chosen for calibration because it is a simulation of a crash test allowing better monitoring of dummy motion with less external factors in effect. On the other side, vehicle finite element model is built using *Radioss.* Finite element results are compared to real crash test results performed at Ford Motor Company's Merkenich Safety Laboratory in Germany. The crash test chosen is the simulation of a light commercial van's, Transit Connect, front offset impact into a deformable barrier at 56 km per hour, which is a legislative requirement for vehicle's approval. Finite element analysis results provide the data that defines vehicle global motion and component intrusions inside the driver compartment. The output data is then used as an input in Madymo model for crash test simulation. Dummy motion during simulation is investigated and pre-determined injury parameters, which are calculated by Madymo, are compared to real crash test results to check the reliability of the model built.

2. INTRODUCTION

According to data from the General Directorate of Highways, GDH (Karayolları Genel Müdürlüğü, KGM), there are more than half a million reported traffic accidents in Turkey each year. Among these reported accidents, 25 percent involve bodily injuries and approximately 4000 people are killed in traffic accidents every year in Turkey, in other words around 10 people every day. Most of these accidents occur in daily city traffic at low speeds usually ending with damage to the vehicle only. However, for the accidents reported in rural areas and highways, the rate of death in accidents rise to 3 percent per accident and the rate of bodily injuries go up to 2 people per accident. Reported injury and fatality numbers in traffic accidents in Turkey from 2000 to 2004 are given in Table 2.1. Interesting point in Table 2.1 is the tendency to decrease in deaths per accident. The tendency to decrease is more clearly shown in Figure 2.1 [1].

Table 2.1. Accident, fatality and injury numbers in Turkey in the last five years

		2000	2001	2002	2003	2004
Accident	Urban Traffic	404167	363528	362979	373531	436187
	Highways	62218	45879	44124	48771	58664
	Rural Areas	34278	33553	32855	33365	42533
	All	500663	442960	439958	455667	537384
Fatalities	Urban Traffic	1542	1309	1215	973	1128
	Highways	2399	1645	1685	1845	1954
	Rural Areas	1625	1432	1269	1148	1346
	All	5566	4386	4169	3966	4428
Injuries	Urban Traffic	71635	62690	62202	59355	67693
	Highways	44242	31807	32023	35969	41988
	Rural Areas	20529	21705	21820	21944	26548
	All	136406	116202	116045	117268	136229

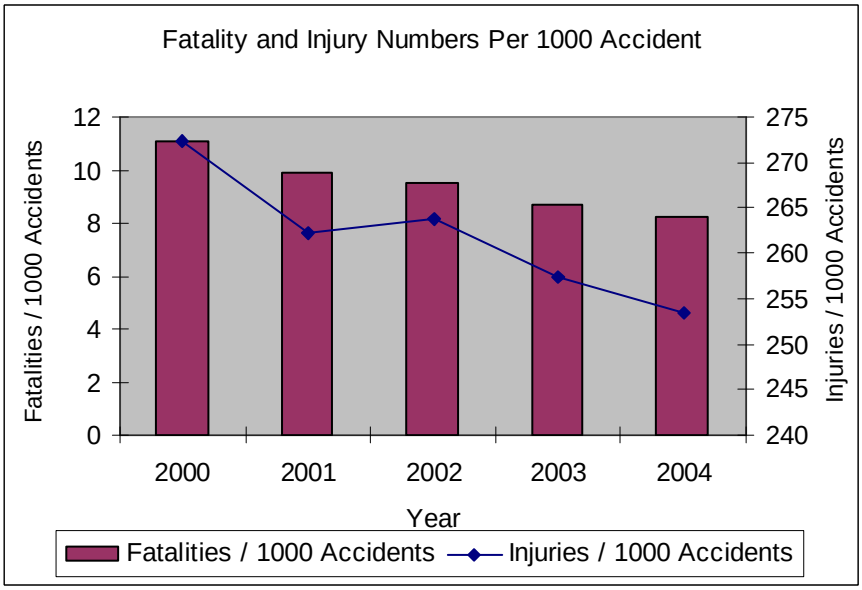

Figure 2.1. Fatality and injury numbers per 1000 accidents

Figure 2.1 displays fatality and injury numbers in Turkey in the last five years. The decrease in fatality and injury numbers might be due to many reasons like improvements in highway design, speed enforcements in highways, alcohol controls or safer vehicles in traffic. After Customs Union agreement with European Union, EU, vehicles manufactured in EU according to the Economic Commission of Europe, ECE, regulations entered the Turkish market. On the other hand, automotive manufacturers in Turkey, both to be competitive in the domestic market and to export the vehicles to EU, improved the safety performance of the vehicles manufactured. As a result, the number of vehicles in Turkey roads satisfying ECE regulations increased year by year, which resulted in more structurally safe cars on the roads and that might be one of the reasons for the decrease in fatalities despite the increase in the number of traffic accidents.

The necessity of the ECE regulations, and their positive effect on occupant life is more clearly explained in Table 2.2. As it can be seen in the table below, the conditions of crash defined by the ECE regulations constitute 88 percent of all reported accidents. Excluding the crash to a pedestrian as in these cases there is usually no harm to the driver or passenger, considering the cases defined by the frontal and side impact regulations which are aimed at securing the driver and passenger only, these cases count for 58 percent of all accidents [2].

Table 2.2. Accident distribution according to type of occurrence

Nature of Accident	Accidents					
	Urban	%	Rural and Highways	%	TOTAL	%
Head to head vehicle crash	17899	37.76	4844	24.00	22743	33.64
Rear end crash	5947	12.54	2842	14.08	8789	13.01
Crash to a wall, obstacle, etc.	4095	8.64	1424	7.05	5519	8.16
Pedestrian crash	13968	29.47	1175	5.82	15143	22.40
Crash to animal	185	0.39	227	1.12	412	0.61
Roll over	2282	4.81	3786	18.75	6068	8.98
Loss of control	2729	5.76	5801	28.74	8530	12.62
Others	300	0.63	89	0.44	389	0.58
TOTAL	47405	100.00	20188	100.00	67593	100.00

From Table 2.2, it can be concluded that ECE regulations cover nearly all aspects of accidents on the roads therefore ECE regulations are obligatory in vehicle approval in all European countries and non-EU member countries including Turkey, Switzerland, Norway, Liechtenstein and Iceland although they are not a member of the EU and are not subject to ECE regulations require that the vehicle satisfy the ECE regulations for vehicle homologation in that country. Other countries like Russia, Gulf Coast countries accept most of the ECE regulations but they omit some of the regulations and add some extra regulations according to the conditions of their country.

2.1. Approval of a Vehicle

Homologation is simply defined as the process to achieve the approval from a government authority. The homologation approval documents transmitted to the government confirm that the product meets all appropriate legal requirements. Without homologating the product, in our case this is the vehicle, the sales of the vehicle in that country is not allowed. Therefore, homologation of a vehicle is not an option to improve brand image or an item in the marketing strategy it is a must for the vehicle’s approval.

Homologation can either be in terms of approval of a single car, or for big manufacturers, the type approval of all cars manufactured by that manufacturer. In type approval, a randomly chosen vehicle of the manufacturer proves compliance with the regulations through witnessed testing. On the other hand, the manufacturer also proves its capability of consistently building identical complying vehicles, which is known as conformity of production.

ECE regulations can be collected under two headings, as the environmental and safety regulations. The environmental regulations include items like engine power, fuel consumption, emissions, diesel smoke, exterior noise and electromagnetic compatibility. There are also some vehicle specific regulations like the LPG equipment installation. These items are aimed at forcing the manufacturer to develop more health and environment friendly vehicles [2].

The rest of the regulations are defined as safety regulations. Safety regulations first aim at developing a safer driving condition for the driver. The regulations also include driver and passenger safety during braking and crash as well as they include pedestrian safety. Safety regulations imposed by the ECE can be summarized under the below headings.

- Horns
- Mirrors
- Brakes
- Lighting
- Forward Vision
- Defrost/Demist
- Wheel Guards
- Wipers
- Tyres
- Safety Glass
- Steering Effort
- Door Latches/Hinges

- Interior Fittings
- Seat Strength
- Protective Steering
- Head Restraints
- Seat Belt Anchorage
- Exterior Projections
- Heating Systems
- Safety Belts & Restraint System
- Towing Hook
- Front Offset Impact
- Side Impact
- Pedestrian Protection

Most of the above listed items are aimed at drivers' and other drivers' safety at traffic like horns, lighting, etc. However, last three items are directly aimed at saving driver, passenger or pedestrian life during a vehicle crash. With the implementation of these regulations in Turkey there has been a decrease in the number of killed or injured occupants during traffic accidents. The table summarizing this was already shown in the above pages.

For the homologation of a vehicle in terms of front offset and side impact regulations, crash tests are performed. Certified authorities also witness the tests. Front Offset Impact Protection regulation, known as ECE94, concern the approval of a vehicle with regard to the protection of the occupants of the front outboard seats in the event of a frontal collision. The regulation applies to all power driven vehicles of category M, better known as passenger cars, of a total permissible mass not exceeding 2.5 tones. During the approval test, the vehicle speed is increased up to 56 km/h and the vehicle hits a deformable barrier at the end of the test track. A deformable barrier is preferred to simulate a real car crash condition and to take into account the energy absorbed by the hit car as well. Similarly Side Impact Protection regulation considers the case of a vehicle hit by another vehicle on the side. Both tests are obligatory and a robust vehicle design is essential to achieve through the tests [2].

2.2. Vehicle Safety and Design

As stated in the previous chapter, design of vehicles from crashworthiness and occupant safety perspectives has become increasingly complex with the addition of new legal requirements every year. United Nations (UN), European Union (EU) and United States National Highway Traffic Safety Administration (NHTSA) impose many legal requirements that limit the design space inside a vehicle including many complexities. Apart from these requirements, vehicle and occupant safety has been one of the critical items in customer's purchasing decision. EUNCAP test in Europe (European Union New Car Assessment Program) and NCAP in North America (New Car Assessment Program) are known worldwide and results of these tests are widely used by manufacturers in advertisements to ensure customers on the safety of their products. With increasing government obligations and customer expectations vehicle manufacturers are investing more on vehicle safety development in recent years [3,4].

Till two decades before, vehicle safety was an expensive area for manufacturers to invest in. The physical nature of crash tests, apart from being expensive, does not also provide the full set of information (crash deformation sequence in detail, occupant envelope regarding out of positions) to guide vehicle structure design. Considering the iterative process of product development, and necessity of shortening product development period, physical crash tests were a major factor slowing product development stage and adding to development costs.

With recent developments in computer industry there has been a marked increase in the usage of computer simulations for safety development. Especially, when supported with controlled test data computer simulations contributed significantly in understanding vehicle and dummy crash behaviors. Nowadays, in automotive industry various simulation programs are used to determine occupant movement and loads during vehicle crash. Two approaches are currently used to perform this type of calculations. Multi Body or Rigid Body Dynamics Approach as used by *Adams* and *Madymo* or Finite Element Approach as used by *Pam Crash, Radioss* and *Dyna3D*. Among these listed approaches vehicle structure analysis, known as crashworthiness, is usually performed using Finite Element approach and occupant safety simulation is usually done using multi body approach. In

addition, most of these programs allow a simultaneous usage of both methods and these methods have proven to give reasonable results if the boundary conditions are defined properly [5].

2.3. Occupant Simulation

Comparing the approaches listed, in the finite element approach, a full vehicle crash model is used and for occupant simulations a finite element model of test dummy is included in the full vehicle model. Full vehicle models prepared to simulate a crash test are large in size compared to other models and need more computing resources. Therefore FE analyses require a significant outlay of time to process. An average finite element model contains around half a million elements and on a Linux cluster using 16 processors, it requires around 8 hours to complete successfully. The time needed for preprocessing and debugging is not included in the above numbers [6,7]. Another disadvantage of the finite element model is the long time needed for contact evaluation. In FE codes the contact definition is over the nodes and surfaces defined by shell elements. At certain cycles nodes and surfaces in defined contact groups are checked for penetration and if penetration occurs additional processing is required to redefine node displacements according to the contact parameters defined by FE analyst. The contact evaluation process in a finite element analysis require checking displacements of thousands of nodes in a large deformation problem and is one of the major factors increasing the time spent on computing.

At this point multi body approach is ahead of finite element approach offering a much shorter computational time. However, multi body approach is not as capable as finite element approach in simulating vehicle deformation. Studies have been performed to simulate vehicle front end by using 3D frame modeling techniques. A vehicle model built with 3D frame modeling technique is shown in Figure 2.2. This technique involves modeling vehicle front structure components with a number of ellipsoids and elliptical cylinders. The results have shown that the 3D frame modeling technique is successful in simulating simple and smooth geometries but the results fail to correlate with real crash tests when geometric details like local reinforcing features are considered. Therefore 3D frame model can be built at the early stages of a car program to define vehicle concept and

safety strategy but at later stages of the development process where front structure component design contain more complexities it should not be preferred [8].

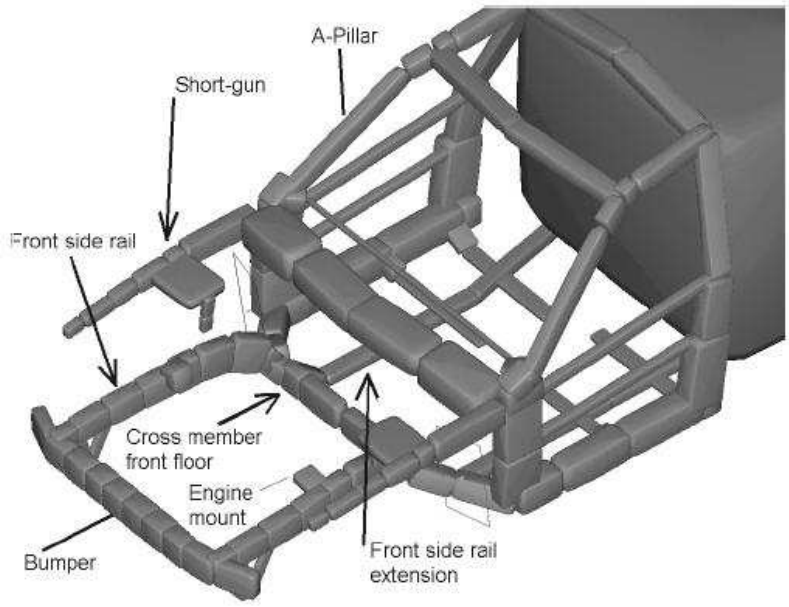

Figure 2.2. 3D frame model of vehicle front end structure

On the other hand multi body approach is very advantageous offering a large number of opportunities to simulate the interaction between dummy and vehicle. In multi body approach contact is defined between the surfaces of two rigid bodies, i.e. the ellipsoid and the plane. Therefore, contact check algorithms and when penetration occurs contact force calculation algorithms take less time to process. This feature brings many advantages in accuracy and time spent. But accuracy depends on contact characteristics pre-defined by the analyst. Software vendors have carried out many tests for a correct definition of the surface compliance of dummy rigid bodies. These tests also supplied valuable information regarding joint stiffness functions used by the dummy. These functions are critical in defining dummy movement during crash. In the end reliable and well-validated dummy databases are available to be used in occupant simulation [9,10].

At this stage, combining finite element analysis vehicle performance and multi body analysis dummy performance capabilities emerge as the most accurate solution to develop a validated model. Most of the commercial software allow a simultaneous processing of both approaches known as coupled approach [4,11]. In the coupled approach vehicle

excluding dummy is modeled in FE. On the other hand components of the FE model that are in interaction with dummy are modeled in multi body model with the dummy. During FE model-processing motion of these components are extracted to multi body simulation at each time step and similarly outputs from multi body simulation is fed back into FE model till an equilibrium is achieved between dummy and vehicle interior. Therefore while simulating the vehicle structure deformation correctly a better representation of the dummy behavior is also achieved. However, the technique mentioned above for performing the coupled analyses require almost double the time necessary for the structural analysis alone. Compared with performing all the work with the FE model, this model seems advantageous both in supplying well correlated data and less time spending, but it is still time consuming when compared to multi body approach.

Instead of coupling both approaches, integrating them is another approach [6,7]. During analyses the major portion of computational time is spent in analyzing vehicle structural deformation and the structural deformation identifies two main injury-causing aspects in vehicle crash, deceleration and intrusions. Successful introduction of these two aspects into the multi body simulation will establish a well-correlated simulation of the real test. As vehicle structure deformation is independent of many design complexities inside the driver and passenger compartment, or these complexities can be considered to have minor effect on vehicle structure deformation, a large number of simulations including different dummies, dummy seating positions, seat-steering column-seat belt-airbag configurations can be evaluated in a short time with the same boundary conditions imposed by the finite element model. Also the existence of a validated FE model enables the chance of evaluating vehicle structure design changes without the necessity of a new test.

Apart from the above, statistical approaches are also available to reconstruct real life accidents. Differing from the above approaches the statistical approach considers the vehicle deformation after crash to simulate the accidents. The vehicle deformation known as crush is one of the key input parameters coupled with vehicle velocity. The approach relies on multi body approach again to estimate the dummy injury criteria. In this accident reconstruction model, the vehicle stiffness and the deceleration are not considered to be a parameter. By the statistical approach many accident scenarios can be created and evaluated in a short time, but compared to the above approaches it is not a reliable

approach in understanding what is happening during a certain well-defined crash scenario. Therefore, statistical approach is not popular in automotive industry but it is widely used in simulating real life accident scenarios [5,12].

Among the above listed five approaches, the integrated approach in which results of the finite element analysis are used as input for multi body simulation will be used to simulate the ECE94 Front Offset Impact. FE model analysis will be performed with the validated commercial software *Radioss*, and multi body simulation will be performed with the well-known multi body simulation software *Madymo*.

2.4. Mathematically Dynamic Modeling

Madymo (Mathematically Dynamic Modeling) is a computer program specially developed for crash simulations. The program predicts behavior of a crash victim or any other structure, which can be represented by a number of connected rigid bodies, based on crash data and environment [13].

In Madymo, systems and system components are defined by rigid bodies or by structures formed by rigid bodies. (Figure 2.3) To define a rigid body; masses, moments of inertia, products of inertia and centers of gravity should be known but it is not obligatory to define the component geometry except when a body has a possibility to interact (contact) other bodies in its environment. The body geometry is usually defined for visual purposes even when there is not a possibility of interaction with other bodies.

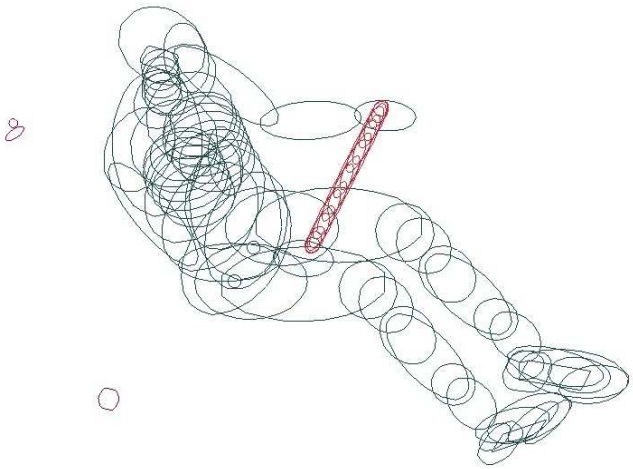

Figure 2.3. Example of a multibody system with tree structure

A local body coordinate system is used to define body properties. The origin of the local coordinate system is the location of the joint connecting the body to its parent body. This is shown in Figure 2.4 where the body j, the child body, is connected to the body i, the parent body. Masses, inertias, centers of gravity are all defined with respect to the shown local coordinate systems. In Figure 2.4, the vector g_j specifies the center of gravity location for body j and the components of the vector g_j are defined in the local coordinate system of body j. The vector c_{ij} defines the joint j on body i, and also the local coordinate system origin for body j. The components of c_{ij} are defined in the parent body i local coordinate system.

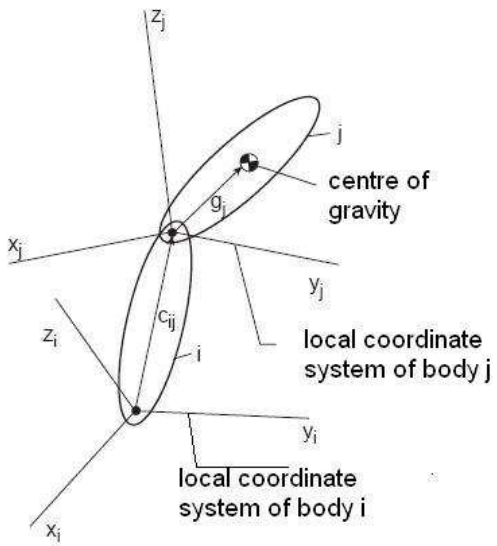

Figure 2.4. Two bodies linked by a joint

A kinematic joint is used to connect a pair of bodies. It defines the relative motion between the two connected bodies, for example a translational joint allows only relative translation. Constraints imposed by the kinematic joint cause a load pair on connected rigid bodies and restrict their relative motion such that they do not violate constraints imposed by the kinematic joint. The relative motion of a pair of rigid bodies can be described by variables like the joint position, joint velocity or joint acceleration degrees of freedom. The joint degrees of freedom assigned determine the motion of systems of bodies.

Besides the relative motion between bodies, prescribed motions can be assigned to joints prior to or during the analysis. Prescribed motions assigned to joints define the motion of the body the joint is attached to. For example, the motion of a vehicle can be assigned to the joint defining the vehicle body or the intrusion of a plane can be assigned to the joint the body of the plane is attached to.

In Madymo, contact interactions between bodies are defined using surfaces of rigid bodies. Rigid bodies do not require a surface definition for calculating rigid body motion but if contact is present then contacting surfaces need to be defined. Madymo uses planes, ellipsoids, elliptical cylinders and facet surfaces to define body geometries in a system. While one plane, ellipsoid or cylinder can be used to define a body's geometry, a combination of these can also be used to define complex body geometries. Different contact interactions between different surfaces of a body can be specified with the body's environment [13, 14, 15].

Planes are defined by defining coordinates of three points as shown in Figure 2.5. The first and second points define the vertices of one edge, A and B. The third is an arbitrary point on the opposite edge and Madymo calculates the vertices on the opposite edge, C and D. The outside normal for the plane constructed is defined by using the right hand rule where the rotation is from point 1 to 2, and to 3 with the outward normal direction determining the material side for the plane [14].

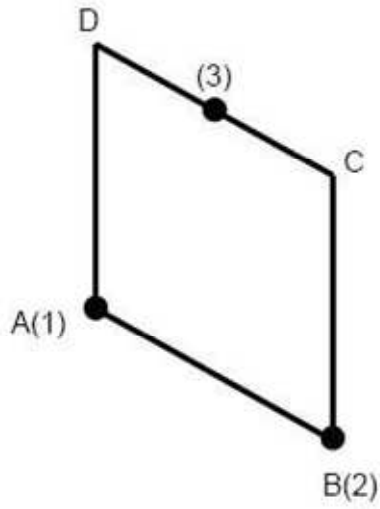

Figure 2.5. Points defining a plane in Madymo 3D

When there are curved surfaces, ellipsoids or hyper-ellipsoids are used. The complex surfaces are also represented by a combination of ellipsoids. The equation defining a hyper-ellipsoid is given by:

$$\left(\frac{|x|}{a}\right)^n + \left(\frac{|y|}{b}\right)^n + \left(\frac{|z|}{c}\right)^n = 1 \qquad (2.1)$$

where *a, b* and *c* are the semi-axes of the (hyper)ellipsoid and *n* is the hyper-ellipsoid degree. When *n* is equal to two the equation describes an ellipsoid. As it is shown in Figure 2.6 with increasing values of *n* the shape of the ellipsoid converge to a rectangular prism [14].

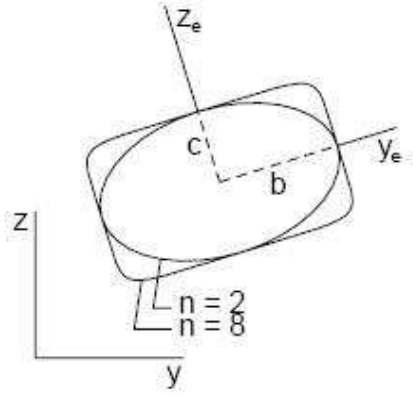

Figure 2.6. Ellipsoid and (hyper)ellipsoid with n=8

(Hyper)elliptical cylinders might also be used to model curved surfaces. The point (hyper)elliptic cylinder differs from the (hyper)ellipsoid is, in (hyper)elliptic cylinder the surface is prismatic in the cylinder axis direction, and has a (hyper)elliptical cross-section perpendicular to the cylinder axis. The end faces are open in a (hyper)elliptical cylinder. A (hyper)elliptic cylinder is shown in Figure 2.7 [14].

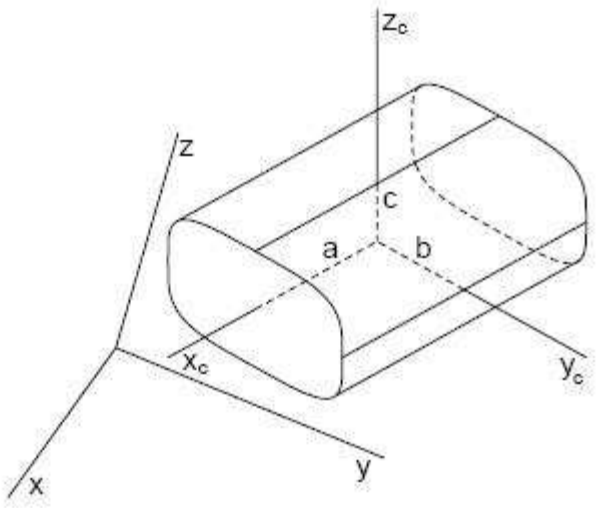

Figure 2.7. Hyperelliptical cylinder for n=4

The equation for a (hyper)elliptical cylinder is given by:

$$-a \le x \le a$$

$$\left(\frac{|y|}{b}\right)^n + \left(\frac{|z|}{c}\right)^n = 1 \qquad (2.2)$$

where a is one half length of the cylinder, b and c are the semi-axes of the (hyper)elliptical cross-section. [14]

When a surface is too complicated as shown in Figure 2.8 to define by using planes and ellipsoids facet surface option is also available. Facet surface is the general name given to surfaces that are approximated by triangular or quadrangular elements. The facet surface is defined by the coordinates of the vertices and for each facet the numbers of the vertices that define the facet. Facet surfaces may be created in Madymo by entering coordinates of

the facet vertices, also importing facet surface information from finite element codes is also available [14].

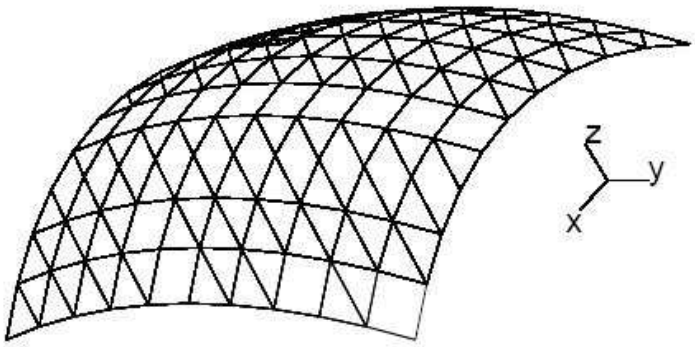

Figure 2.8. Facet surface

Once the rigid body surfaces involved in contact are specified by means of planes, ellipsoids, elliptical cylinders and facet surfaces, contact interaction may be assigned to these surfaces. A possible contact between two surfaces is only evaluated if a contact interaction is specified between two surfaces.

There are two contact models available in Madymo, the elastic and the kinematic contact model. The elastic contact model can be used for all plane, ellipsoid and cylinder contacts. In elastic contact model shown in Figure 2.9 contacting surfaces do not deform and penetration of surfaces is allowed. The resulting contact force is a point force that consists of an elastic, damping and friction part. The elastic contact force (including hysteresis) is a user-defined function of the penetration of the surfaces. A force-penetration characteristic can be defined for each surface separately or as the characteristic of the contact between two surfaces. The damping and friction force depend on the relative velocity of the contacting surfaces.

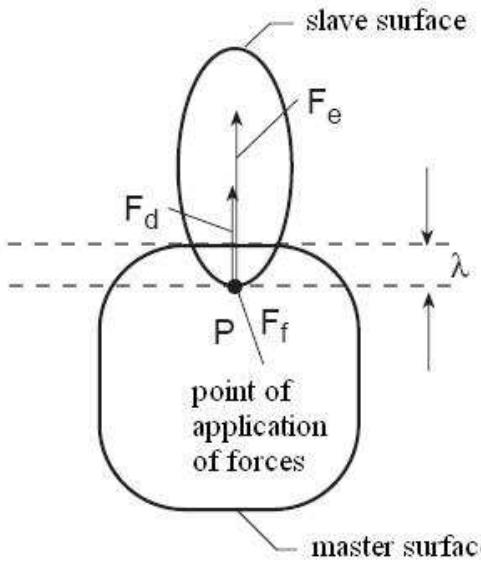

Figure 2.9. Contact loads in an elastic contact model
(only forces acting on slave surface are shown)

The elastic force is perpendicular to the tangent planes. The point P of application of the contact force depends on how the contact characteristic has been specified. There are four options to define the characteristics. In user-master, the contact characteristic of the master surface is used. Point *P* coincides with the contact point on the master surface P_1 since the master surface is considered to be infinitely stiff. In user-slave, the contact characteristic of the slave surface is used. Similarly, point *P* coincides with the contact point on slave surface P_2 and the slave surface is considered to be infinitely stiff. In user-midpoint the combined contact characteristic of the interacting surfaces are used and point *P* lies in the middle of the line between P_1 and P_2. In user-combined the contact characteristic is combined from the characteristic defined separately from both surfaces. The combined contact characteristic is obtained by adding the penetrations of master and slave surfaces for each value of the contact force. The elastic force is used to calculate the penetration into surface $x_{e,m}$ from the master surface contact characteristic and the penetration into surface $x_{e,s}$ from the slave surface contact characteristic. Next point *P* is calculated from

$$P = P_1 + \frac{x_{e,m}}{x_{e,m} + x_{e,s}}(P_2 - P_1) \tag{2.3}$$

where

P_1 contact point on master surface

P_2 contact point on slave surface

To define damping and friction forces a reference plane is introduced as shown in Figure 2.10. This plane contains the point P and is parallel to the contact plane in case of plane-ellipsoid contact. For the ellipsoid-ellipsoid and cylinder-ellipsoid contact, the reference plane is parallel to the tangent planes corresponding to a minimum value of λ.

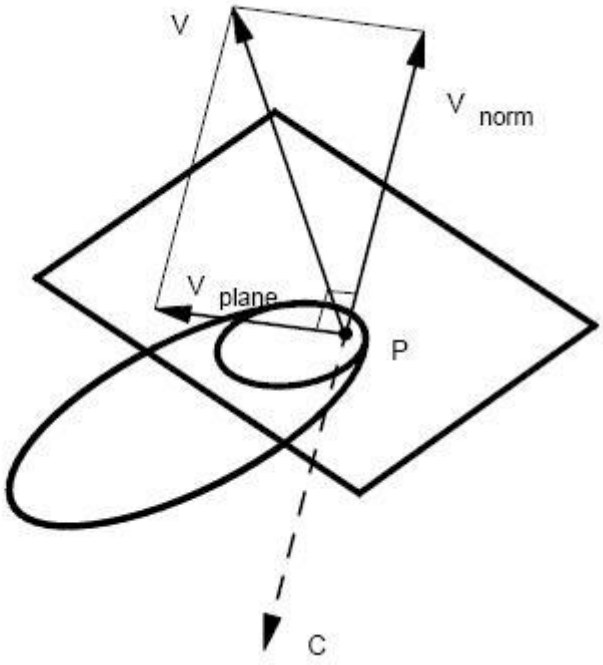

Figure 2.10. The relative velocity *v* resolved into components

The relative velocity *v* between the interacting contact surfaces is defined as the relative velocity at the point *P* of the two contacting objects. This velocity vector is resolved into two components: a component v_{plane} in the reference plane and a component v_{norm} normal to this plane. The damping force F_d is defined as

$$F_d = C_d * |v_{norm}| \tag{2.4}$$

$$C_d = C_{1d}(v_{norm}) * C_{2d}(F_e) \tag{2.5}$$

where C_d is the (positive) damping coefficient, which is defined as the product of a function of v_{norm} and a function of the elastic force F_e. A damping coefficient cannot be defined separately for each contact surface.

In the case of increasing penetration (loading) the damping force is added to the elastic force as shown in Figure 2.11. If the penetration decreases (unloading) the damping force counteracts the elastic force. Since contact forces are resistive forces no contact forces are applied during unloading if the damping force exceeds the elastic force.

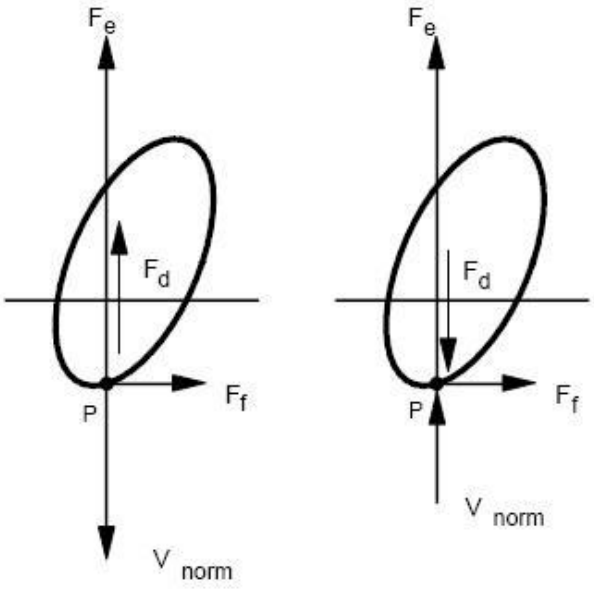

Figure 2.11. Damping in loading and unloading

In addition to the damping force, a dry friction force F_f can be specified. This friction force acts in the reference plane in the direction opposite to the relative velocity component v_{plane}:

$$F_f = C * f(|F_e - F_d|) * |F_e + F_d| \tag{2.6}$$

where $f(|F_e - F_d|)$ is the Coulomb friction coefficient and C a so-called ramp function (Figure 2.12). This ramp function varies between 0 and 1 as a function of the relative velocity v_{plane}. The ramp function has been introduced in order to avoid vibrations

induced by dry friction. The friction coefficient can be defined as a function of the magnitude of the normal force. Note that the same ramp function is used for all contacting surfaces.

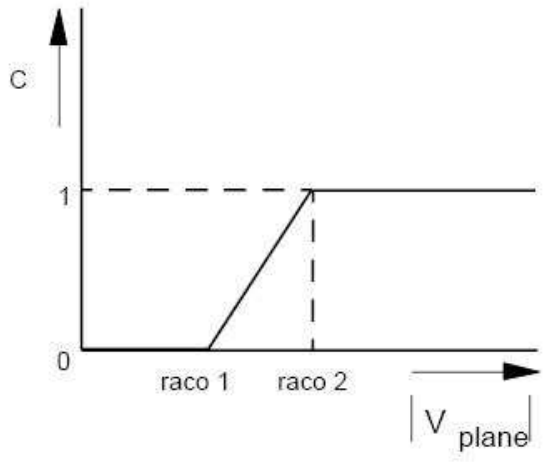

Figure 2.12. Definition of the ramp function *C*

Contact between nodes of a finite element model and an ellipsoid surface is defined by the kinematic contact model. In kinematic contact model, penetration of a node in the contact surface is not allowed and the contact force is based on the inelastic impact of the node and the surface. In the contact algorithm nodes are treated as point masses and contact surfaces impenetrable. Each time step the relative position of the node and the corresponding contact surface is evaluated. If a node is inside the contact surface contact algorithm is activated [13].

Contact forces are calculated based on the relative velocity of the node and the contact surface. A normal impulse is applied to the node and the contact surface such that the component of the relative velocity perpendicular to the contact surface becomes zero. The penetrated node is placed on the contact surface. To account for friction a tangential impulse, that is equal to the product of the normal impulse and the friction, is applied such that the resulting relative velocity of the node and the contact surface equals zero [13].

Apart from the above, Madymo offers a large database of reliable and validated test dummy models included in the software package. The existence of a large dummy database is an important requirement for the effective use of computer models in the field

of crash victim simulations [15]. Madymo is also able to present the results of injury parameter calculations in addition to the standard output quantities like accelerations, displacements and contact forces. A more detailed explanation of the injury parameters Madymo calculates will be given in 2.5.

2.5. Injury Parameters

Dummies are used in the simulation of traffic accidents to generate data like mechanical loads. Dummies cannot be used to simulate injuries during an accident. Therefore a relationship between the dummy's reaction to crash, and real injuries need to be defined. In Madymo, acceleration, velocity and displacement of rigid bodies, joints can be calculated but the calculated data needs to be processed with the help of injury biomechanics to identify the severity of the injury.

Injury biomechanics deals with the effect of mechanical loads, in particular impact loads on human body. Due to a mechanical load, a body region will experience mechanical and physiological changes, the so-called biomechanical response. Injury will take place if the biomechanical response is of such a nature that the biological system deforms beyond a recoverable limit, resulting in damage to anatomical structures and alteration in normal function. The mechanism involved is called injury mechanism and the severity of the resulting injury is indicated by the expression "injury severity" [14].

An injury parameter is a physical parameter or a function of several physical parameters that correlates well with the injury severity of the body region under consideration. Many schemes have been proposed for ranking and quantifying injuries. Anatomical scales describe the injury in terms of its anatomical location, the type of injury and its relative severity. These scales rate the injuries themselves rather than consequences of injuries. The most well known worldwide accepted anatomical scale is the Abbreviated Injury Scale (AIS). Although originally intended for impact injuries in motor vehicle accidents, the updates of the AIS allow its application now also for other injuries like burns and penetrating injuries. The AIS distinguishes the following levels of injury:

0 no injury,
1 minor,
2 moderate,
3 serious,
4 severe,
5 critical,
6 maximum injury (cannot be survived).

The AIS ranking is a so-called “threat to life” ranking. The numerical values have no significance other than to designate order. A biomechanical tolerance is the magnitude of a biomechanical response of human body to an impact which causes a certain defined level of injury, often given by the AIS level. It is important to note that the tolerance is not the same for each individual in a population and varies from low to high values within the population. Thus the tolerance in general is related to a certain percentage of the population to be protected. [14]

Injury criteria, based on data of these experiments or mathematical simulations, can be used for an efficient analysis of car safety design and optimization. Most injury criteria are based on accelerations, relative velocities or displacements, or joint constraint forces and most injury criteria need some mathematical evaluation of a time history signal. [14]

2.5.1. Head Injury Criterion (HIC)

Injury criterion for the head was first defined by the U.S. government, the Head Injury Criterion (HIC):

$$HIC = \max_{T0 \le t_1 \le t_2 \le TE} \left[\frac{1}{t_2 - t_1} \int_{t_1}^{t_2} R(t)dt \right]^{2.5} (t_2 - t_1) \qquad (2.7)$$

where *T0* is the starting time of the simulation, *TE* is the end time of the simulation, *R(t)* is the resultant head acceleration in *g*'s (measured at the head's centre of gravity) over the

time interval $T0 \leq t \leq TE$, t_1 and t_2 are the initial and final times (in s) of the interval during which the HIC attains a maximum value. For practical reasons, the maximum time interval (t_2 - t_1) which is considered to give appropriate HIC values was set to 36 ms. This time interval greatly affects HIC calculation and recently, this time interval has been proposed to be further reduced to 16 ms in order to restrict the use of the HIC to hard head contact impacts. A value of 1000 is specified for the HIC as concussion tolerance level in frontal (contact) impact.

An injury criterion and associated tolerance level, should relate to injury severity. Limitations of the HIC are:

- HIC only considers linear acceleration, while biomechanical response of the head also includes angular motion which is believed to cause head injury,
- HIC is only valid for a hard contact, thus the time duration of impact is limited,
- HIC is based on the Wayne State Tolerance Curve, which is derived from subjects loaded in anterior-posterior direction only.

Despite these drawbacks, HIC is the most commonly used criterion for head injury in automotive research and is believed to be an appropriate discriminator between contact and non-contact impact response [2,14,16].

2.5.2. Neck Injury Criteria (FNIC)

Neck injury is often assessed by peak forces and moments in the upper and lower neck. (The keyword FNIC is used in order to discriminate with the NIC criterion for rear impact neck injury assessment which is based on the motion of the head relative to the thorax.) The FNIC is a measure of the injury due to the load transferred through the head/neck interface. The FNIC consists of three components: the neck axial force, the fore/aft neck shear force and the neck bending moment about a lateral axis at the head/neck interface. The FNIC injury calculation is applied to dummy's neck upper joint constraint load signals.

As axial force, the component of the constraint force in neck upper joint z-direction is used, as fore/aft shear force, the component of the constraint force in neck upper joint x-direction is used and as bending moment, the component of the constraint moment about neck upper joint y-axis is used. Duration curves of these time history signals are made. A duration curve is constructed by plotting the force in y-axis and the time the force is above this value in x-axis. The neck axial force and neck shear force duration curves must not exceed the values shown in Figure 2.13 and Figure 2.14; the neck bending moment must not exceed 57 Nm in extension [2,14,16].

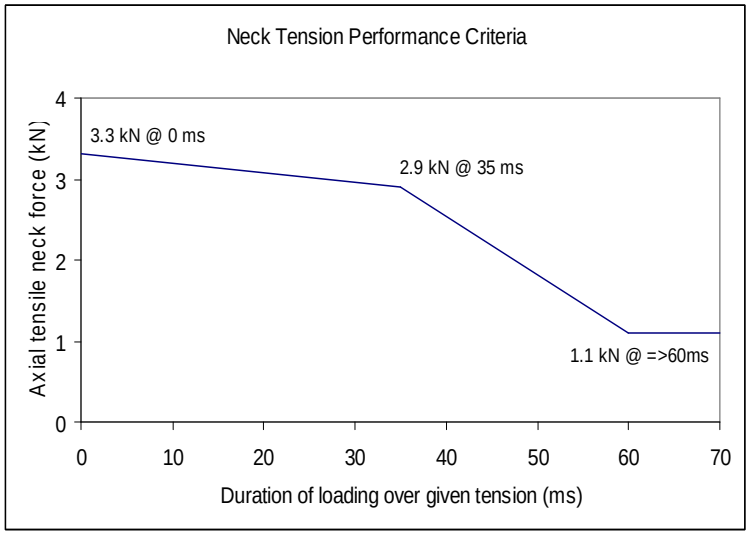

Figure 2.13. Neck tension performance criteria

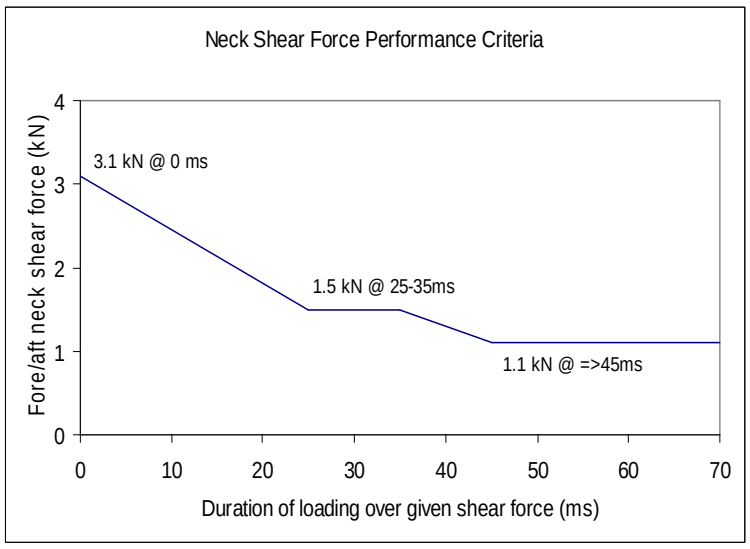

Figure 2.14. Neck shear force performance criteria

2.5.3. Viscous Injury Response (VC)

The vital organs of the chest, the heart and great vessels and the lungs are built of soft tissues. The acceleration of bony structures like the ribs and the spine, or the chest deflection and the applied force do not address the injury mechanism at high velocity rates of soft tissues and can therefore not be used as an injury criteria. Therefore the understanding of the mechanism of soft tissue injury is critical for improvement of occupant protection systems. Research in the past years has lead to the knowledge that soft tissue injury is induced by rate sensitive deformation of the chest. It was found that some occasions of pulmonary and cardiac injuries occurred in conditions of high impact velocities with very little chest deformation. This fact is also reported from injuries caused by the impact of a bullet on a bullet-proof vest, or a baseball hitting the chest directly. It was found that some of these impacts were fatal, even without any visible damage of the chest [2,14,16].

The viscous response, denoted as *VC*, is the maximum value of a time function formed by the product of the velocity of deformation (*V*) and the instantaneous compression function (*C*):

$$VC = \max\left(\frac{dD(t)}{dt} \frac{D(t)}{SZ} \right) \tag{2.8}$$

where *D(t)* is a deflection and *SZ* is a prescribed size (the distance between dummy chest and back at the accelerometer location)

Analyses of data from experiments on human cadavers show that a frontal impact which produces a *VC* value of 1.3 m/s has a 50% chance of the introduction of severe thoracic injury (AIS $\geq$ 4). A value of 1 m/s may be used as a reference value for human tolerance in blunt frontal impact to the chest [2,14,16].

2.5.4. Femur Force Criterion (FFC)

The Femur Force Criterion (FFC) is a measure of the injury of the femur. It is the compression force transmitted axially on each femur of the dummy as it is measured by the femur load cell. The FFC injury calculation is applied to the joint constraint force in the bracket joint located at a femur load cell.

As axial force, the component of the constraint force in the joint z-direction is used. A duration curve of this time history signal is made. The resulting femur axial force duration curve must not exceed the values shown in Figure 2.15 [2,14,16].

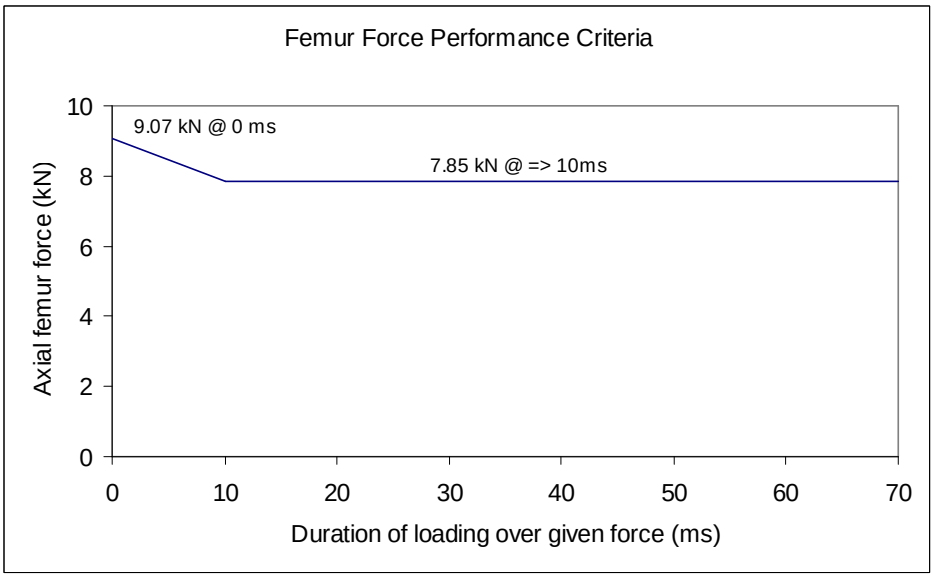

Figure 2.15. Femur force performance criteria

2.5.5. Tibia Compressive Force Criterion (TCFC)

The Tibia Compressive Force Criterion (TCFC) is a measure of the injury of the tibia. It is the compressive force F_Z expressed in kN, transmitted axially by a tibia load cell. The TCFC injury calculation is applied to the joint constraint force in the bracket joint located at a tibia load cell. As axial force, the component of the constraint force in the joint z-direction is used [2,14,16].

2.5.6. Tibia Index

The Tibia Index (TI) is a measure of the injury of the tibia. The TI injury calculation is applied to the joint constraint load in the bracket joint located at a tibia load cell. As the axial force, the component of the constraint force in the joint z-direction is used and as the bending moment, the component of the constraint moment about the joint z-axis is used. The equation for the calculation of TI is given by

$$TI = \left|F_Z/(F_C)_Z\right| + \left|M_R/(M_C)_R\right| \tag{2.9}$$

where

F_Z = compressive axial force in joint z-direction

$(F_C)_Z$ = critical compressive force and should be taken to be 35.9 kN

M_X = bending moment about the joint z-axis

M_Y = bending moment about the joint n-axis

M_R = $\sqrt{(M_X)^2 + (M_Y)^2}$

$(M_C)_R$ = critical bending moment and should be taken to be 172.8 N.m

The tibia index is calculated for the top and bottom of each tibia. For each joint, the corresponding axial force F_Z is used [2,14,16].

2.6. ECE 94 Requirements

According to the injury criteria mentioned above the ECE regulations have set targets for front impact crash tests. [2] These targets are;

- The head performance criterion (HIC) shall not exceed 1000 and the resultant head acceleration shall not exceed 80 *g* for more than 3 ms, the latter shall be calculated cumulatively, excluding rebound movement of the head,
- The neck injury criteria (NIC) shall not exceed the values shown in Figure 2.13 and Figure 2.14,

- The neck bending moment about the y-axis shall not exceed 57 Nm in extension,
- The thorax compression criterion (ThCC) shall not exceed 50 mm,
- The viscous criterion (VC) for the thorax shall not exceed 1.0 m/s,
- The femur force criterion (FFC) shall not exceed the force-time performance criterion shown in Figure 2.15,
- The tibia compression force criterion (TCFC) shall not exceed 8 kN,
- The tibia index (TI) measured at the top and bottom of each tibia, shall not exceed 1.3 at either location,
- The movement of the sliding knee joints shall not exceed 15 mm,

The above criteria indexes are obtained by measuring data on the dummy. The following criterions are also checked to ensure vehicle safety.

- Residual steering wheel displacement, measured at the centre of the steering wheel hub, shall not exceed 80 mm in the upwards-vertical direction and 100 mm in the rearward horizontal direction,
- During the test no door shall open,
- During the test no locking of the locking systems of the front doors shall occur,
- If there is continuous leakage of fluid from the fuel-feed installation after the collision, the rate of leakage shall not exceed 30 g/min,

3. MADYMO MODEL CONSTRUCTION

The steps involved in developing a MADYMO model of vehicle's driver compartment are summarized in this chapter. In a Madymo model, all vehicle components are not modeled; instead subsystems which are in interaction with dummy during crash or which may affect dummy behavior during crash are included in the model. Major subsystems affecting the dummy's behavior during vehicle crash are selected after studying FE model animations and crash test videos. Investigations show that floor pan, pedals, instrument panel, front driver seat, steering column subsystem, safety belt subsystem and airbag are the critical components in the analysis. Among these subsystems airbag and belt subsystems are in the supplier's responsibility and these subsystems are constructed by the supplier (Autoliv) and delivered in a separate include file. Rest of the subsystems are constructed by defining the mass, inertia and geometry information. Also internal motion (kinematics) of subsystems like seat and steering column are defined by using the appropriate joints. A detailed explanation of how each subsystem is modeled and the role of each subsystem during crash is summarized in the following lines [17, 18].

3.1. Vehicle Interior Modeling

Model construction starts with the construction of the interior space of the vehicle. The interior space is divided into two systems for better model handling and better model monitoring. The first system is made up of a floor pan, a carpet, crash pads and pedals; while the second system is made up of an instrument panel, windshield and roof headliner. The modeled parts and their counterparts in Madymo can be seen in Figure 3.1 and Figure 3.2.

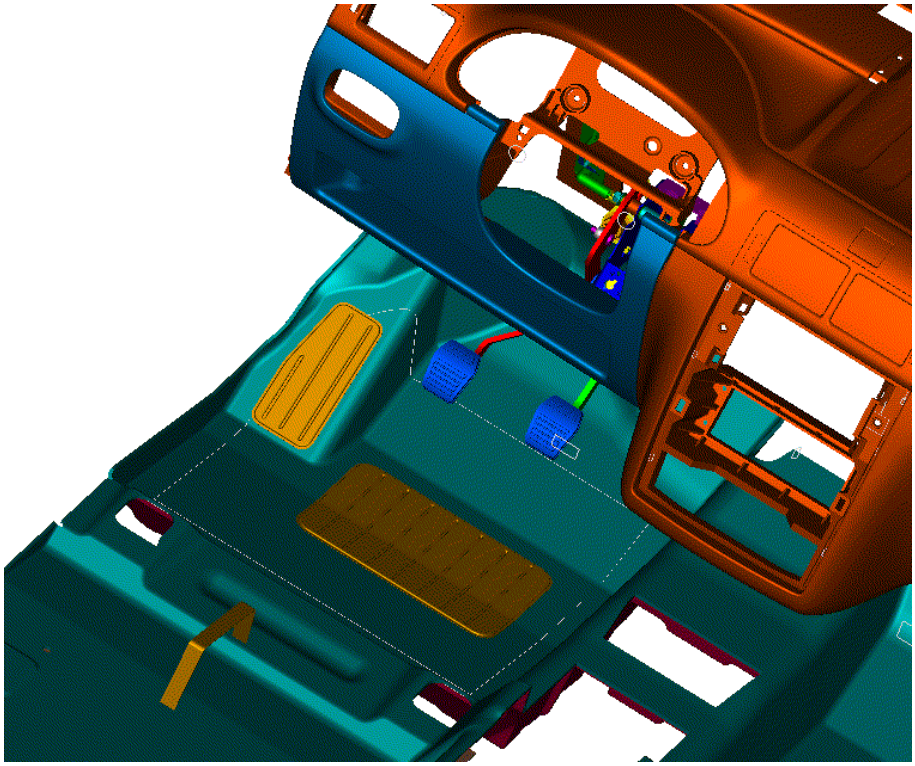

Figure 3.1. Vehicle interior space (CAD data)

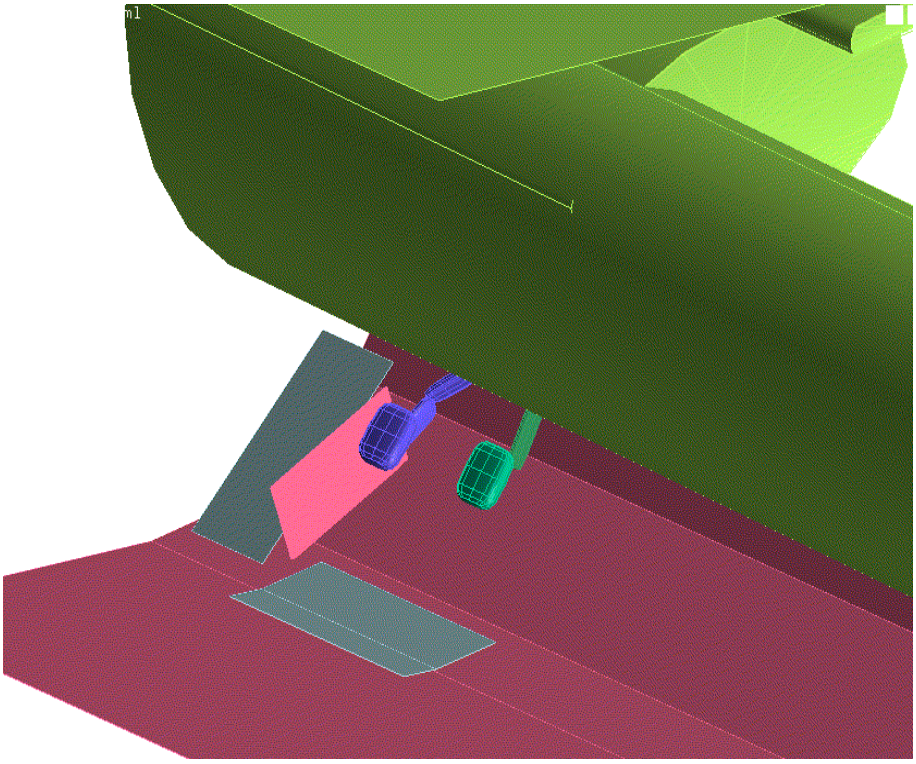

Figure 3.2. Vehicle interior space (Madymo)

3.1.1. Floor Pan Modeling

Floor pan is modeled by using planes to construct floor pan surfaces. The critical item in modeling the floor pan is the definition of contact between the dummy and the floor pan components. As shown in Figure 3.1 and Figure 3.2, crash pads are placed at areas where there is more resistance to dummy from floor. These pads are for improving leg performance. The crash pads are modeled as additional planes of Madymo with lower resistance to forces exerted by the dummy heel and shoes. However, when the foot penetration to floor is close to the thickness of the crash pad, the resistance reaches the resistance of the floor pan. This is illustrated in Figure 3.3, the red curve is the force displacement curve of a floor pan with no crash pad while the blue curve shows the curve of a floor pan with crash pad.

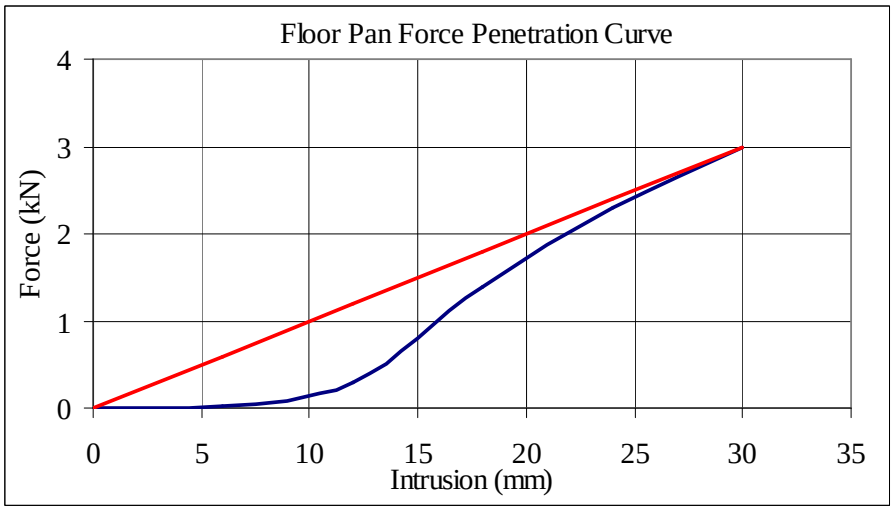

Figure 3.3. Floor pan characteristics function (with and w/o crash pad)

3.1.2. Pedal Modeling

Another critical item to consider during vehicle interior modeling is pedal modeling. Pedals are usually modeled with high degree ellipsoids due to their geometry. Unlike floor pan and crash pads, pedals are considered to be infinitely stiff compared to dummy's shoe and do not deform under forces exerted by the dummy. Therefore the contact definition between the pedals and the dummy shoe is extremely stiff compared to floor pan curve. However, the pedals are attached to a pedalbox with springs, and pedals rotate around their

fixing points and are free to travel forward during crash with the force exerted by the dummy's shoe. This is modeled by a revolute joint at the pedal rotation axis with a rotational stiffness equal to the pedal travel stiffness.

Madymo representaion of the pedalbox and pedals subsystem is shown in Figure 3.4. The pedal attachments for the clutch and brake pedals are only for visual purposes and they are not included in the contact definition between the shoes and pedals. Revolute joint positions at the pedalbox attachment points are also shown in the figure. The rectangle behind the pedals (body-pedalbox motion) is only for visual purposes and is defined to specify the pedalbox intrusion into the interior space during crash.

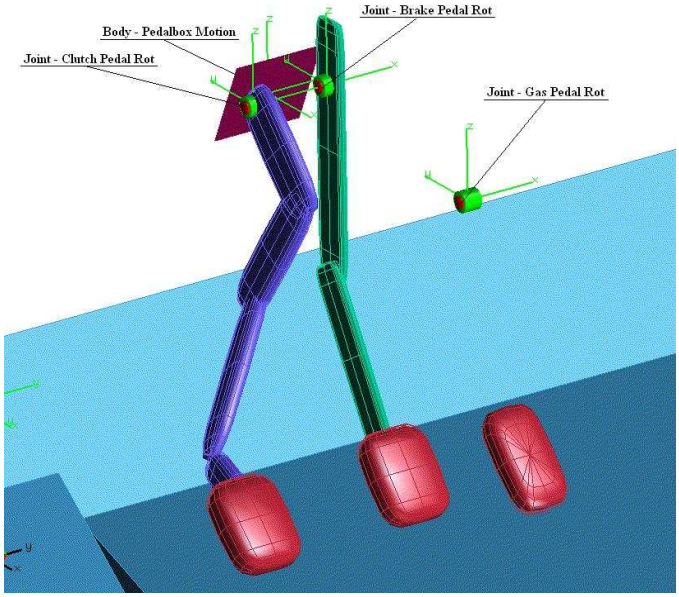

Figure 3.4. Madymo representation of pedalbox and pedals

3.1.3. Instrument Panel Modeling

Instrument Panel modeling is similar to floor pan modeling. However, instead of planes, elliptic cylinders are used to model the instrument panel. The contact characteristics defined for the instrument panel defines the dummy knee intrusion into the instrument panel and critical as in the floor pan contact characteristics.

3.2. Seat Modeling and Dummy Positioning

The seat is the first item in contact with the dummy during crash. The deformation of the seat during crash directly affects the dummy's behavior. A seat with small horizontal stiffness will tend to push the dummy forward resulting in a larger dummy motion, higher safety belt forces and early contact with the airbag while a robust seat will enable a better dummy performance. On the other side seat cushion will tend to damp the dummy motion preventing hard contact between the seat structure and dummy.

A seat model constructed in Madymo is shown in Figure 3.5. The blue ellipsoids and blue planes define seat cushion, while the green ellipsoids and green planes define steel structure. The whole seat does not need to be modeled; instead seat surfaces in contact with the dummy are modeled. Among these surfaces a stiff contact characteristic exists between the dummy and the steel structure, while a soft contact characteristic allowing intrusions up to 100 mm exists between the seat cushion and the dummy. Contact characteristics for the seat foam and steel structure are measured by the seat manufacturer. During these tests the pelvis of the dummy is used as the load application device and the corresponding intrusions on the seat steel structure and seat foam are measured. (Figure 3.6)

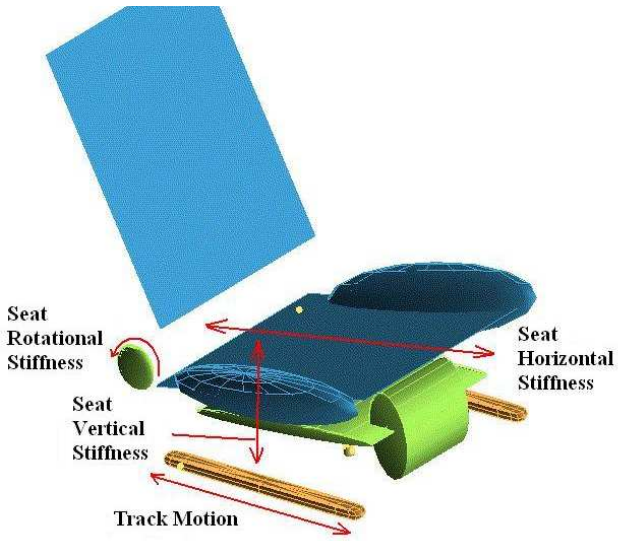

Figure 3.5. Madymo seat model

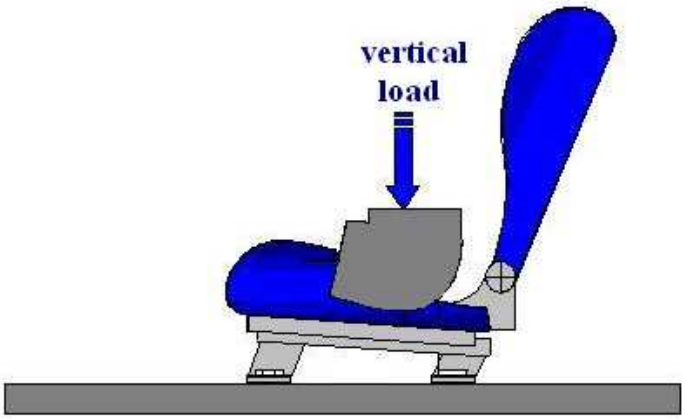

Figure 3.6. Test setup to measure seat characteristics

Seat height adjusting and seat back adjusting mechanisms are not modeled but their effect on seat deformation is included in the analysis by joints. Planar joints are defined for seat horizontal and vertical adjusting mechanism stiffness and a revolute joint is defined for seat back rotating mechanism stiffness. The planar joints act as horizontal, vertical springs allowing a relative motion between seat ramp and track while the revolute joint does the same for the relative motion between seat back and seat ramp. The stiffness functions for seat deformation is also derived from the test mentioned above for seat contact characteristics.

Once the seat is modeled, the dummy is positioned in the seat. The dummy used in the model is the Madymo representation of the standard “Hybrid III %50 male dummy”. The dummy joint positions and angles are modified to achieve the same dummy seating position between the test and the Madymo model. Note that when the dummy is positioned the dummy ellipsoids penetrate the seat cushion both on the back and the bottom. (Figure 3.7) This is made on purpose to simulate the seat cushion deformation when the dummy is first placed in the seat during test.

Figure 3.7. Dummy and seat model together (Madymo)

3.3. Steering Column Modeling

Steering column system is one of the most complex systems in the vehicle's Madymo model. The system consists of a number of revolute and translational joints to represent steering wheel rotation, steering column position adjusting mechanism and steering column ride-down during crash. Steering wheel also holds the airbag housing and therefore directly affects airbag behavior during crash.

Steering wheel rotation and steering column position adjusting mechanisms are modeled with revolute joints at the steering column lower shaft end. In the revolute joint, for steering wheel rotation, data supplied by the manufacturer is used. The revolute joint for adjustment is either locked or a very stiff function can be defined for this joint.

Apart from the detailed modeling above, the column's ride-down behavior needs to be modeled. In steering columns with ride-down feature, the upper shaft is attached to the column bracket such that the attachment breaks at a certain force. This force is generated by the inflation of the airbag and the dummy head hitting the airbag. Under these forces outer shaft starts to travel downwards over the inner shaft until it is stopped by the stopper at the end. This feature prevents a hard impact between the dummy head and the wheel and

results in lower head acceleration values. It also increases the distance between dummy chest and steering wheel preventing chest wheel contact. The steering column and the corresponding Madymo model is shown in Figure 3.8 and Figure 3.9.

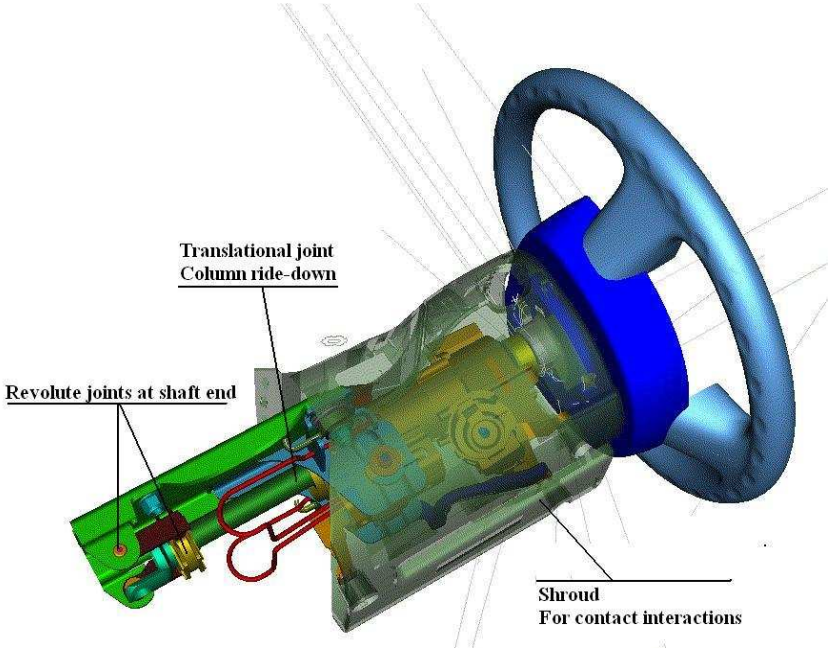

Figure 3.8. Steering column (CAD data)

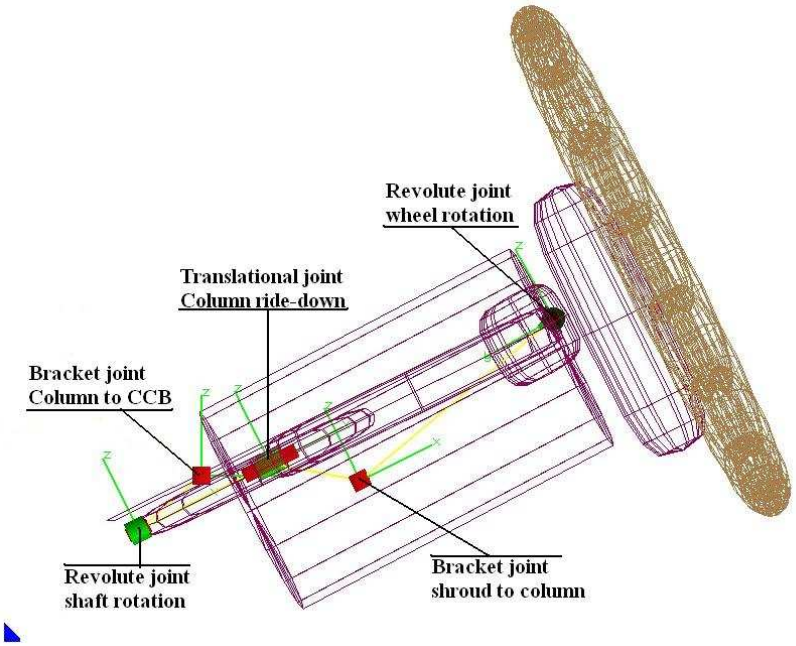

Figure 3.9. Steering column model in Madymo, coordinate systems shown are joint local coordinate systems

The steering column's ride down function is difficult to calculate analytically or using finite element codes. The most common method used to derive the function is to use a linear impactor test. The test gives the load under which the ride down starts and the force displacement characteristics during ride down action. Also during crash tests a sensor is placed in the steering column to measure the steering column ride down start time, which enables better correlation between Madymo results and test.

The results of the steering column ride-down test performed by the manufacturer and the Madymo function derived from these results are shown in Figure 3.10 and Figure 3.11. The negative ride-down at the beginning is caused by the airbag's inflation. This is not included in Madymo as it has no effect on airbag or column behavior. Instead, in Madymo a very sharp increase to the breakaway force and then a sudden drop is modeled, after all the overall behavior of the steering column system is the same throughout the crash. Negative values of the test results are used in Madymo because in the translational joint to represent the column's ride-down, x-axis points inside the vehicle and the force acting on the joint is always negative during ride-down.

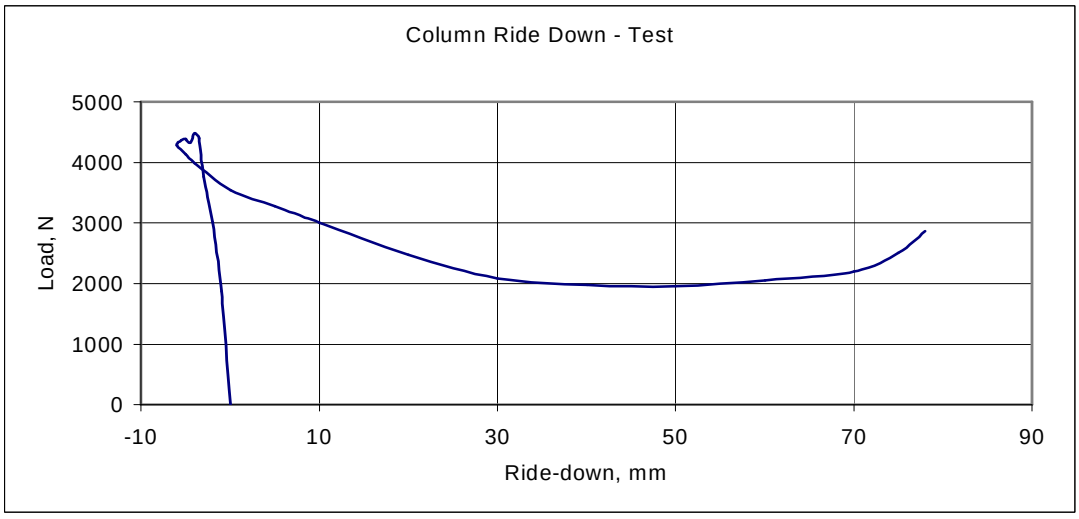

Figure 3.10. Steering column's ride down, test results.

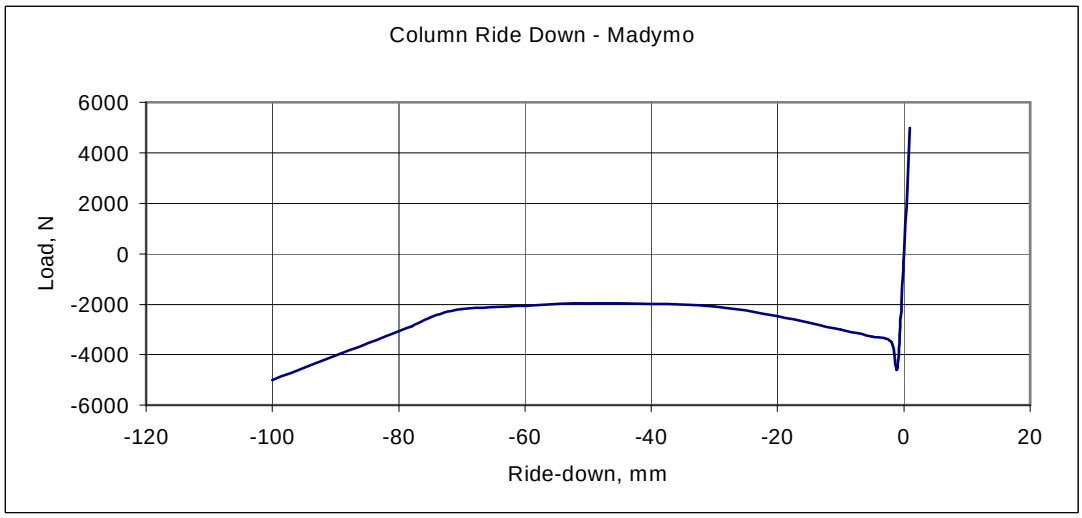

Figure 3.11. Steering column's ride down function in Madymo

To model the column's ride down action, sensors and switches need to be defined besides the joints. As mentioned before, a translational joint controls steering column's ride-down. The joint is locked at the beginning of the analysis. A sensor is used to measure the force acting on the joint. When the force measured is greater than the breakaway force the sensor activates a switch. The switch sets the joint status from locked to free and the column's ride down action starts according to the function defined in Figure 3.11. At the same time another sensor on the joint starts to measure the outer shaft travel. When the travel is equal to the column stroke it activates another switch, which locks the joint again. In this manner, the column ride down is modeled in Madymo.

3.4. Safety Belt System Modeling

The safety belt system consists of a retractor, d-ring, buckle, anchor point and the belt. These are all modeled as separate systems in Madymo as shown in Figure 3.12. The D-ring and the anchor point are just point items, which are defined in routing the belt while the buckle and retractor are complex structures defining the belt behavior during crash. The buckle and retractor may have many features from pretensioners to load limiters to hold the dummy in the seat during crash. This will be explained briefly in the following lines. [19]

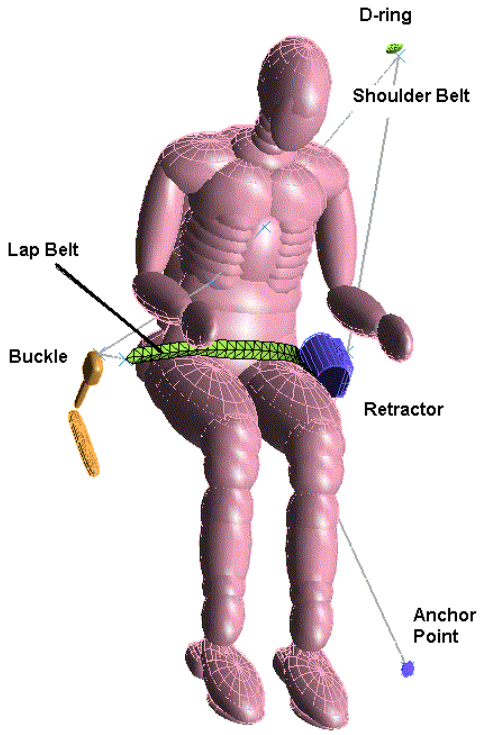

Figure 3.12. Safety belt system

There are two options to model a safety belt in Madymo. Segment belts or finite element (FE) belts. Segment belts are 1-D items created between two points and carrying the stiffness of the belt material. The segment belt ends may contain points on the retractor, D-ring, dummy, buckle, etc. The points where the segment belt ends are attached are special points defined as sliprings, which allow transition from one segment to another. This feature ensures that the belt can slip along the axis it is routed but the belt has no relative motion with respect to the dummy [18].

On the other hand, the FE belt consists of 2D triangular elements for which the belt properties and material is defined. Unlike the segment belt, the FE belt is not attached to the dummy. Instead contact is defined between the dummy ellipsoids and the FE belt. Unlike the segment belt, the FE belt can slip on the dummy and relative motion between dummy and belt is possible [18].

As long as the belt characteristics defined are the same, the segment belt and FE belt resistance to the dummy motion is similar and both can be used to define the seat belt. The difference between the two belt models lies in contact definitions. To decide on which type

of belt to use, the test animations or Madymo simulations need to be examined. The belt behavior during crash on dummy will define whether segment belt or lap belt will be used. In the model constructed, the chest motion is perpendicular to seat belt alignment while the lap motion is parallel to the seat belt alignment. Therefore segment belts will be used to model shoulder belt and FE belt will be used to model lap belt. The two belt models are attached to each other at the buckle end.

3.4.1. Buckle and Retractor Modeling

Buckle and retractor systems shown in Figure 3.13 and Figure 3.14 are the two critical hard points of the safety belt system. These two systems may have many features to affect the dummy's behavior. Without them, retractor is no more different than anchor point and buckle is no more different than D-ring. But features like pretensioners and load limiters are added to these two systems for better dummy performance during crash.

Figure 3.13. Buckle

Figure 3.14. Retractor

When crash is sensed through sensors on the vehicle, the aim of all restraint systems is to keep the driver away from intrusion zones. As the driver is considered to be free in his seat, and the seat decelerates with the deceleration of the vehicle, the driver will have a relative motion with respect to the seat. At this stage, the buckle and retractor work as systems, which tighten the driver to the seat. However, decelerating the driver at the same speed as the vehicle decelerates will result in high deceleration loads on the driver, so that the driver needs to be released slowly at some instant during the crash to reduce the risk of internal injuries. This is achieved by pretensioners and load limiters.

The two types of pretensioners are shown in Figure 3.15 and Figure 3.16. Pretensioners usually contain a propellant, which is fired following a signal from the airbag sensor. In buckle pretensioner, the cable holding the buckle end is pulled by the impact force generated and the lap belt is tightened. In retractor pretensioner, the belt is rewound inside the retractor case and the shoulder belt is tightened. Both pretensioners restrain the driver to the seat so that the driver's relative motion to the seat is prevented [20, 21].

Figure 3.15. Buckle pretensioner

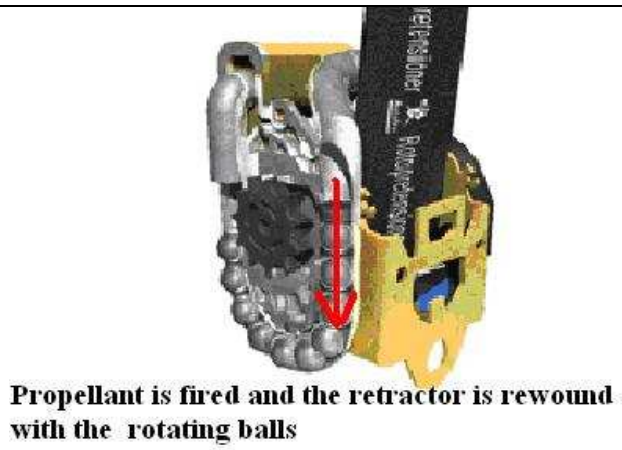

Figure 3.16. Retractor pretensioner

Once the driver is restrained in the seat, at a certain deceleration the driver needs to be released to avoid internal injuries due to the high deceleration. This is achieved by the load limiter shown in Figure 3.17. The load limiters absorb the load in a crash in a very efficient way by keeping the belt force at a controlled and pre-defined level. This is accomplished by a mechanism in the retractor that allows webbing to be pulled out slightly - and in a controlled way - if and only if the load on the driver's body becomes too high in a violent crash, that means if the driver needs to be released at some degree. The load limiter is typically integrated with the retractor, where a specially designed bar holds the spindle with the webbing. As long as the force from the webbing exceeds a pre-set limit, the end of the bar will turn, twisting the bar and thereby gradually reducing the load on the driver's chest [20, 21].

Figure 3.17. Retractor load limiter

After the entire belt is webbed from the retractor, the belt's plastic deformation begins. Belts are usually made of high strength materials, which can resist very high forces, more than that can be generated during, crash. So a belt failure is not expected. The plastic deformation of the belt also acts as a load limiter and helps in controlling the driver by releasing the driver slowly [20, 21].

Pretensioners and load limiters are modeled as a system of rigid bodies connected to each other by translational joints. Stiffness values of joints are defined by force-displacement functions that are derived by belt manufacturers. It is the belt manufacturer's responsibility to create the retractor and buckle models for the Madymo analysis. They are included in the Madymo analyses as separate files.

3.5. Airbag Modeling

Airbags, as a safety item in a vehicle, were first introduced in the 1970s and since then they are used as the most known safety feature in a vehicle. Although effectiveness studies on safety items show that the safety belt is the first item absorbing 35% of the total kinetic energy of the dummy, airbags prevent head, neck and thorax injuries which are more severe compared to abdomen, pelvis, leg and foot injuries [22].

Airbags cannot be modeled as a rigid body like other items modeled in Madymo. Therefore, a detailed FE model of the airbag is needed. An airbag positioned on the

steering wheel is shown in Figure 3.18. There are two approaches to model an airbag, folded airbag approach; which represents the complete behavior of the airbag during airbag inflation; and the scaled airbag approach, which does not reflect the real behavior of the airbag during inflation process but which is less time consuming and cheaper.

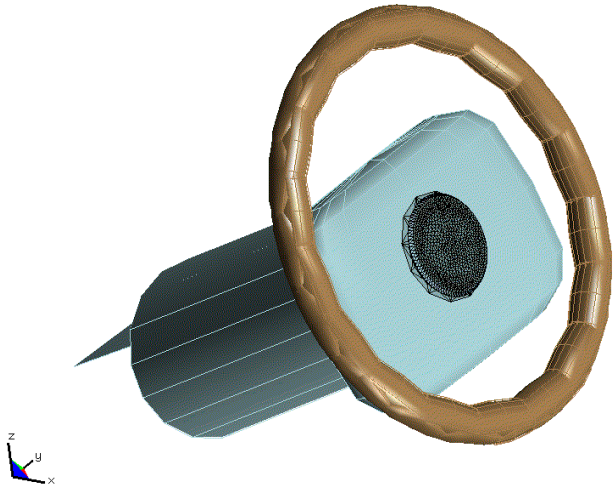

Figure 3.18. Airbag positioned on the wheel (scaled to initial size)

In scaled airbag approach, the inflated airbag is scaled to fit in the steering wheel. When the airbag switch is triggered, and the gas starts to fill in, the airbag is scaled up to its original size. The inflation process does not simulate a real airbag inflation process, but investigations on Madymo simulations show that the airbag's critical role in crash starts when the airbag reaches its full size and the pressure inside the airbag is close to maximum. After the airbag is fully inflated, the behavior of a folded airbag or a scaled airbag is the same. The head-airbag contacts usually occur after the airbag is inflated as in this manner the force generated by the inflation process does not add to head's deceleration. [18]

Scaled and fully open models of an airbag are shown in Figure 3.18 and Figure 3.19. The fully open airbag is a flat surface of two layers. The airbag starts to fill in and acquires its shape when the inflation process starts. The inflation and ventilation behaviors of the airbag need very detailed modeling techniques and they are all modeled with functions derived from airbag tests on rigid walls and airbag head impact tests. Therefore, there is always a good correlation between the airbag behavior in a test, and Madymo simulations.

The airbag tests and the corresponding Madymo airbag modeling is performed by the airbag manufacturer and the airbag subsystem is supplied in a separate include file.

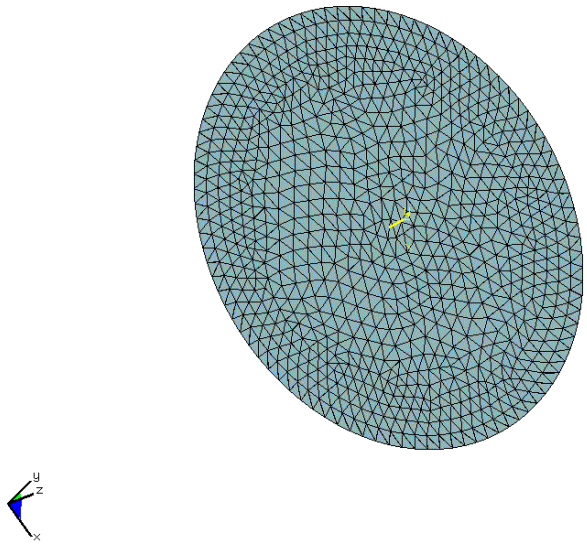

Figure 3.19. Airbag open (reference-original size)

4. MADYMO SLED TEST SIMULATION RESULTS

There are many difficulties involved when trying to correlate a real crash test and a Madymo simulation; most difficult one being the monitoring of dummy behavior. The behavior of the dummy cannot be estimated because the dummy is inside the vehicle, and its entire motion cannot be monitored. On the other hand, during the crash the vehicle adds extra motion and intrusions to driver survival space, which makes the correlation even more difficult. As a result, sled tests are used to correlate the Madymo model and to derive necessary functions to be used in Madymo. The benefits of first correlating the Madymo model with the sled test are; better monitoring of subsystems because during sled test all dummy, airbag, steering column and safety belt motion can be monitored and contact interactions between subsystems can be better monitored and investigated.

A sled test can be defined as a simpler version of the physical crash test with no actual crash of the vehicle taking place since there is no vehicle deformation. This feature makes sled tests popular since they are cheaper and repeatable. During the sled test instead of placing the vehicle on sled, a certain portion of the vehicle, usually called the buck, is mounted on a rigid non-deformable sled and is accelerated up to the speed of the vehicle before crash. After some constant speed travel, the vehicle is suddenly braked to zero speed by means of energy absorbing obstacles or a hydraulic system. During the deceleration period, at known time steps the airbag and the belt pretensioners are fired. The pulse the buck undergoes during the sled test is obtained from the data gathered from the vehicle's physical crash test. As a result the dummy behavior is similar to the dummy behavior in a real physical crash test. However, sled test results are not accepted for final approval purposes, rather their results produce important data in vehicle's product development period. The picture of a sled test system and the corresponding Madymo model can be seen in Figure 4.1 and Figure 4.2.

Figure 4.1. Sled test

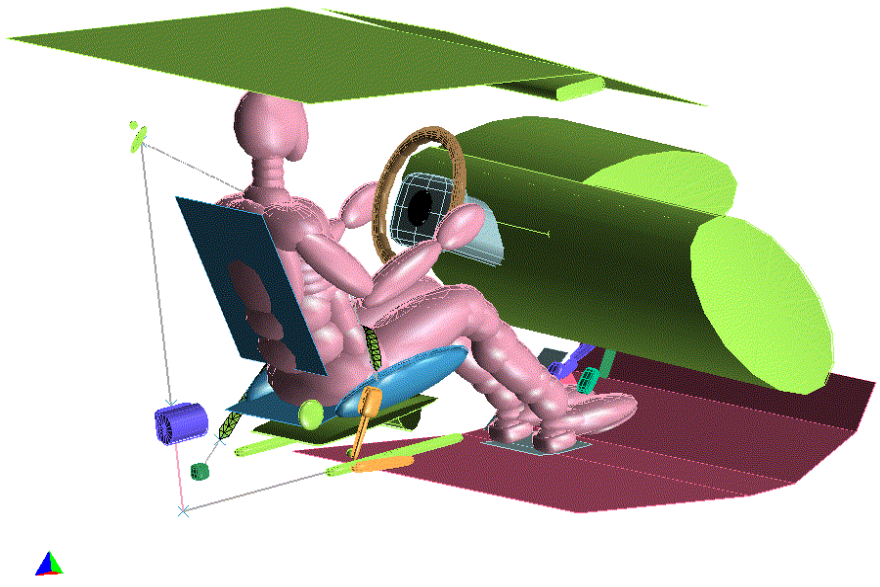

Figure 4.2. Madymo representation of sled test

The sled test chosen for Madymo correlation was performed in Ford Motor Company's Dunton Safety Laboratories. The sled test's purpose was to evaluate the seat structural integrity and corresponding dummy motion. The sled deceleration data for the test was gathered from Ford internal physical crash tests. Ford internal physical crash tests impose more strict conditions on the vehicle and dummy performance than the homologation tests. Also the test conditions are harder compared to the homologation tests. Therefore, sled tests to represent homologation tests are not preferred, instead the sled tests are performed at harder conditions. In the physical crash test the data for our sled test was gathered, the vehicle was a light commercial vehicle. (Transit Connect) The vehicle was hit to a rigid wall instead of a barrier resulting in more deformation, the vehicle speed was 56 km/h and the vehicle was lighter than the homologation vehicle to achieve higher decelerations, therefore higher forces on the seat and the dummy for a worst case simulation. The velocity and acceleration profile gathered from the physical crash test and used in the sled test can be seen in Figure 4.3.

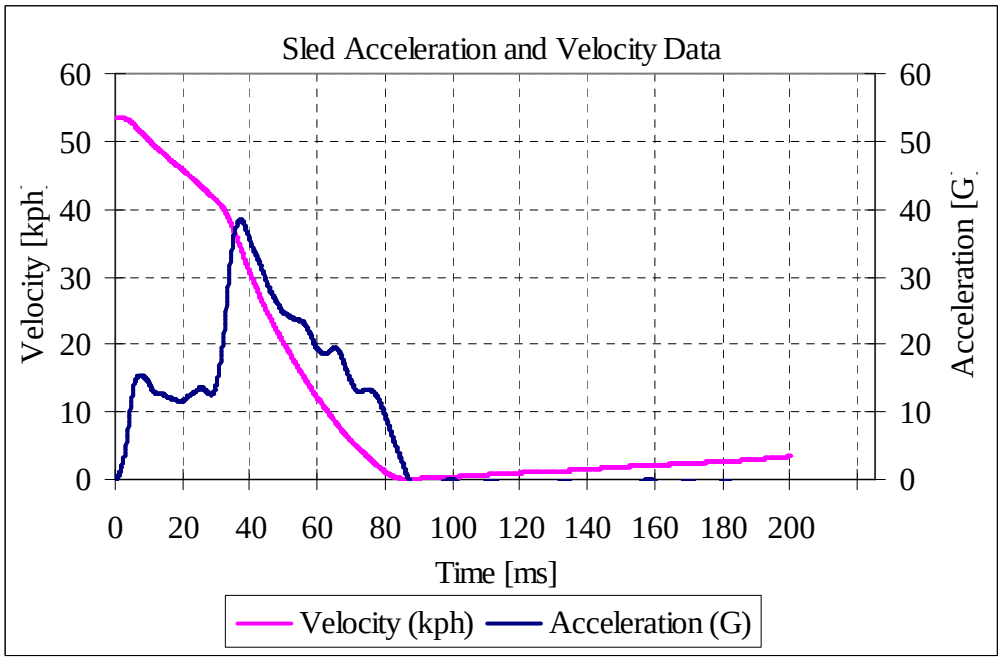

Figure 4.3. Sled acceleration and velocity data

The Madymo model constructed was modified to match the sled test conditions. The following modifications performed on the model.

- The seat was moved to mid-track travel and the seat height was adjusted to the lowest position as in the test.
- The steering column was adjusted such that the height and travel was in mid-mid position.
- The airbag and belt pretensioner firing times were set to 10 ms.
- In the buck, pedals and steering column shroud was not included. The contacts involving these parts were deleted.
- Dummy joint positions and angles (neck, pelvis, hip, knee) were modified according to the pre-test measurements to achieve the same distances between the dummy and interior space parts.
- The motion of the sled was generated integrating the velocity profile and this was assigned to the sled as prescribed motion.
- D-ring (shoulder belt upper attachment) was in highest position during the test, d-ring moved into the test position.
- Shoulder belt was defined with segments tying points on dummy, belt routing was defined by measuring points on a 50% male dummy, and the corresponding points were assigned to segment belt dummy attachment points.

In the following (Figure 4.4 and Figure 4.5), the captured photo from the sled test video at the beginning of sled deceleration and the corresponding screenshot from Madymo model are shown.

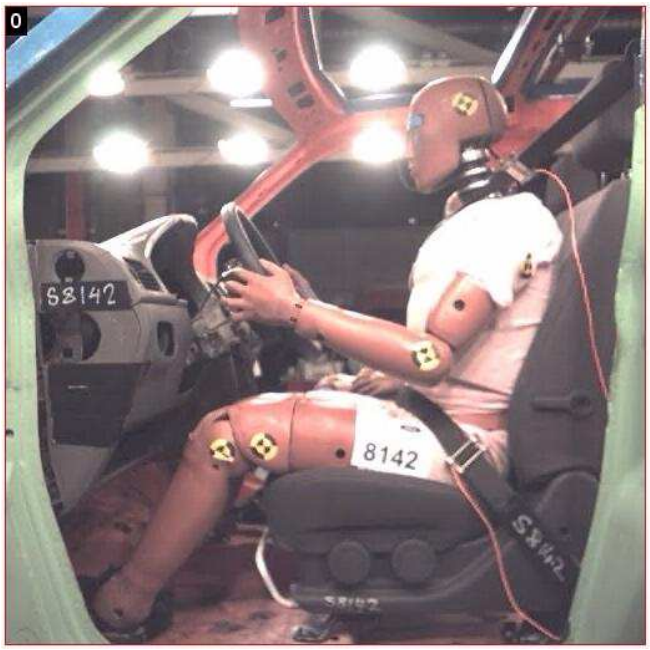

Figure 4.4. Sled test t = 0 ms

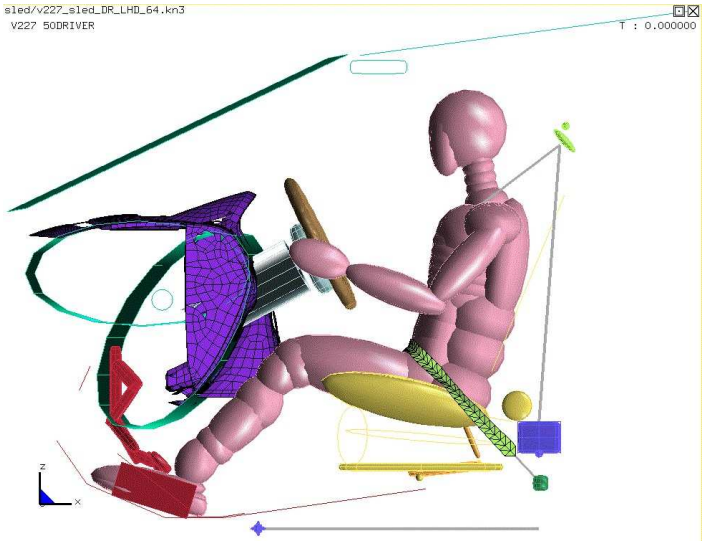

Figure 4.5. Madymo model t = 0 ms

4.1. Sled Test and Madymo Simulation Comparison

From Figure 4.6 to Figure 4.11 sled test and Madymo simulation screenshots after the above modifications are listed. Looking at the figures overall head to airbag contact, chest to airbag contact, chest and head behavior during crash is similar. Also note that the steering column's ride down effect is successfully included in the model.

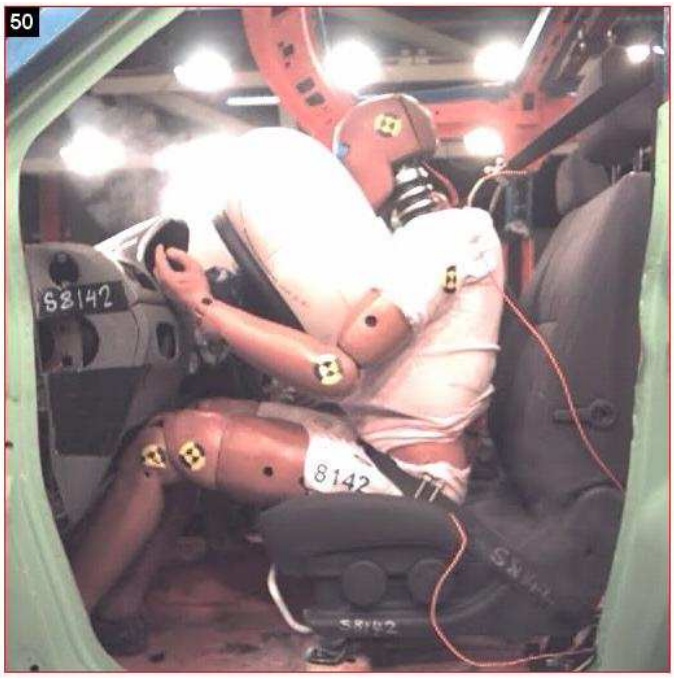

Figure 4.6. Sled test at t = 50 ms

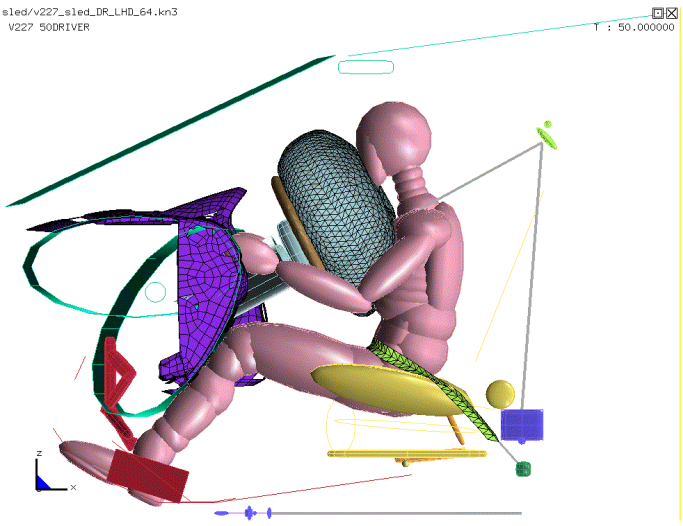

Figure 4.7. Madymo model at t = 50 ms

At 50 ms, the head contacts the airbag. The behavior of the head and chest in both simulations, and the video images are similar. Note that airbag ventilation already started allowing a soft contact between the dummy and the airbag. At this stage, the steering column ride-down has not started yet, but it is about the start. Also the knee IP contact has occurred.

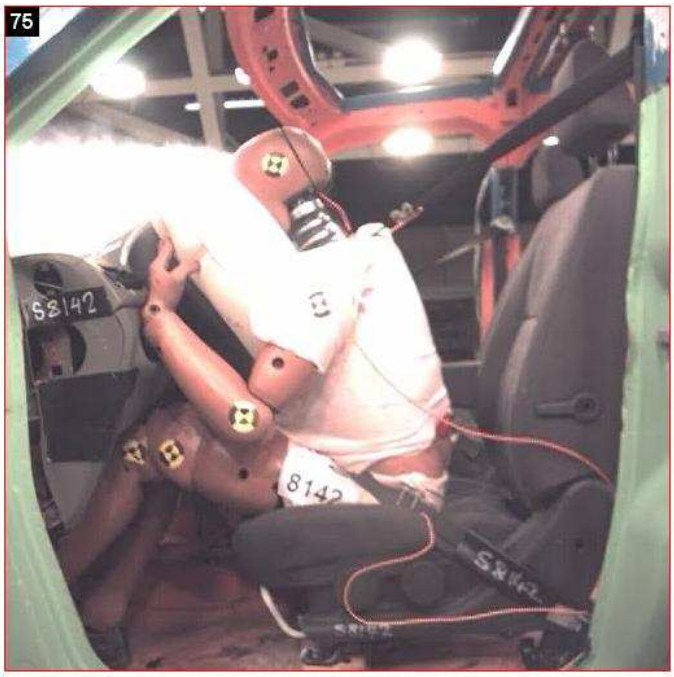

Figure 4.8. Sled test at t = 75 ms

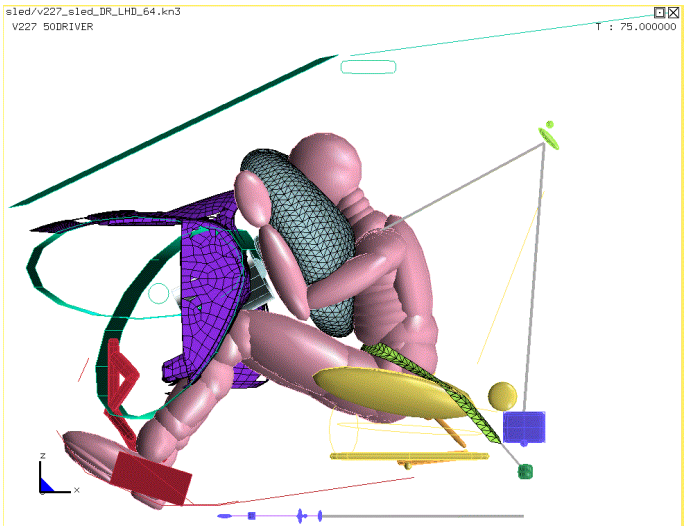

Figure 4.9. Madymo model at t = 75 ms

At 75 ms, dummy's head is totally buried in the airbag and the steering column rides down with the contact force generated by the airbag and the head contact. Although the steering column position cannot be seen clearly in the picture from the positions of the airbag and the head, it is clear that it has ridden down and is buried in the instrument panel.

Figure 4.10. Sled test at t = 100 ms

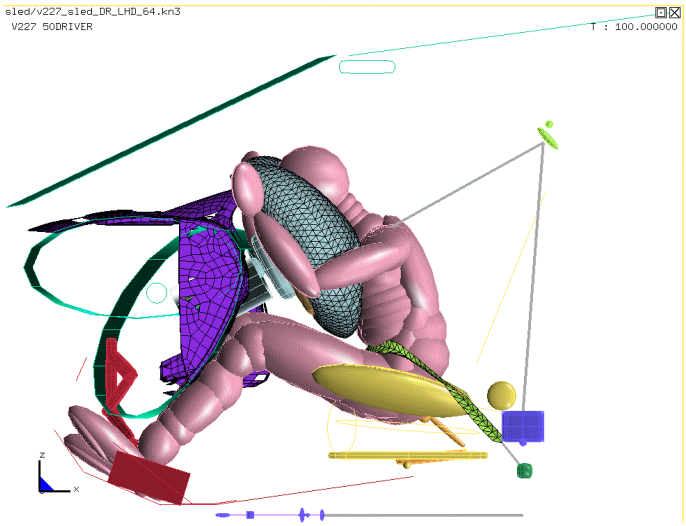

Figure 4.11. Madymo model at t = 100 ms

At 100 ms, dummy's spring back starts. This can be understood from the head and knee positions. From then on, crash ends for the dummy and no further critical damage to dummy is expected. The acceleration and force values in figures also verify this. After 100 ms, all values have a tendency to decrease.

The first shot analyses showed a good correlation with the test results. The airbag (Autoliv), safety belt (Autoliv), seat (Hanil) and steering column (NACAM) models in the Madymo simulation were all constructed using component test data supplied by the manufacturers mentioned in parentheses. Each component, on its own was subjected to physical component tests and the coefficients in the model that determine the subsystem's characteristics were modified to match the best correlation between the physical test and the model constructed. However, little tunings were necessary for better correlation.

4.1.1. Head x and y Accelerations Comparison

First shot analyses predicted the head resultant acceleration higher than the sled test. A breakdown of the resultant acceleration showed that the misalignment was in head x and y accelerations. The x-dir acceleration tended to be higher while there was an unexpected acceleration in negative y-dir. For x-dir acceleration to be higher there might be two reasons; either airbag ventilation may be less than actual so the airbag resists more to the head motion or the shoulder belt is not holding the dummy upper portions as strong as in the test. Iterations changing airbag ventilation did not affect head impact, on the other side increasing the friction coefficient between d-ring and the shoulder belt from 0.1 to 0.2 improved the results. (Figure 4.12) The change in the friction coefficient also affected the shoulder belt force calculated in Madymo. With the higher friction coefficient, the shoulder belt force is higher and close to the measured belt force in the sled test. (Figure 4.13)

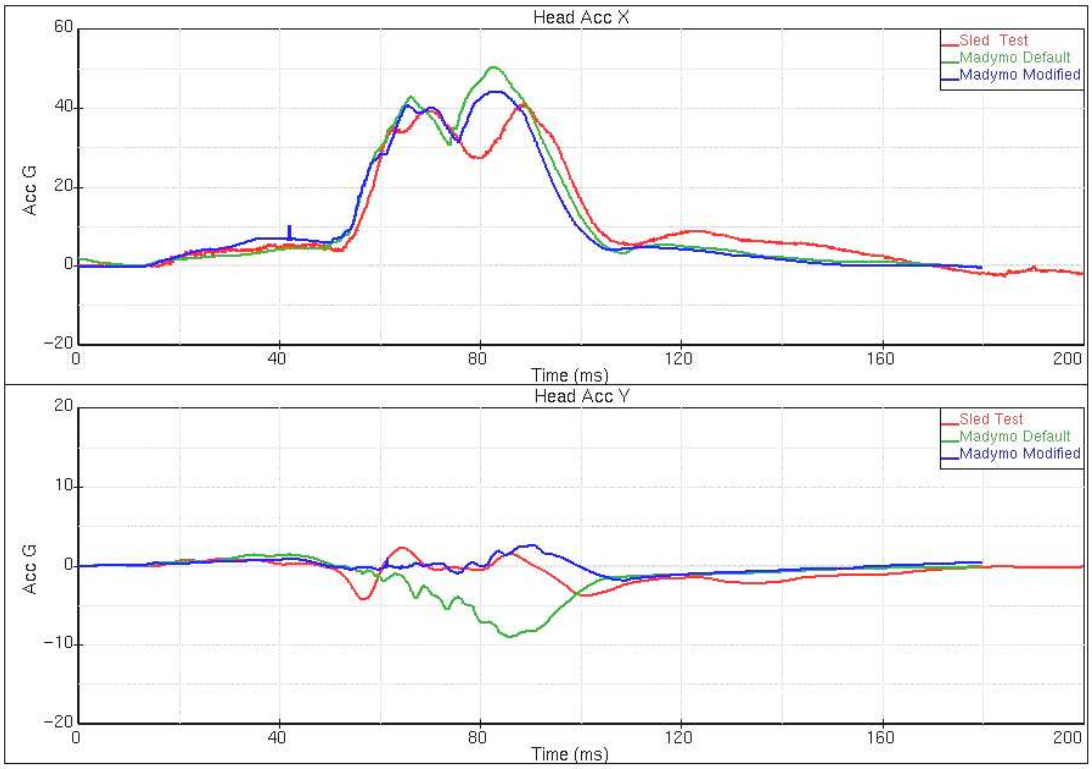

Figure 4.12. Head x and y direction acceleration values

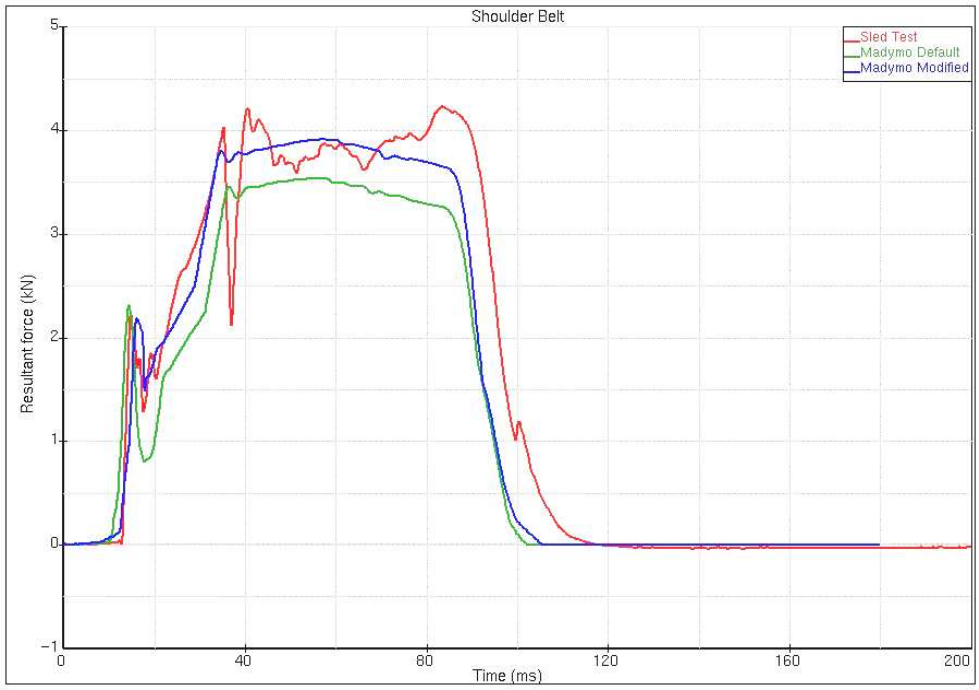

Figure 4.13. Shoulder belt forces with different friction coefficients at d-ring

The differences in the head y-dir accelerations resulted from the head rotation after head contacts the airbag. Looking at Figure 4.12, it can be seen that the head y-dir

acceleration increases after 60 ms, the head's contact with the airbag. The default friction coefficient (0.3) specified between the airbag and the dummy head is higher and dummy head is pushed to rotate due to the friction. This is shown in Figure 4.14. Decreasing the friction coefficient from 0.3 to 0.15 a better representation of dummy head was achieved.

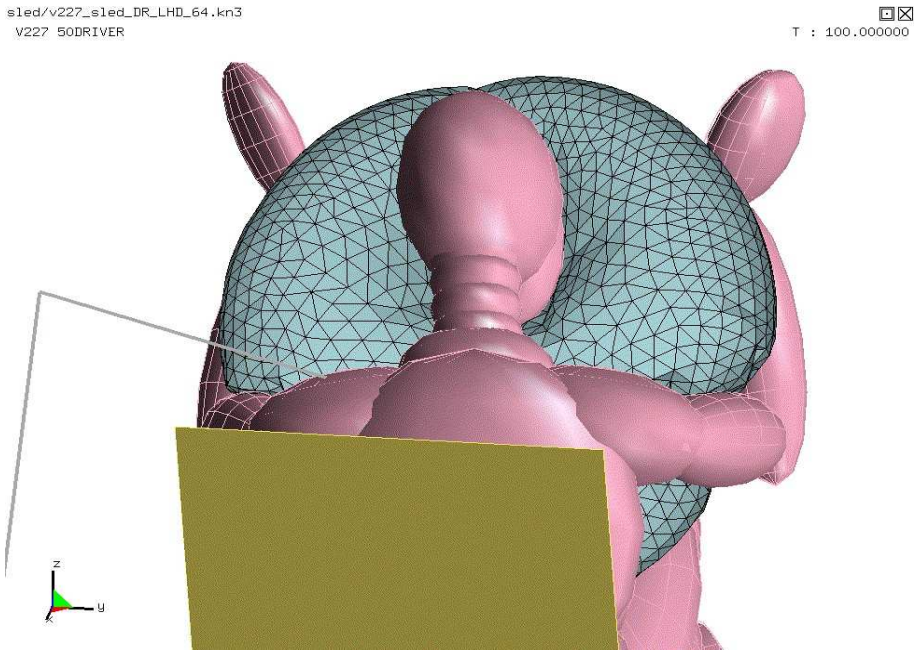

Figure 4.14. Head rotation at 100 ms due to friction between airbag and dummy head

4.1.2. Chest z-dir and Pelvis x-dir Accelerations Comparison

The next mismatching item is the chest z-dir acceleration. Actually, no reason could be found for the mismatch in z-dir accelerations. Iterations were done by increasing the friction between airbag and dummy chest to prevent the negative z-dir acceleration but the iterations did not help. Changing shoulder belt stiffness caused variations in x and y-dir chest accelerations which were already in good correlation. However, iterations done to improve pelvis x-dir accelerations helped to improve the chest z-dir acceleration results up to 80 ms as shown in Figure 4.15.

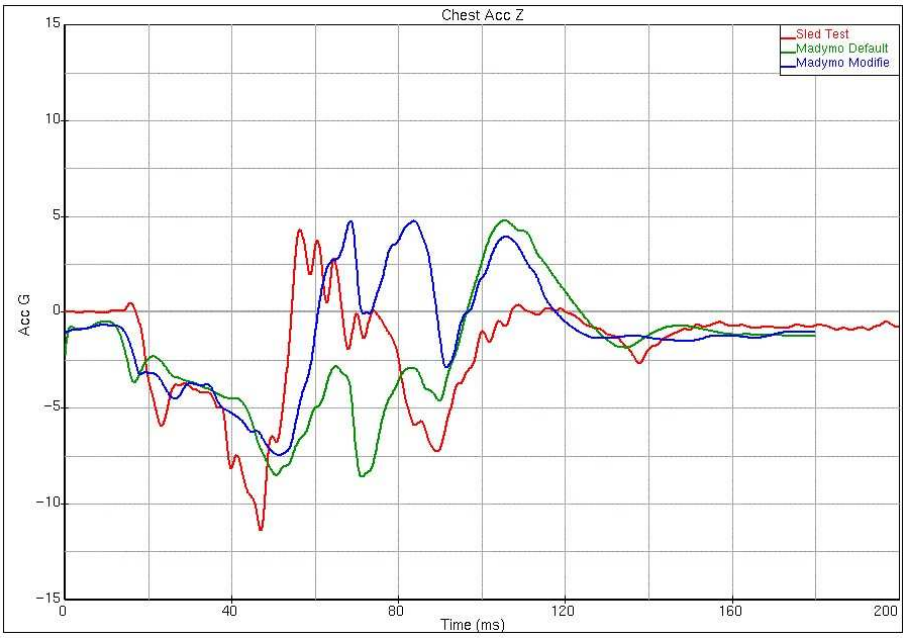

Figure 4.15. Chest z-dir accelerations

Comparing the animations of the sled video and Madymo simulations, it is realized that the lap belt is tighter in the sled test compared to the Madymo simulation. The lap belt in the sled test prevents dummy pelvis motion more than in the Madymo simulation. Except the belt, also the buckle in the Madymo simulation has a motion towards the vehicle. (See Figure 4.16 and Figure 4.17) The contact defined between the buckle and the seat cushion has a friction coefficient of 0.35 that needs to be higher to prevent buckle motion. Increasing lap belt friction coefficient from 0.1 to 0.15 and buckle seat cushion friction coefficient from 0.35 to 0.50 the pelvis x-dir acceleration values increased. (Figure 4.18) This modification also affected the chest y-dir acceleration values in a positive manner up to 80 ms.

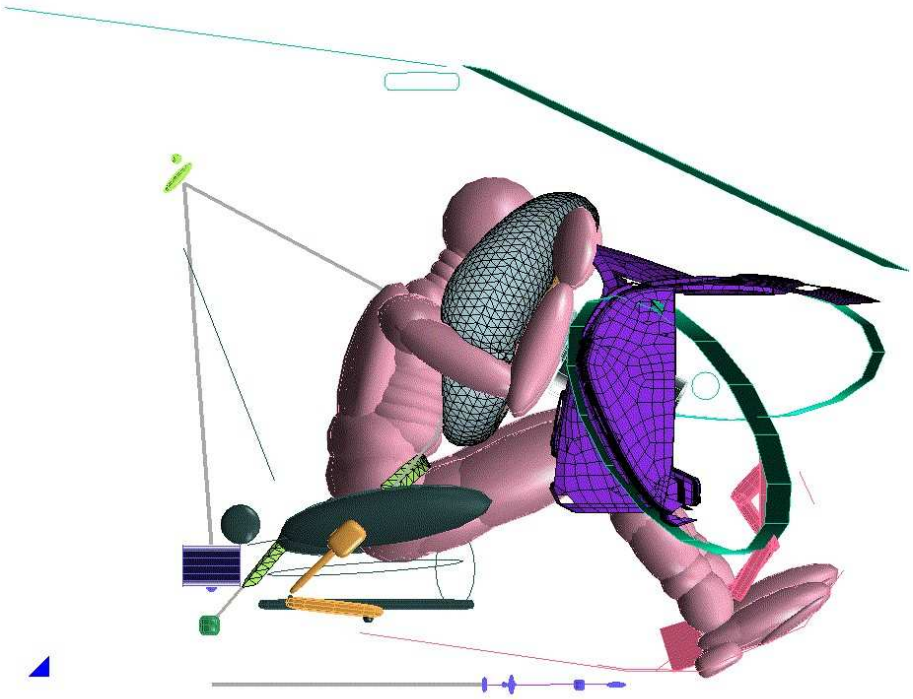

Figure 4.16. Dummy position at 80 ms, default lap belt coefficients

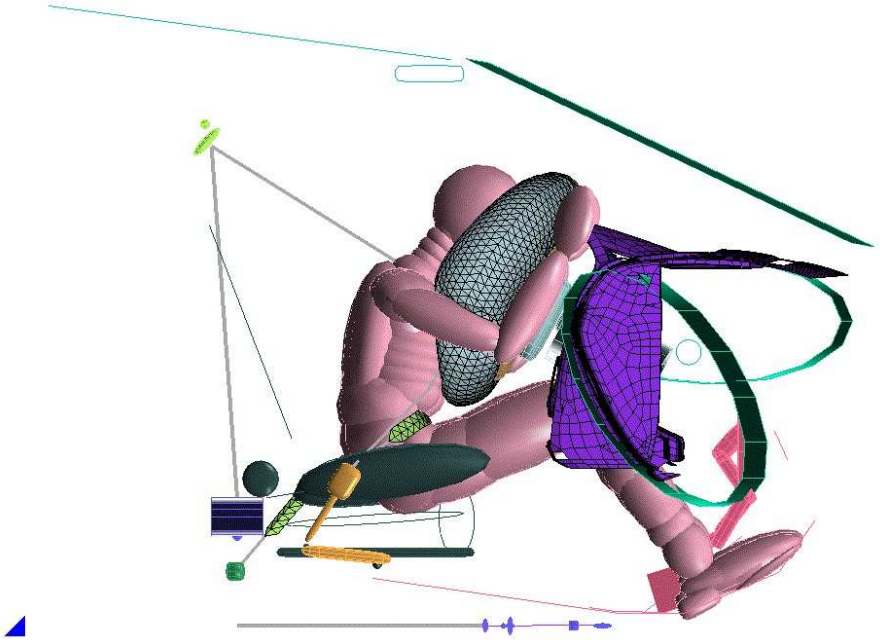

Figure 4.17. Dummy position at 80 ms, tighter lap belt coefficients

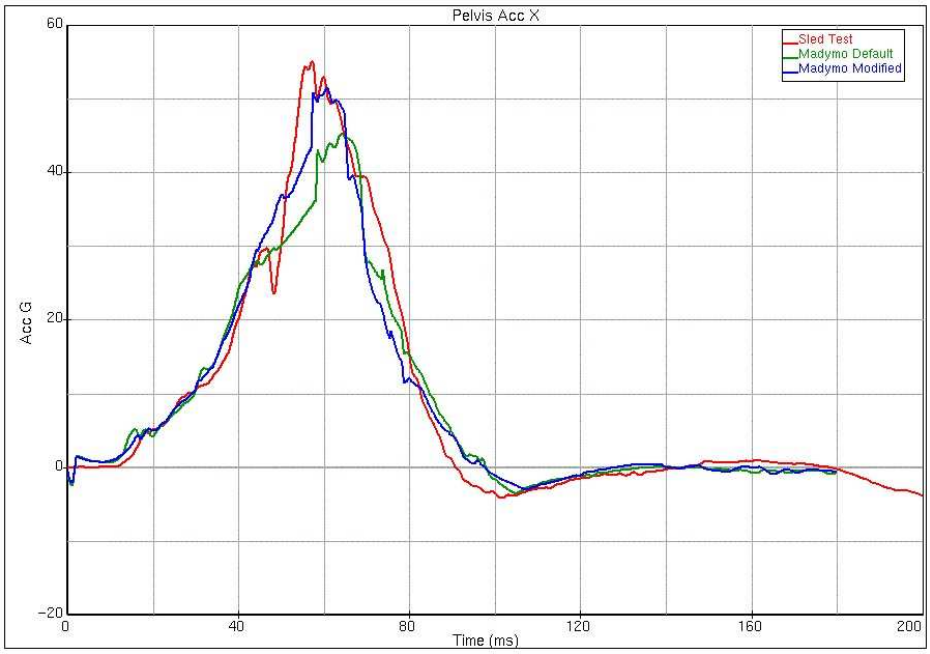

Figure 4.18. Pelvis x-dir accelerations

4.1.3. Knee Instrument Panel Impact Force

On the other hand, the lower portions of the dummy (knee, femur, tibia) are in contact with the instrument panel (IP) and the default instrument panel contact characteristic was used to define the relationship between the knee, femur, tibia and IP interactions. The default characteristics were measured by applying dummy knee to a smooth instrument panel surface. However, in the vehicle instrument panel there is a pocket on the instrument panel under the steering wheel adding stiffness to the instrument panel at the knee impact zone. (See Figure 4.19) The pocket could not be modeled and ignored because modeling of such a geometric detail in Madymo is not easy and requires many ellipsoids to define the geometry. And the existence of many ellipsoids in contact brings difficulties in contact force calculations. Therefore first shot results of femur forces calculated in Madymo were lower than femur forces measured in sled test. (0,817 vs. 1,28 for femur right and 0,964 vs. 1,548 kN for femur left) A set of different contact characteristic functions were defined for the knee instrument panel contact force until the femur forces correlated with the femur forces from sled test data. (Figure 4.20)

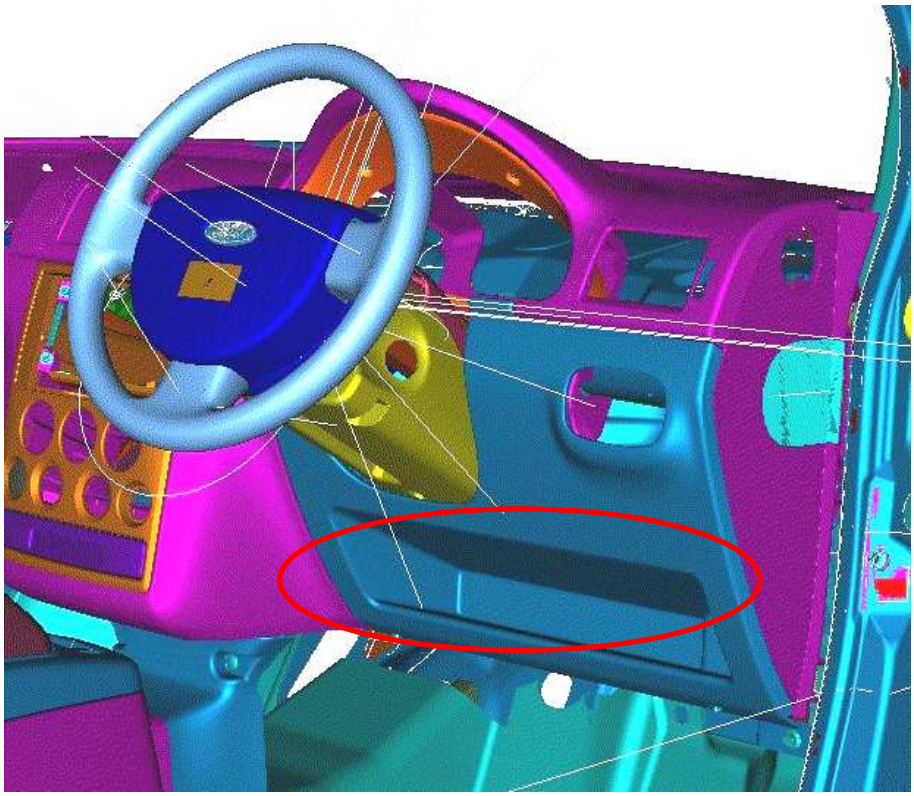

Figure 4.19. Pocket on instrument panel stiffening the knee impact zone

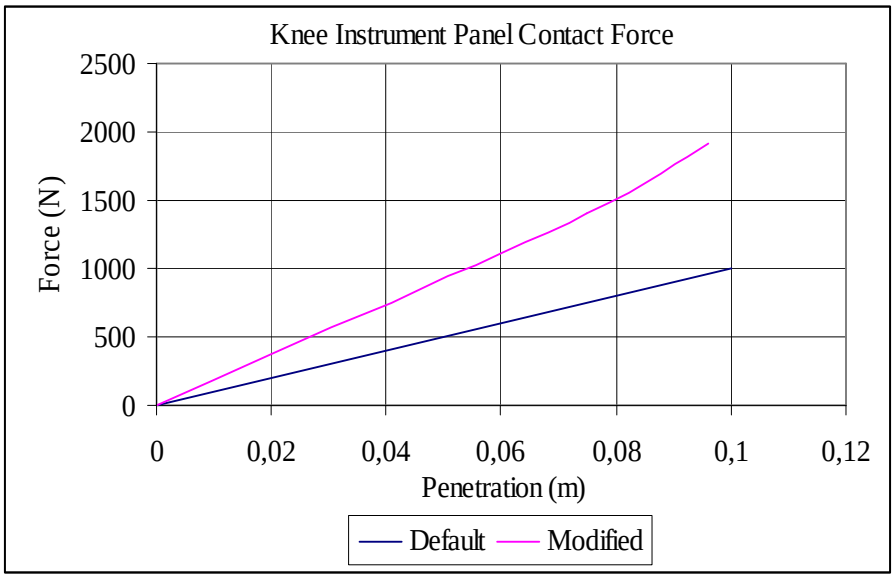

Figure 4.20. Knee instrument panel contact force

With the above modifications a better correlation between the sled test and Madymo simulations were achieved. Final status of the Madymo simulation results vs. sled test results are shown in Figure 4.21 to Figure 4.24.

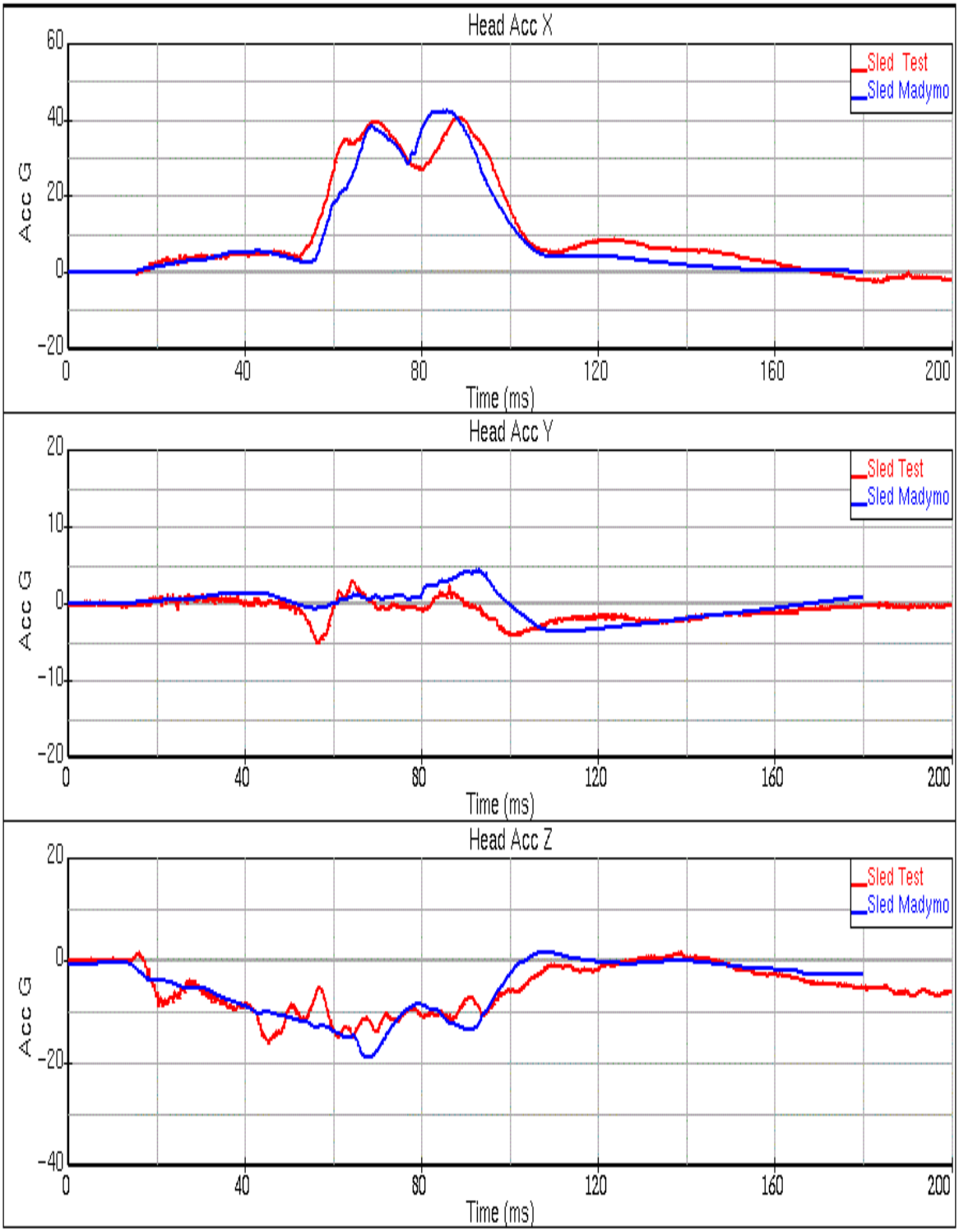

Figure 4.21. Sled test vs Madymo, head x, y and z accelerations comparison

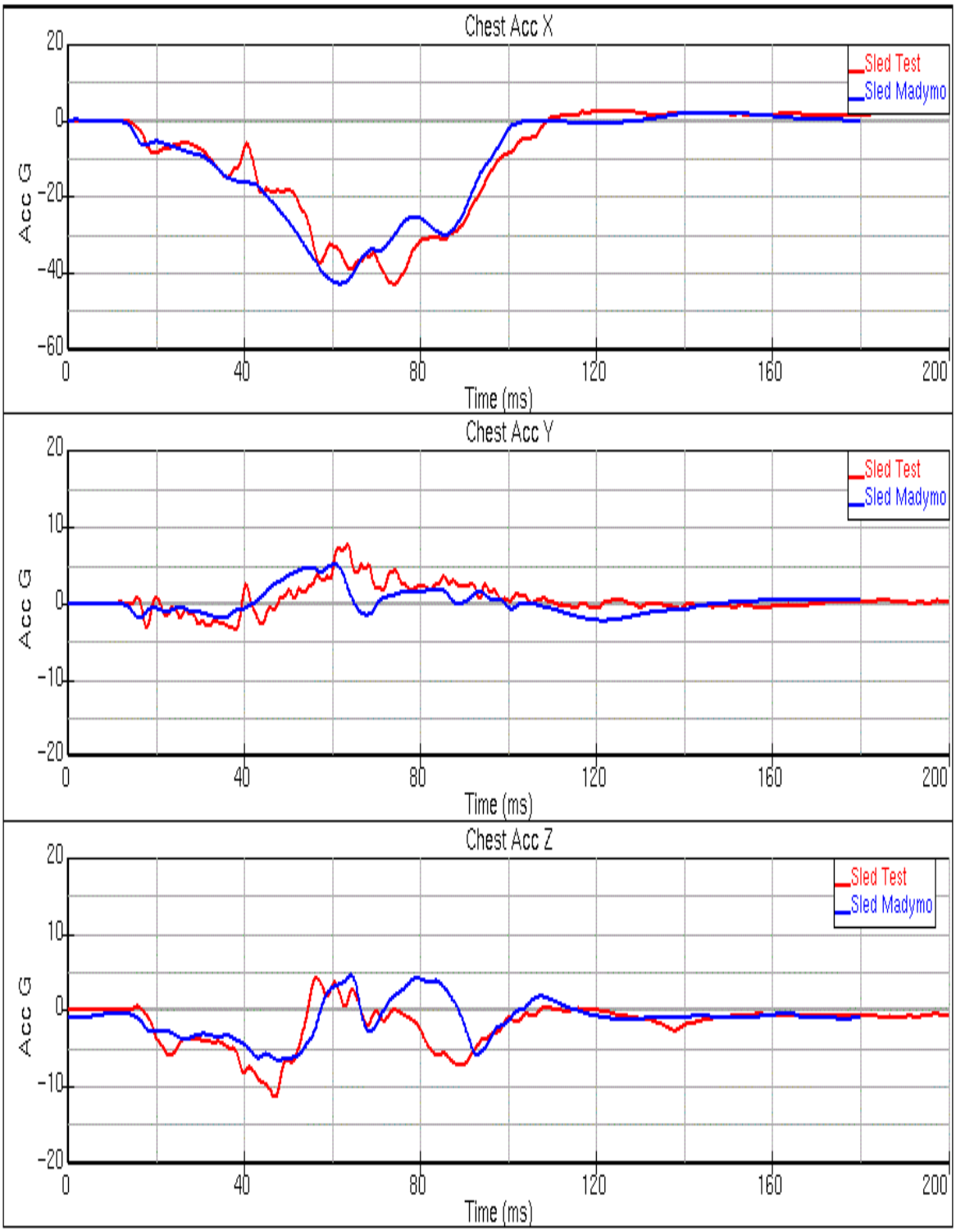

Figure 4.22. Sled test vs Madymo, chest x, y and z accelerations comparison

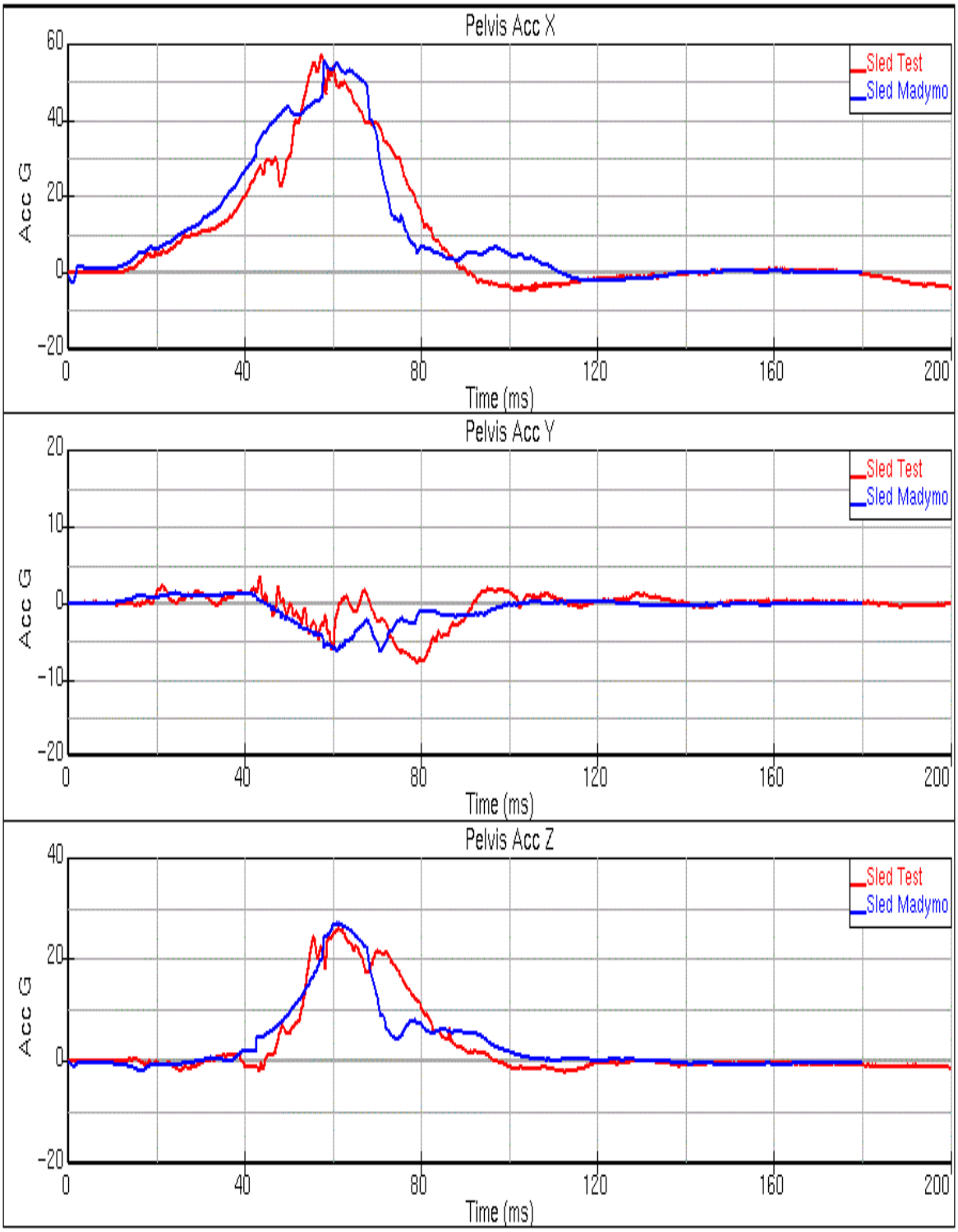

Figure 4.23. Sled test vs Madymo, pelvis x, y and z accelerations comparison

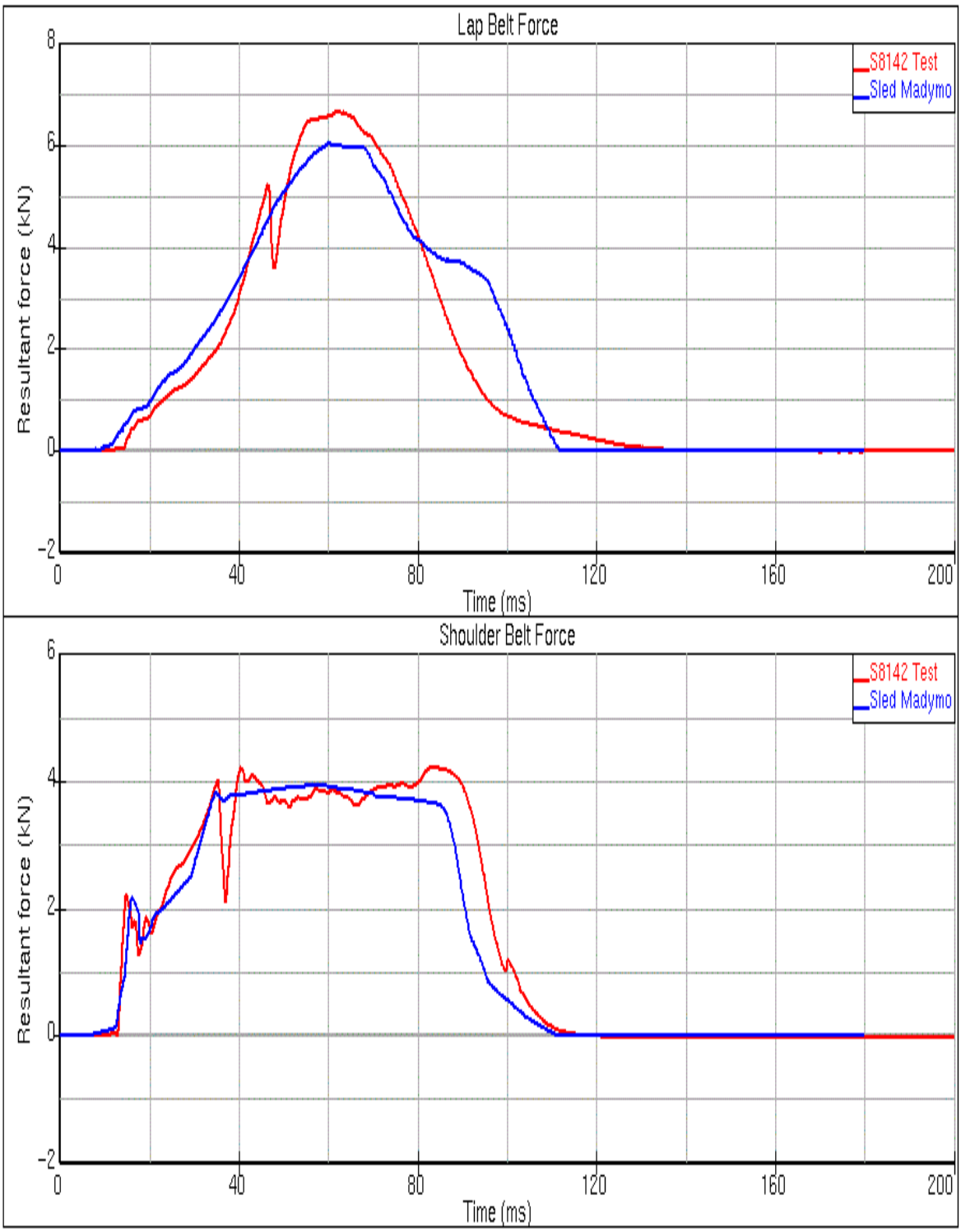

Figure 4.24. Sled test vs Madymo simulation, lap and shoulder belt forces comparison

5. FINITE ELEMENT MODEL DESCRIPTION AND RESULTS

The simulation of a real crash test (Figure 5.1) contains additional difficulties compared to a sled test. In a sled test, the buck undergoes no deformation. The airbag, safety belt, seat and steering column data are all derived from tests that have similar test conditions to the sled test. The dummy used in the Madymo analysis is also validated by the software's vendor, *TNO*, with many tests [15]. Therefore, the contact interactions between the dummy and surrounding parts are all well defined and similar results are achieved at the end.

Figure 5.1. Front offset impact test setup for a light commercial vehicle hitting a deformable barrier at a speed of 56 km/h

However, in a real crash test, vehicle undergoes deformation. The dash, pedalbox, instrument panel and floor pan intrudes into the driver survival space. On the other hand, seat and steering column are also not stationary and they also deform during crash. Ignoring these effects, a good correlation between dummy results from a physical test and

Madymo analysis can not be achieved. The contact between the knee and instrument panel may occur earlier than calculated by Madymo because the intrusion is not defined or airbag inflation may be different than actual because the steering column rotation is not included.

Tracking the motion of these items during crash needs more instrumentation on the vehicle, i.e. accelerometers on the instrument panel, pedals, seat and steering wheel. This is not favored because instrumentation on these components may lead to unrealistic contact between these components and the dummy. Unrealistic results may occur, i.e. a spike on the femur force due to an accelerometer on the instrument panel. Instead, results from a finite element analysis may be used to define intrusions and motion of these parts inside the vehicle. The motion of these parts can be monitored in a finite element analysis and the motion monitored can be assigned to these parts in Madymo as prescribed motion. However, to do that, the overall vehicle behavior in the finite element analysis and the physical test should be similar.

As mentioned above, the tracking of items inside the vehicle is not favored during the test. Therefore, post-crash deformation values measured after the physical test is compared with the results of the finite element analysis. The items that will be checked are shown in Figure 5.2 to Figure 5.5;

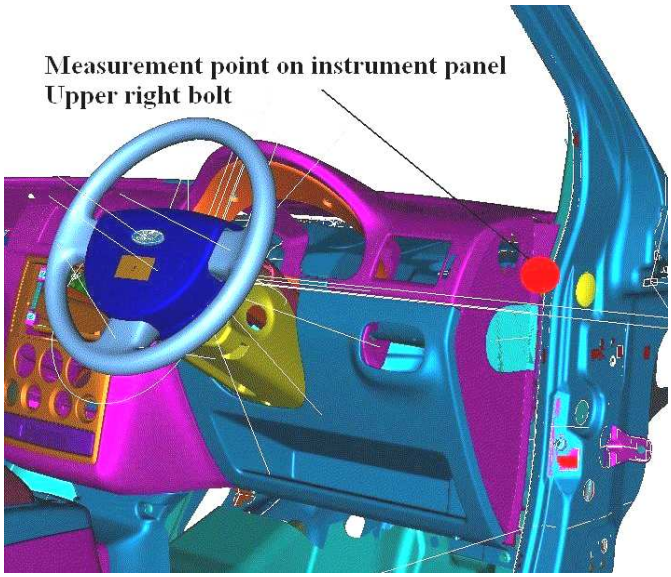

Figure 5.2. Instrument panel upper right attachment point x, y, z deformations

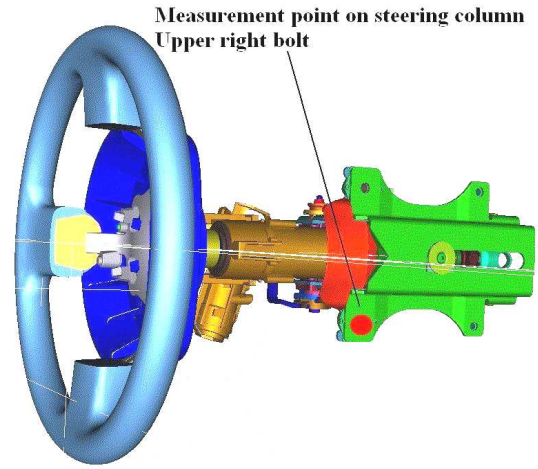

Figure 5.3. Steering column upper right attachment point x, y, z deformations

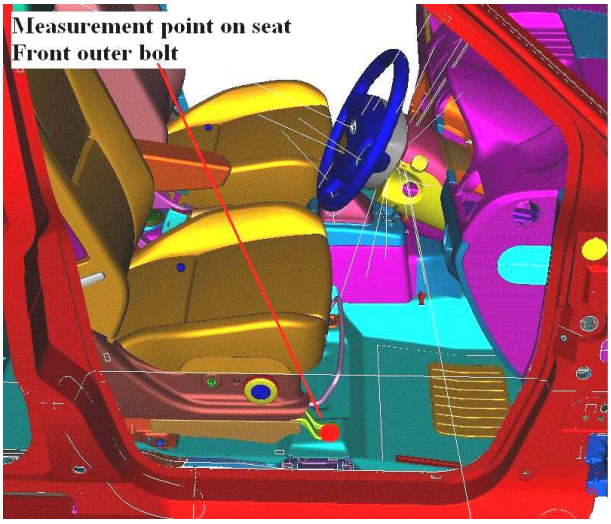

Figure 5.4. Seat front outer attachment to floor pan x, y, z deformations

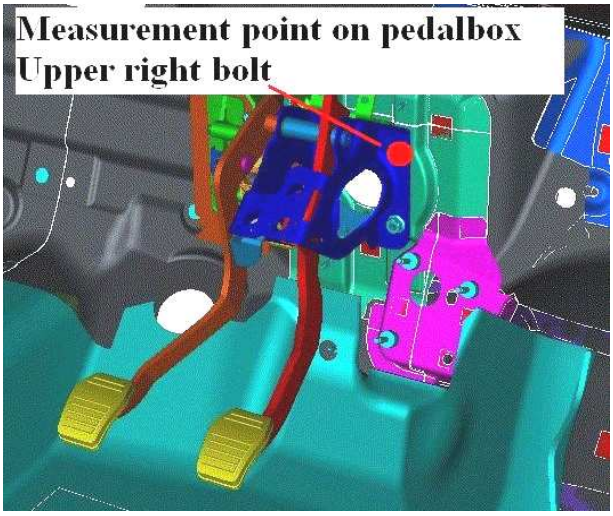

Figure 5.5. Pedalbox upper right attachment x, y, z deformations

Correlation of the items above may not be a good indication of these items behavior during crash. The deformation of these items in the end may be the same but the deformation behavior through the crash may be different. This may lead to wrong estimations of vehicle behavior from the beginning to the end of the crash. So it is important to see that the vehicle in a physical test and the vehicle in the finite element model decelerate in a similar way. This is achieved by comparing the pulses measured at the b-pillar lower ends of the vehicle. The accelerometer location is shown in Figure 5.6 in more detail. Similar accelerometer is placed on vehicle left hand side as well. The accelerometer locations chosen on the vehicle are at regions where there is negligible deformation of the structure and are a good indication of the deceleration the dummy is subject to during crash. Therefore, in addition to the post crash displacements, pulses measured at the LH and RH b-pillar lower ends should also be similar for a better correlation.

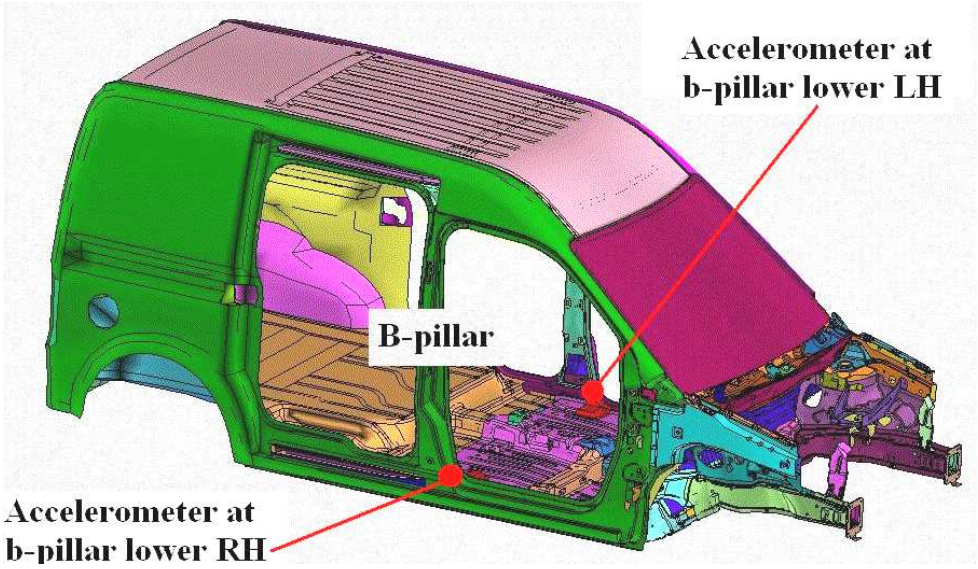

Figure 5.6. Accelerometer location at b-pillar lower right hand side

5.1. Finite Element Model Description

The finite element model represents a right hand drive light commercial vehicle's ECE94 56 km/h front offset impact test. The test is performed by crashing the vehicle into a stationary deformable barrier at a velocity of 56 km/h. The vehicle includes the driver and passenger dummies and mass of the vehicle is balanced to match the mass of a

production level vehicle with full option (all accessories) and with allowed maximum luggage. Data is collected through the test from the dummy and the passenger. Collected data are later processed and criteria mentioned in injury parameters section are calculated.

The finite element model shown in Figure 5.7 and Figure 5.8 is generated using *Altair Hypermesh* and *Mecalog M-Crash* [23, 24]. The model contains around 398672 nodes and 402274 elements, containing 2392032 degrees of freedom. All structural parts are modeled as surfaces consisting of triangular and quadrilateral shell elements. The spotwelds, bolts and adhesives that are connecting parts are modeled using beams or spring type 1-D elements. The model does not contain the driver and passenger dummy but their masses are distributed over the seat structure and included in the vehicle mass.

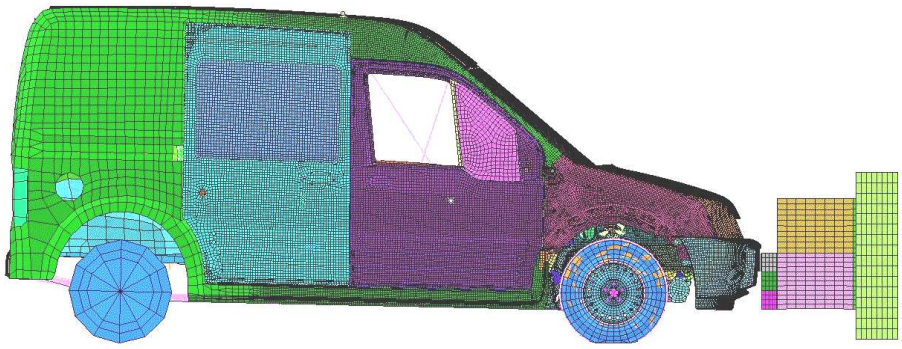

Figure 5.7. Finite element model side view

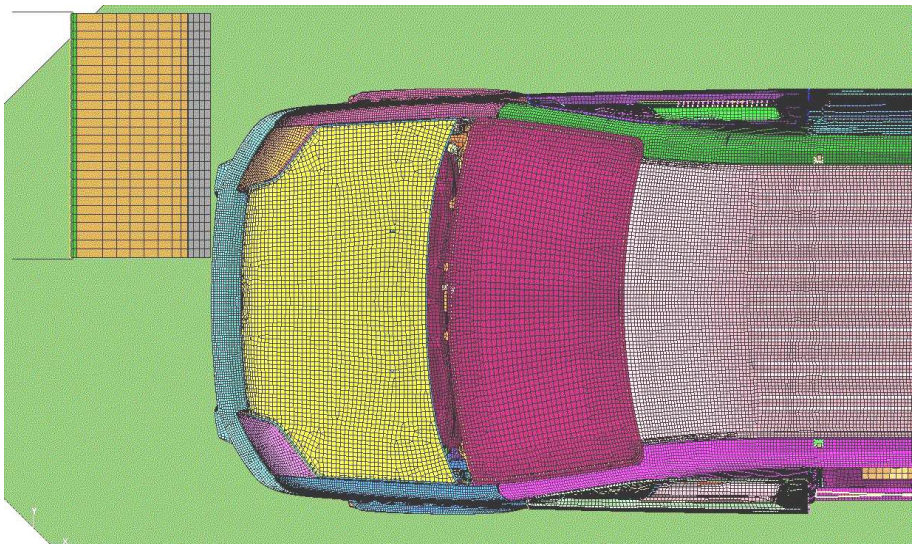

Figure 5.8. Finite element model top view

5.1.1. Modeling of Structural Items

All structural components of the vehicle absorbing energy (body, suspension, engine, doors) are modeled in detail as shown in Figure 5.9. Other items, which absorb negligible energy but have a mass effect like the hood, bumper, fender, cooling pack are also included in the model to catch the best correlation with the physical test. For 2D elements, element size chosen to model the front structure parts changes between 8-10 mm. No element smaller than 4 mm is used to avoid a small time step. Element size increases gradually to the rear of the front side doors and at vehicle rear an element size of 50 mm is used. Components at vehicle rear like rear suspension, fuel tank, rear wheels are not modeled in detail. This is done to reduce the total number of elements and to save from the computation time.

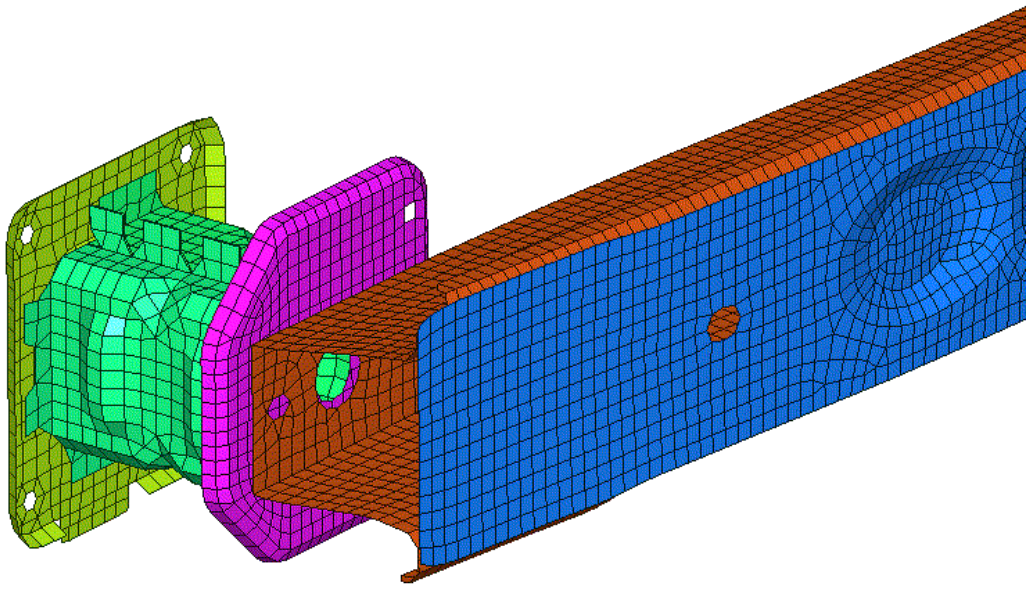

Figure 5.9. Finite element mesh in detail, bumper beam and crash can

In a front offset impact, vehicle parts especially parts in the front structure experience big deformations and strain-hardening behavior of materials become a major factor in the parts' structural response. A proper description of the strain hardening at large plastic strains is needed. For many plasticity problems, the hardening behavior of the material can be characterized by the strain-stress curve of the material. For proportional

loading cases like the case in a frontal impact this may be done but in cases where there are combined loadings this is no longer adequate.

From many of the material models offered by *Radioss*, Johnson-Cook plasticity model is chosen. [25] In this model, the material behaves as linear elastic when the equivalent stress is lower than the yield stress. For higher values of stress, the material behavior is plastic. The model is applicable to brick, shell, truss and beam element types in *Radioss*. The equation defining the relation between equivalent stress and the corresponding plastic deformation is given as:

$$\sigma = \left(a + b\varepsilon_p^n\right)\left(1 + c\ln\frac{\dot{\varepsilon}}{\dot{\varepsilon}_0}\right)\left(1 - T^{*m}\right) \tag{5.1}$$

where:

σ = Flow Stress (Elastic + Plastic Components)

ε_p= Plastic Strain (True Strain)

a = Yield Stress

b = Hardening Modulus

n = Hardening Exponent

c = Strain Rate Coefficient

$\dot{\varepsilon}$ = Strain Rate

$\dot{\varepsilon}_0$ = Reference Strain Rate

m = Temperature exponent

$$T^* = \frac{T - 298}{T_{melt} - 298}$$

where T_{melt} is the melting temperature in Kelvin degrees. However, this factor is usually omitted in the equation assuming a room temperature of 25ºC for the analysis.

In Figure 5.10 stress-strain curve for the Johnson-Cook material law is shown. On the curve, when the maximum stress is reached, the stress remains constant and material undergoes deformation until the maximum plastic strain. Element rupture occurs if the plastic strain is larger than ε_{max}. The rupture is simulated by deleting the element that reached the maximum plastic strain.

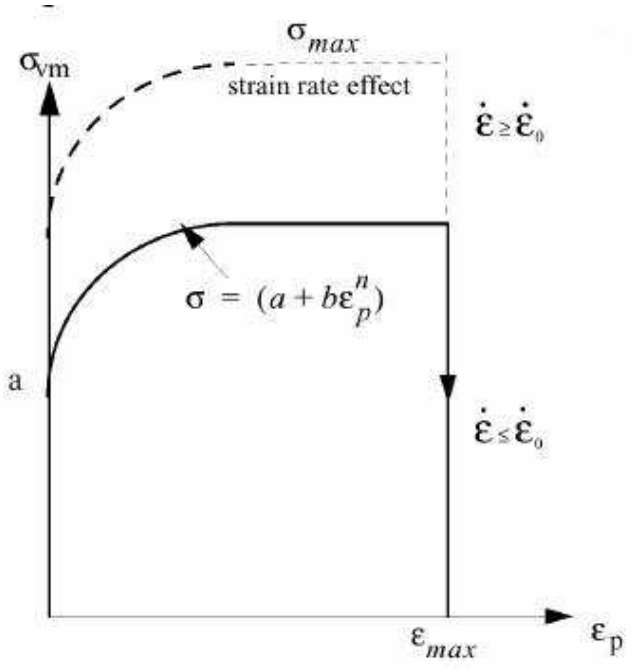

Figure 5.10. Stress vs plastic strain curve

For steel structures in the model, generic material data from suppliers were used initially. The data is listed Table 5.1. However, post crash measurements from the test and finite element model were not similar. Vehicle's test performance was better compared to the finite element simulation. A detailed investigation on the model showed that parts were absorbing less energy in the finite element model. This was due to using the generic material data and ignoring deep drawing effects. The generic data supplied is obtained through specimens from sheet metals from which the parts are drawn and this data is assigned to the parts. However, during the drawing process parts undergo strain hardening and the coefficients in Table 5.1 are no longer valid for these parts.

Table 5.1. Generic material data from suppliers

Steel	A	B	n	C	$\dot{\varepsilon}_0$
Mild steel	0.170	0.196	0.45	0.0683	1×10^{-6}
ZSTE180	0.218	0.334	0.45	0.0265	1×10^{-6}
ZSTE220	0.258	0.334	0.45	0.0265	1×10^{-6}
ZSTE260	0.287	0.400	0.50	0.0265	1×10^{-6}
ZSTE300	0.332	0.468	0.64	0.0275	1×10^{-6}
ZSTE340	0.363	0.482	0.70	0.0295	1×10^{-6}
ZSTE380	0.389	0.482	0.70	0.0295	1×10^{-6}
ZSTE420	0.429	0.638	0.57	0.0209	1×10^{-6}
DP600	0.640	2.000	0.80	0.0200	1×10^{-3}
DP800	0.800	0.671	0.25	0.0200	1×10^{-3}
BORON	1.113	9.402	0.93	0.0200	1×10^{-3}

A study was performed to see the effect of deep drawing on stress-strain curve. Test post-crash pictures and *Radioss* animations were investigated to define the critical parts in crash. These parts are shown (highlighted in blue) in Figure 5.11) and these parts create the major load path on the vehicle starting from the crash cans at the front and ending with longitudinal rails at the center of the vehicle. Specimens were extracted from these parts and subjected to tensile testing. The specimens extracted from one of these components (right hand side inner side rail) and the measured yield stress values during tensile test are shown in Figure 5.12.

The material for inner side rails is ZSTE340. Looking at Table 5.1 the yield stress for the material is 0.363 for a specimen cut out from sheet metal. However, tensile test results showed that yield stress value for inner side rail is around 0.48. The actual value is much higher and the difference between the supplied data and actual data caused the difference in post-crash displacements between the finite element model and the physical test. Similarly, material data for the other critical parts were also updated and analysis was rerun. Vehicle post-crash displacements decreased and a better correlation between the test and analysis was achieved.

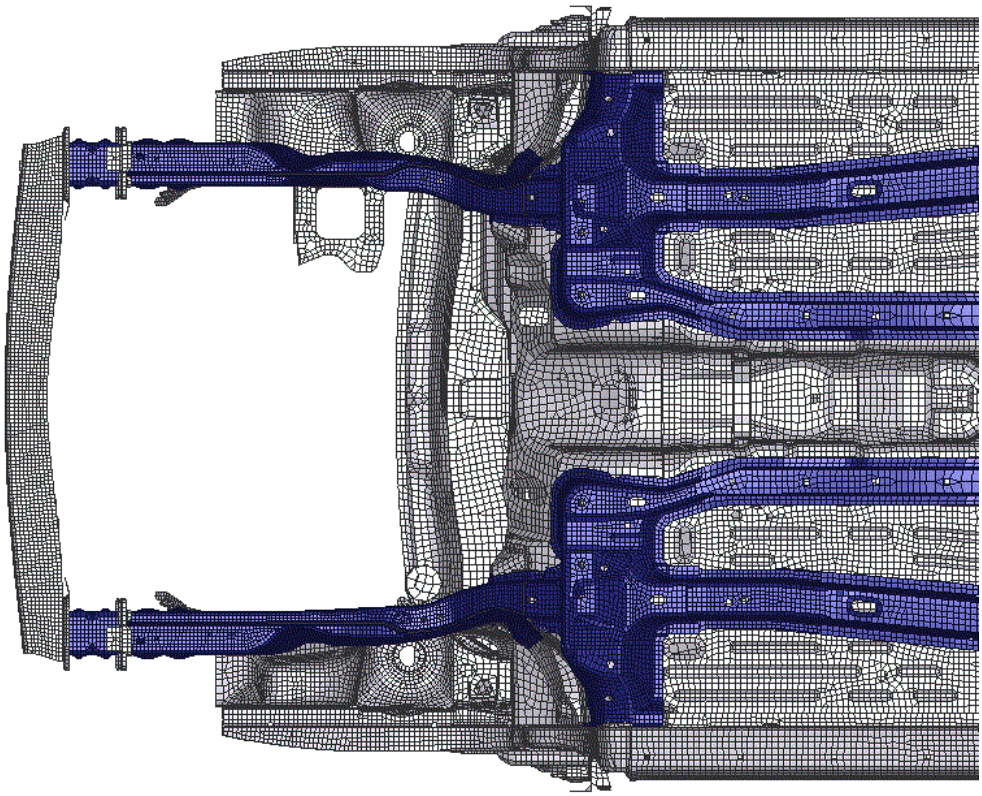

Figure 5.11. Critical parts playing an important role in front offset crash

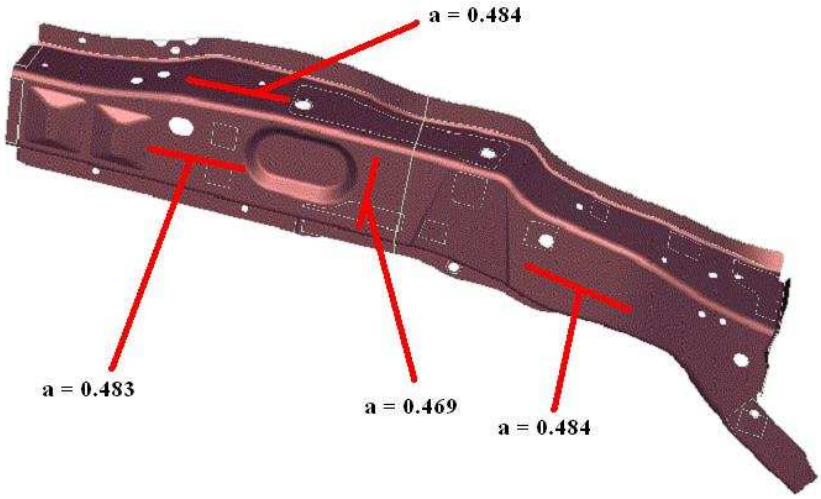

Figure 5.12. Specimen locations on inner side rail and corresponding yield stress values

5.1.2. Modeling of Deformable Barrier

Full front impact test purpose is to simulate a vehicle's crash into a rigid wall while front offset deformable barrier impact test purpose is to simulate a vehicle to vehicle crash condition. To simulate the vehicle crashed into deformable barriers are used. Dimensions and structure of a deformable barrier is shown in Figure 5.13 [2].

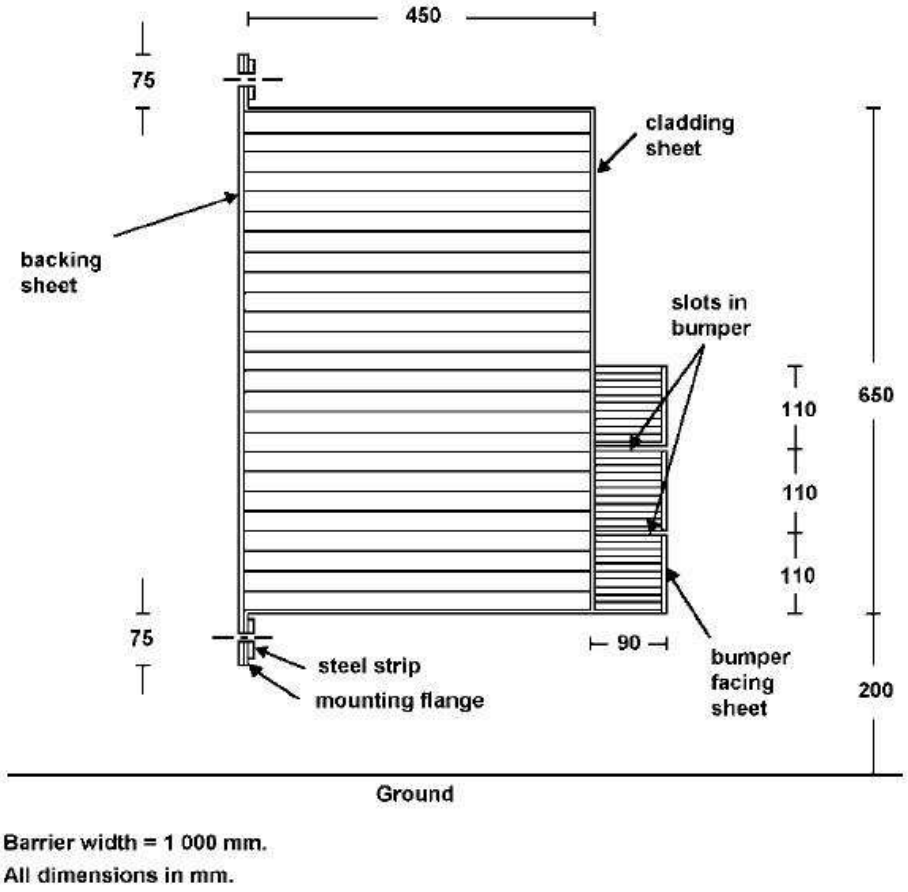

Figure 5.13. Deformable barrier for ECE94 test [2]

The deformable barrier consists of honeycombs cladded in sheets. The main part consists of aluminum honeycombs 19.1mm in size. The smaller part in front, known as the bumper honeycomb consists of smaller size aluminum honeycombs (6.4 mm in size) Smaller size honeycombs at front makes this part stiffer compared to the rear. The stiffer honeycomb facing the crashing vehicle's bumper enables a better representation of the crashed vehicle's structure. Both structures are cladded in aluminum sheets and glued to each other by structural adhesives (polyurethane) to maintain the barrier's integrity during crash.

The deformable barrier used in the analysis is obtained from the *Mecalog M-Crash* database (Figure 5.13) [23]. In this model, the barrier's aluminum honeycombs are simulated with solid elements instead of using shell elements to define the honeycomb geometry. This is due to the fact that during crash aluminum honeycombs experience a large deformation and modeling the honeycombs with shell elements result in hourglass problems. Excessive hourglass energy is generated to account for the large deformation and barrier behaves stiffer than it is in actual.

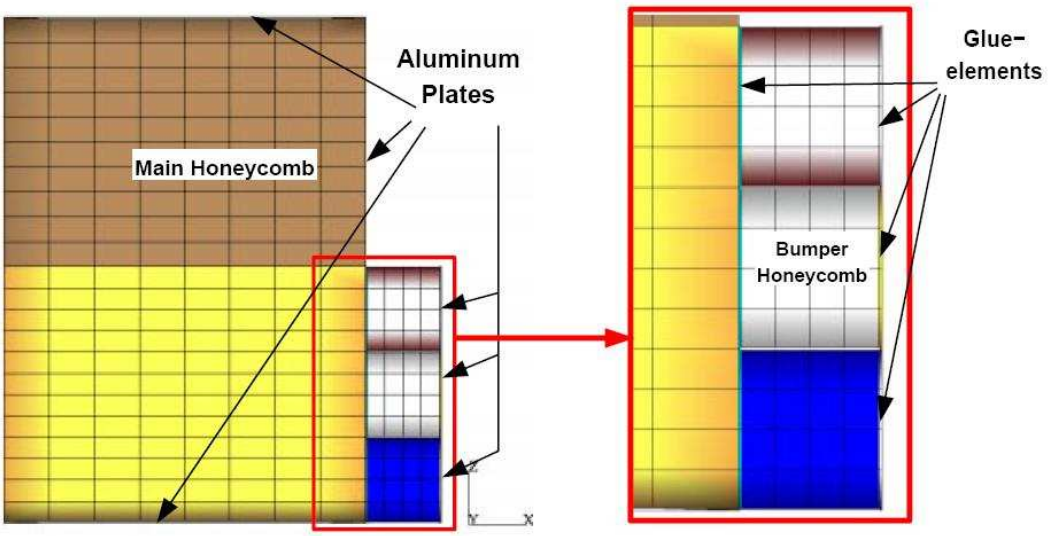

Figure 5.14. Deformable barrier finite element model

Modeling of aluminum honeycombs with solid elements causes extra difficulties as well. The barrier deformation is large and zero or negative volume 3D solid elements are formed during analysis stopping the analysis. To avoid this, *Radioss* developed small-strain option for 3D solid elements to simulate the crushed honeycomb. With the small strain option negative or zero volume elements are avoided. Also small time steps due to large element contractions are also prevented. It may be unusual to use small-strain option for a large deformation case, but small strain option offers a better solution than element deletion to avoid zero or negative volume elements. On the other hand, because honeycomb material has no Poisson effect the small strain limitation is corrected by an appropriate stress strain curve.

5.1.3. Modeling of Tyres

Tyres play a major role in frontal crash because they are on one of the major load paths to the rear of the vehicle. The main load path on the vehicle is the front end structure side rails. The deformation and load absorbing capacity of the side rails determine other important parameters like dash, pedalbox and steering column intrusions which directly effect dummy kinematics. The front tyres create the second load path acting as a linkage between vehicle rockers below the front side doors and deformable barrier. The more load transferred on the tyres to the vehicle, the less will be the side rail deformation, therefore the intrusions inside the driver compartment. Therefore a correct modeling of front tyres needs to be built to have a correct representation of the driver compartment intrusions.

Tyre parts are modeled with three different modeling schemes in *Radioss* as shown in Figure 5.15. Tyre outer (rubber part) and tyre rim is modeled with quadrilateral shell elements. The appropriate rubber and rim material data and thicknesses are assigned to the shell elements. Tyre radial cords are simulated with beam elements created between the shell elements nodes on the rubber part. The last part to model is the air inside the tyre. The air is modeled with the monitored volume option of *Radioss* [25].

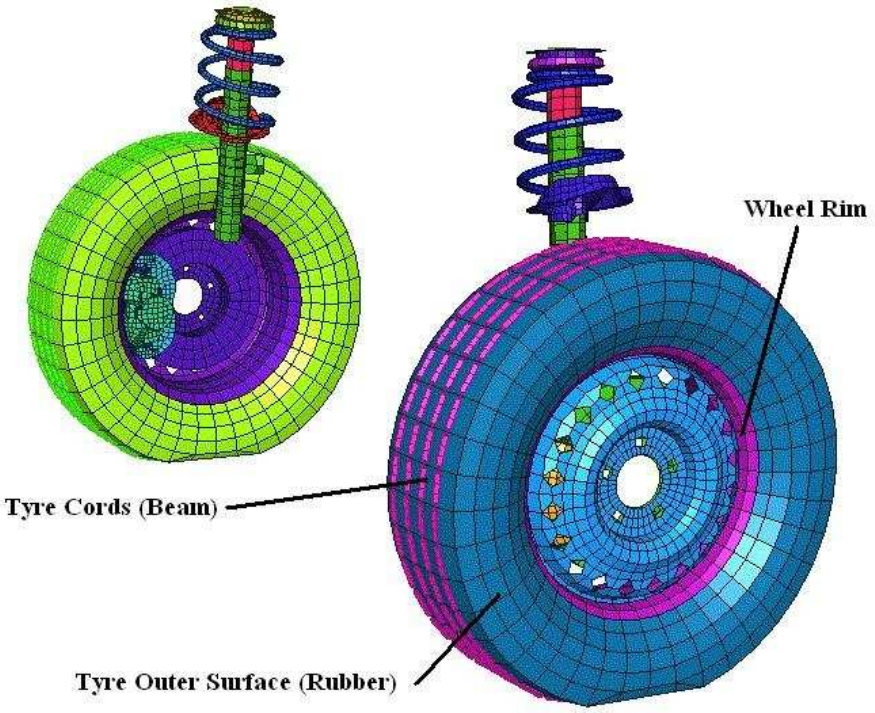

Figure 5.15. Tyre finite element model

Monitored volumes are defined inside closed volumes. In the tyre model, the rubber part and the tyre rim creates the closed volume needed to define the monitored volume. Once the monitored volume is defined *Radioss* solves the general gas equation to calculate the pressure inside the tyre.

$$P\upsilon = RT \tag{5.2}$$

where P is tyre pressure, v is specific volume, R is gas constant and T is ambient temperature. R and T are constant for the crash simulation therefore tyre pressure and volume at any time step t, during an analysis can be calculated from:

$$P_0 * V_0 = P_t * V_t \tag{5.3}$$

where P_0 is initial tyre pressure, V_0 is initial tyre volume and P_t and V_t are pressure and volume values at time step t. P_t increases as tyre is squeezed during crash and an

equivalent force, P_t times element area on tyre outer surface, is generated to react the loads from the barrier.

5.2. Crash Test and Finite Element Model Results

To perform the analysis an initial velocity of 15.66 m/s in negative x direction is applied to all the nodes on vehicle. Deformable barrier steel plate at the back is constrained in all six degrees of freedom to simulate a rigid wall. Vehicle bumper and barrier are positioned so that at the first millisecond of the analysis bumper contacts the deformable barrier and crash begins. Analysis runs until vehicle springs back from the barrier after crash and stays still on the ground (200 milliseconds). Final displacements are calculated at the mentioned points on the model and the displacements are compared to post-crash measurements taken on the vehicle during real life crash tests. In Table 5.2 the lowest and highest values measured on vehicles in previous offset front crash tests (ECE94) are listed.

Table 5.2. Post crash measurements on vehicle

Bolt Location		Difference (in mm)		
		Δx	Δy	Δz
Instrument panel upper right	Lowest	15,7	1,9	-1,3
	Highest	38,6	14,8	-2,9
Steering column rear right	Lowest	9,5	-13,5	-21,3
	Highest	22,7	-7,5	-35,1
Seat front outer	Lowest	-0,1	-0,9	-2,6
	Highest	0,4	-1,7	-9,6
Pedalbox upper right	Lowest	113,5	-16,0	16,5
	Highest	124,4	-24,1	25,7

Below are listed the finite element results for the instrument panel and pedal box intrusions starting from Figure 5.16 to Figure 5.21. The results are compared against the highest and lowest post-crash displacements measured on the vehicles after ECE94 crash tests. As seen in these figures pedalbox post-crash intrusions are within the values measured during the tests. Instrument panel x and y direction intrusions are also within the test range but there is a small deviation in the z direction intrusion. When the dimensions

of the instrument panel are considered, instrument panel z direction intrusions are relatively small and a small deviation as in Figure 5.18 will not affect overall dummy behavior.

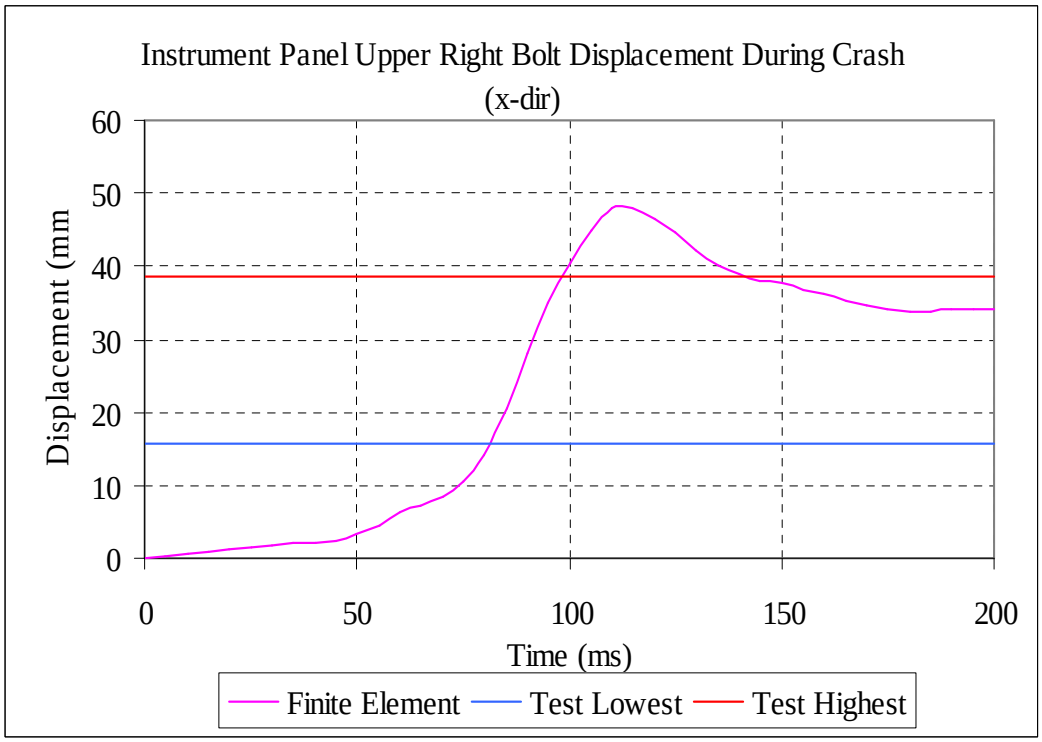

Figure 5.16. Instrument panel intrusion x-dir (FE vs.Test)

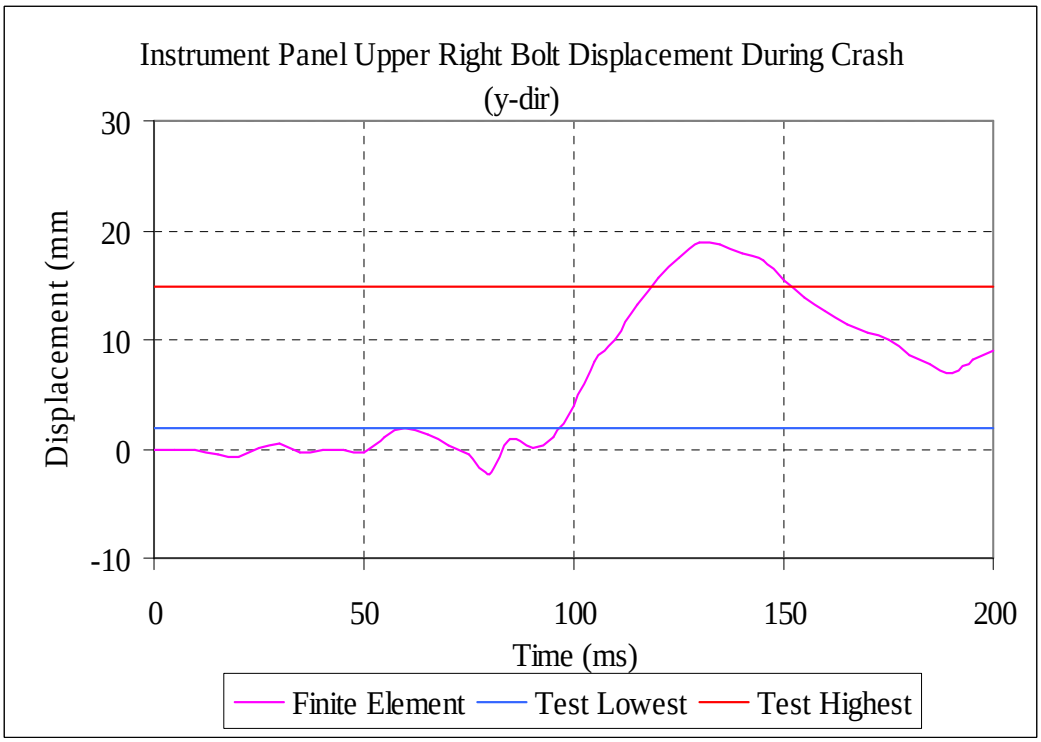

Figure 5.17. Instrument panel intrusion y-dir (FE vs.Test)

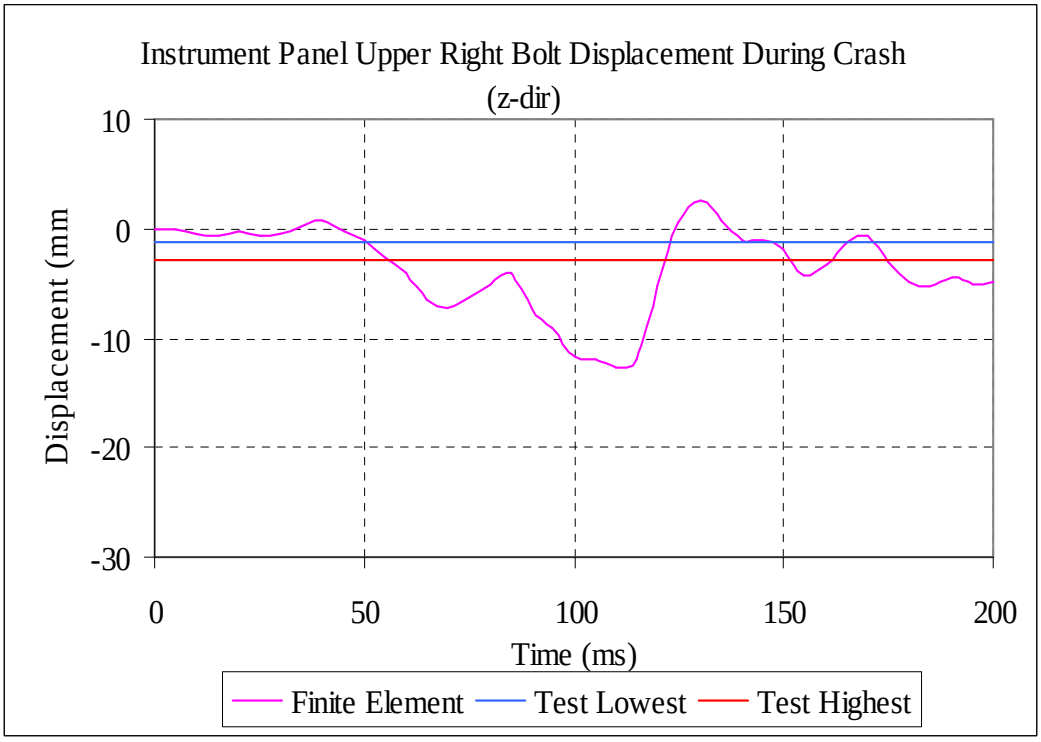

Figure 5.18. Instrument panel intrusion z-dir (FE vs.Test)

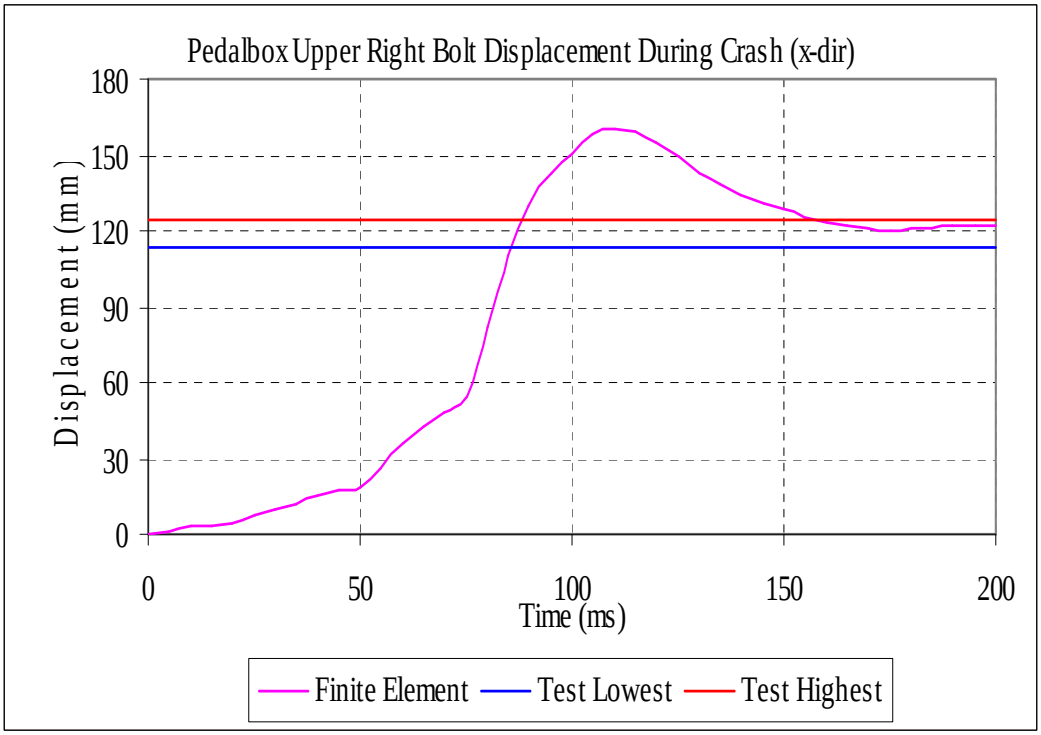

Figure 5.19. Pedalbox intrusion x-dir (FE vs.Test)

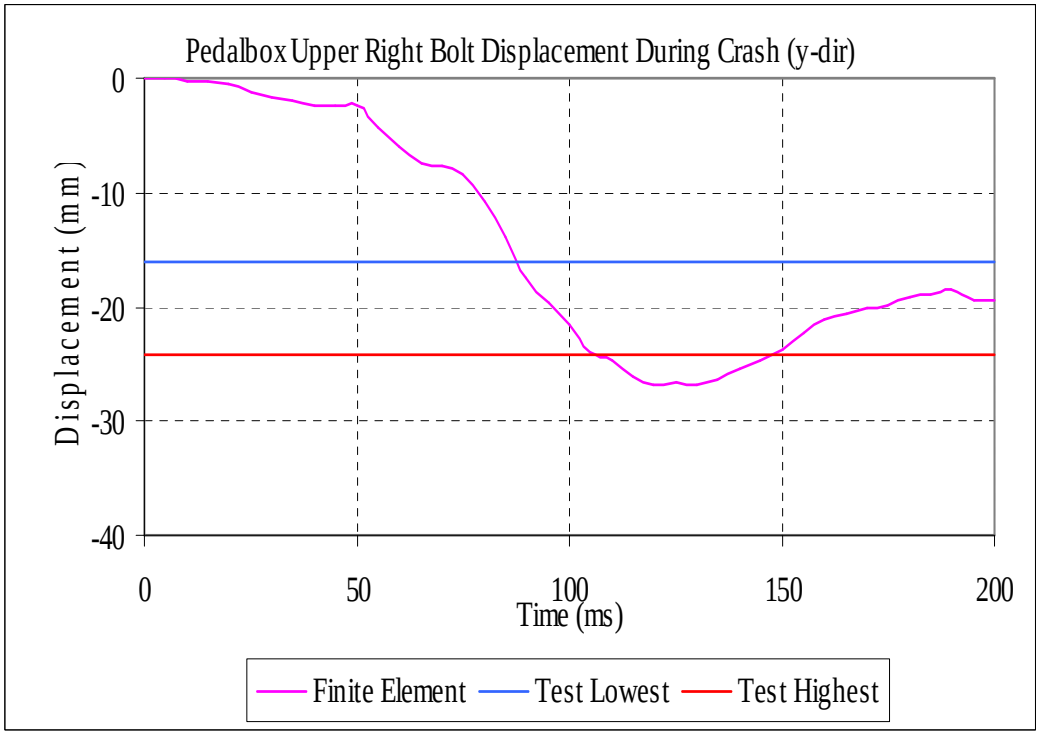

Figure 5.20. Pedalbox intrusion y-dir (FE vs.Test)

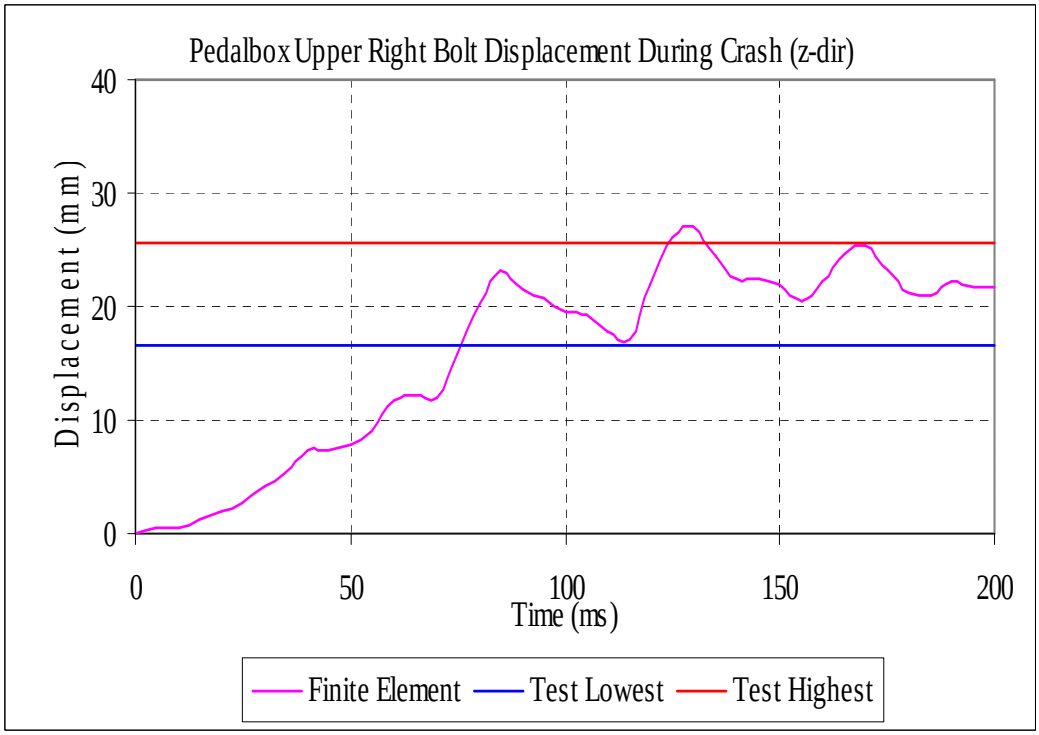

Figure 5.21. Pedalbox intrusion z-dir (FE vs.Test)

Similar to these figures, steering column and seat displacements are also measured on the finite element model. In finite element model, the steering column's ride down action is not included. 70 mm ride down effect is subtracted from final x direction intrusion and similarly, 34,9 mm is subtracted from final z direction intrusion. The calculated x-direction intrusion is 19,4 mm and z direction intrusion is –28,7 mm and these results are within the test range. For the seat motion, the measured x, y and z intrusions on the finite element model are 0,1, -0,4 and –4,8 mm and these are also within the test range.

In Figure 5.22 and Figure 5.23, pulses measured in the physical test and pulses calculated using finite element model are compared. A good correlation is achieved in maximum decelerations measured. This enables a better prediction of maximum head and chest accelerations. In b pillar lower right hand side pulses, between 75 and 85 ms there is a mismatch between the test and the finite element model. This is due to the rupture of the engine's attachment to the vehicle at 78 ms. The jump in the acceleration curve can not be modeled precisely due to the capability of the finite element model. In b pillar lower left hand side pulses, the curves are more similar except that the pulses from the finite element model has a 5 ms delay compared to the test pulses. This delay is expected to result in 5 ms

delays in the passenger head and chest peak accelerations. However, in the Madymo model, the passenger is not included and the delay has a negligible effect on driver accelerations.

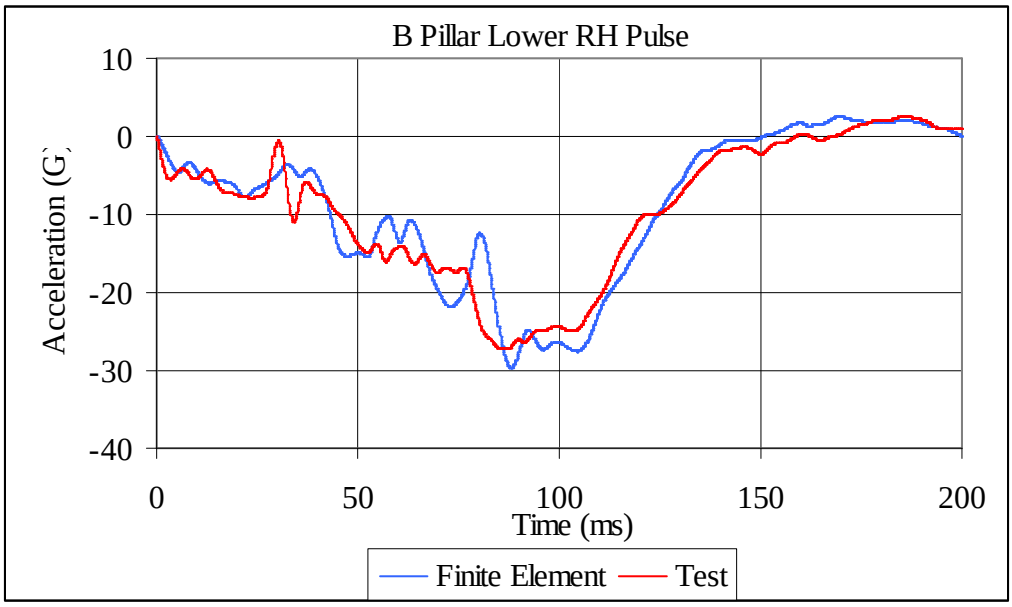

Figure 5.22. B-pillar lower RH pulse

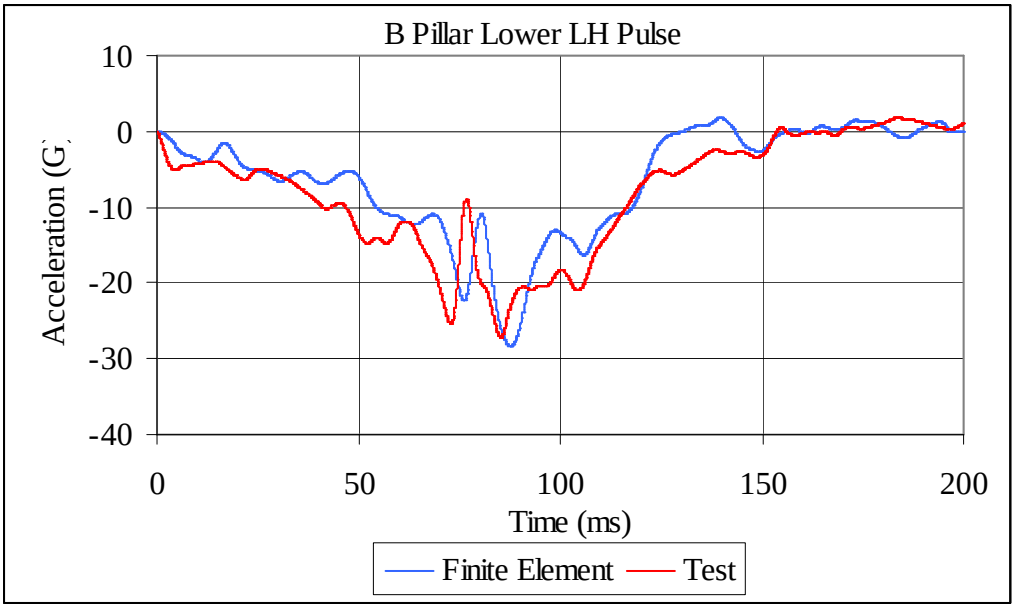

Figure 5.23. B-pillar lower LH pulse

According to the above results, the finite element model is considered to be in good correlation with the tests and the results of the finite element model can be used in Madymo as input functions. As a last additional subjective check, the physical test video and the finite element animations are visually compared. (Figure 5.24 and Figure 5.25)

Figure 5.24. Vehicle deformation during 56 km/h offset impact test, (t=150ms)

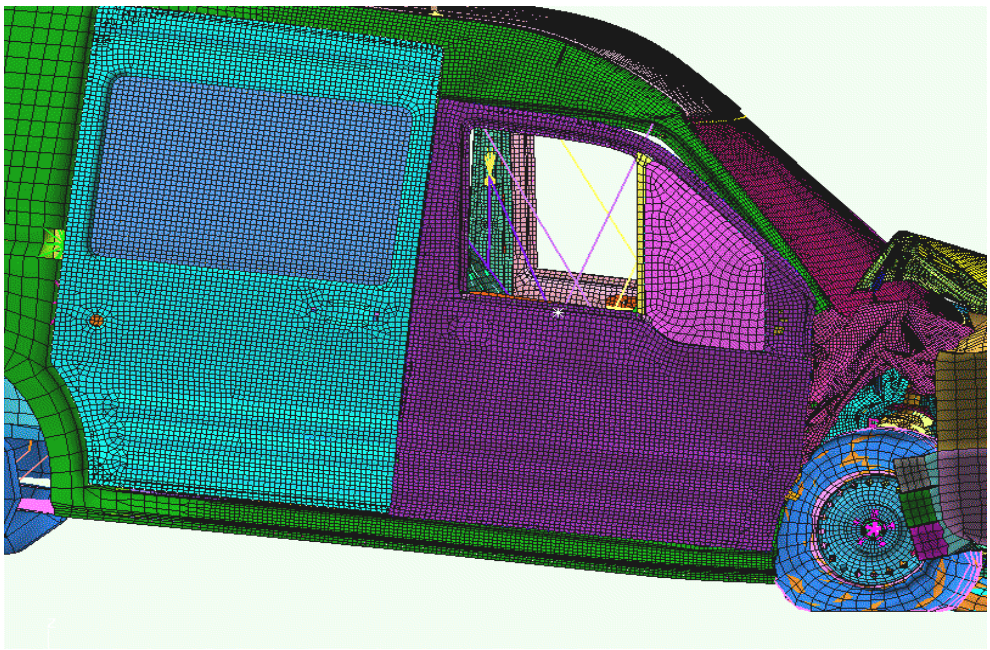

Figure 5.25. Vehicle deformation (finite element, t=150ms)

6. MADYMO SIMULATION OF CRASH TEST

6.1. Defining Initial Conditions for the Analyses

In a physical crash test, after hitting the rigid wall or deformable barrier, the vehicle decelerates. But the dummy continues its motion at vehicle crash speed and has a relative motion with respect to the vehicle during crash. This motion is restrained by the airbag, safety belt and seat systems during crash. In other words, during crash all systems decelerate at the same level with the vehicle, but dummy tries to continue his motion at the crash speed. This behavior of dummy has led to the acceleration driven Madymo initial condition specification.

In acceleration driven methodology vehicle interior is assumed stationary and subsystem intrusions are defined relative to their initial positions as prescribed motions assigned to the defining joints. And the vehicle deceleration pulse is inversed and the positive acceleration is assigned to the dummy as initial acceleration. This way, dummy's relative motion with respect to the vehicle interior is modeled and final dummy motion is determined by the restraint system. The methodology is very advantageous because it decreases the number of initial conditions for the analysis and usually successful in predicting the dummy behavior when there is a full front impact test.

But the restraint system design is predominantly driven by front offset impact test performance. Unlike full front impact tests, in offset tests vehicle motion cannot be considered to be unidirectional. Offset impact contains multidirectional motion in all directions also involving vehicle rotations. These rotations have a major effect on dummy behavior and the acceleration driven methodology is not suitable for offset front impact simulation. Instead, overall vehicle translations and rotations are derived from either finite element or from crash test data and the calculated motion is imposed to the whole vehicle subsystems except for the dummy. For the dummy, instead of the inverse acceleration the crash speed is assigned as the initial velocity.

6.1.1. Defining Global Vehicle Motion

To define the vehicle global motion, vehicle global x, y and z displacement data from an undeformed region of the vehicle (in this model, b-pillar lower and upper accelerometers) is transformed to local x, y and z displacements and x, y and z-axis rotations in the local coordinate system created at the accelerometers plane. The transformation is achieved by an internal Matlab code developed at Ford Motor Company. The transformed motion data is then assigned to the joint defining the plane as prescribed motion. The plane constructed for this purpose is shown in Figure 6.1 [26].

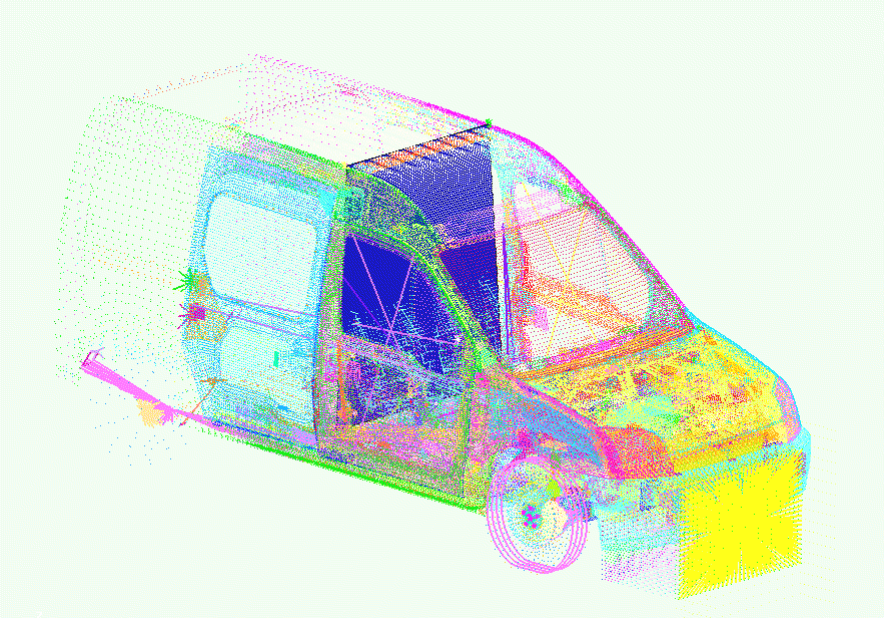

Figure 6.1. Plane constructed to define global vehicle motion

6.1.2. Defining Intrusions in Madymo

Subsystems in the vehicle deform or move during crash test and their motion should be included as input functions in Madymo. These subsystems are already constructed and contact characteristics are defined and correlated with sled test data but ignoring their intrusion or motion during crash causes unrealistic dummy behavior. For example ignoring instrument panel intrusion will result in less femur forces and ignoring steering column motion will result in incorrect airbag inflation and incorrect head and chest acceleration values. For the mentioned subsystems the geometries are all modeled as planes, ellipsoids

or cylinders and the nodal displacements of these components from FE model can not be inserted directly into Madymo model. A similar methodology like defining the vehicle global motion is used to include the motion of these subsystems in the model and planes are defined inside the FE model to monitor subsystem motion as shown in Figure 6.2 [26].

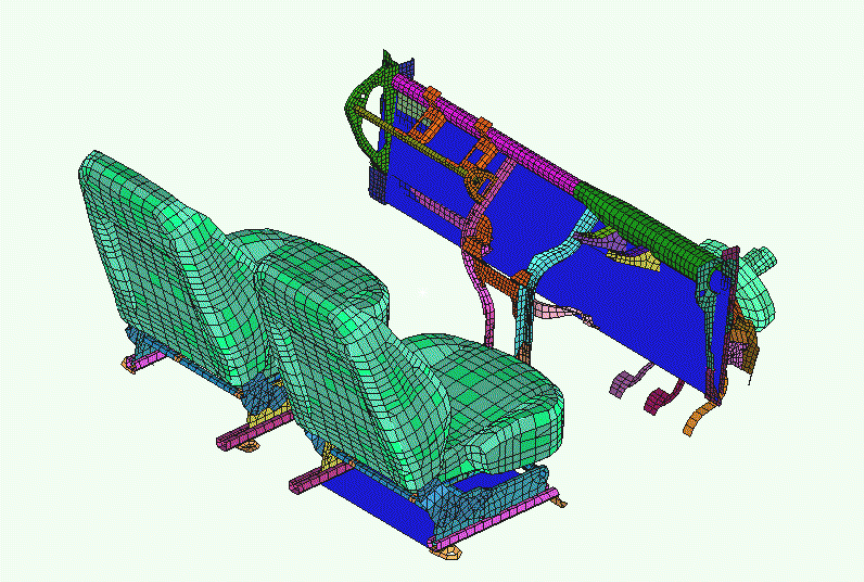

Figure 6.2. Planes defined for instrument panel, seat and steering column intrusion

Planes are created in the FE model as shown in the above picture and the global motion of these planes are extracted using the displacement values of the nodes the plane is attached to. The nodal displacements measured are all defined with respect to the planes defining the geometries and transferred into Madymo as translations and rotations.

The Cross Car Beam (CCB) shown in Figure 6.3 is one of the key components in the Madymo model. The instrument panel and the steering column are rigidly attached to the CCB and the motion of the mentioned components are driven by the CCB. The instrument panel is critical in femur forces. Steering column directly effects airbag and therefore head acceleration values and the steering wheel and airbag together effect chest behavior. Therefore a good representation of the CCB motion during crash is essential.

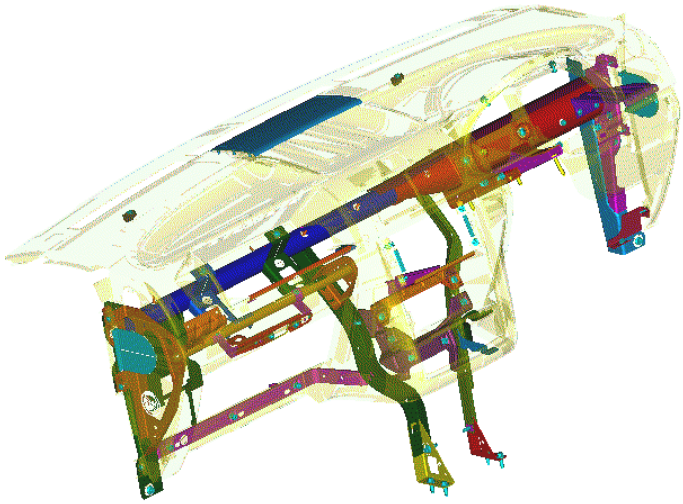

Figure 6.3. The instrument panel and the cross car beam structure

The CCB FE model is shown in Figure 6.4. In the finite element analyses, the instrument panel is usually not included and its mass is distributed over the CCB structure. This is due to the varying material properties of the instrument panel making it hard to model correctly and its negligible effect on vehicle crash performance. On the finite element model, the CCB attachment points to the vehicle body structure are used to define the CCB plane. The displacement of these points are added to the output file of the finite element analysis. After the analysis is complete, the output data is processed, and the input files for Madymo is generated. Generally, CCB motion is defined with respect to the local coordinate system created at the center of the plane constructed. The data input to Madymo is in terms of displacement vs. time and rotation vs. time. In this manner, the motion of the instrument panel and the steering column is described over the Cross Car Beam. Similarly by tracking the data at seat attachment points, seat motion and tracking the data at pedalbox attachment points pedalbox motion is incorporated into the Madymo model.

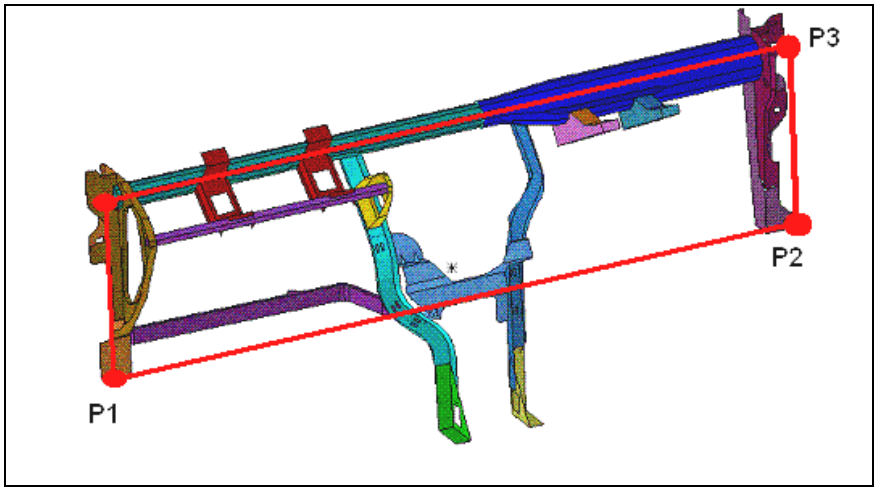

Figure 6.4. Cross car beam finite element model

After defining the vehicle global motion and intrusions, the model is updated to reflect the offset front impact test conditions. Following changes are made on the model.

- Test vehicle was a right hand drive vehicle, model was reflected about vehicle y=0 axis.
- Seat pan and cushion was raised 15 mm to seat mid-mid position from low-mid position
- Dummy was raised 15 mm for the new seat position.
- D-ring attachment point was lowered 45 mm from highest to lower position.
- Belt was rerouted according to the new dummy, d-ring and seat positions.
- Airbag firing and retractor pretensioner times were updated to 32 ms from 10 ms. The values are taken from the test.
- Steering column shroud and pedal contacts which were deleted in sled test were added to the model.

6.2. Results and Discussion

After setting the above mentioned initial and boundary conditions in the model the constructed model is run for 200 milliseconds. Results from Madymo simulation are compared with crash test results in Table 6.1.

Table 6.1. Front offset crash test and Madymo simulation comparison

		Test	Madymo	Limit Value
Head performance criterion (HPC)		304	267	≤ 1000
Resultant Head acceleration	[g]	40.89	41.12	≤80
Neck injury criteria (NIC tension)	[kN]	Figure 6.6	Figure 6.6	Figure 2.13
Neck injury criteria (NIC shear)	[kN]	Figure 6.7	Figure 6.7	Figure 2.14
Neck bending moment (M_{NY})	[Nm]	11.22	11.78	≤ 57
Thorax compression criterion ThCC	[mm]	35.2	30.6	≤ 50
Viscous criterion (V*C) for the thorax	[m/s]	0.20	0.14	≤ 1.0
Femur force criterion (FFC) left/right ($F_{Z(-)}$)	[kN]	1.33 / 0.63 Figure 6.8	1.39 / 0.55 Figure 6.9	Figure 2.15
Tibia compression force (TCFC) ($F_{Z(-)}$)				
upper left / right	[kN]	0.65 / 0.89	0.71 / 0.94	≤ 8.0
lower left / right	[kN]	0.99 / 1.05	1.13 / 1.14	≤ 8.0
TI Tibia index left/right				
upper left / right		0.32 / 0.26	0.38 / 0.26	≤ 1.3
lower left / right		0.31 / 0.26	0.31 / 0.33	≤ 1.3
Movement of the sliding knee L / R	[mm]	1.14 / 0.88	1.24 / 0.83	≤ 15

Head resultant acceleration curves calculated by Madymo and measured in crash test are shown in Figure 6.5. The curve tendencies are similar up to 107 ms if we omit the region between 40 and 80 ms. The reason of the increase in this region is possibly due to the vehicle deceleration difference between the test and finite element model. At this time interval, the dummy's head motion is determined only by two factors, the safety belt and

the vehicle pulse. The safety belt parameters are correlated with sled test data, which makes vehicle pulse difference the major factor in the difference between the curves. However, much attention will not be paid in this area as the difference has no affect on the peak acceleration and HIC values.

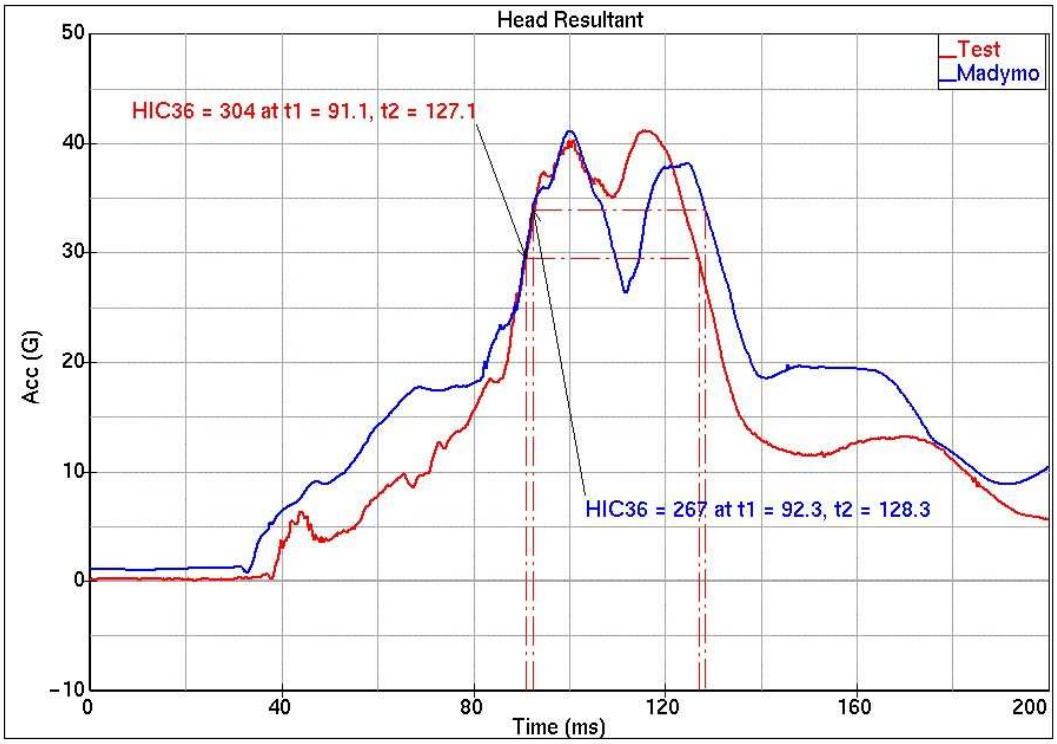

Figure 6.5. Comparison of dummy's head resultant accelerations

The difference in HIC value is caused by the curve local minimum at 107 ms. In the test, at 107 ms the resultant acceleration increases again while in Madymo the resultant acceleration drops until 115 ms. This delay in the local minima causes a lower acceleration after 115 ms, also reducing the area under the curve results in a lower HIC value. The local minimums at 107 and 115 ms are caused by sudden decelerations of dummy's head. Looking at the Madymo offset front impact simulations at 115 ms the steering column's ride down ends. The steering column's ride down starts at 97 ms. Start of steering column's ride down causes a decrease in the acceleration because the opposing force to the dummy's head decreases. The decreasing trend continues till the column's ride down ends and when the column stops the head acceleration starts to increase again until head velocity reaches zero and head's springback starts. Test head resultant acceleration curve shows that the steering column's ride down ends at 107 ms. The 8 ms delay in the steering

column's ride down results in a lower acceleration after 115 ms allowing a softer contact interaction between dummy's head and steering wheel and therefore lower HIC values for the dummy.

Neck performance curves are shown in Figures 6.6 and 6.7. Neck tension forces measured in Madymo are lower because there is a smoother contact between the head and the wheel putting less force on the neck joint. On the other hand, the duration neck suffers the load is longer compared to the test. This is in conjunction with Figure 6.4. The softer but longer contact between dummy's head and wheel resulted in a lower but longer acting axial force on the neck upper joint. Similarly, the long lasting contact results in a higher and long lasting shear force for the upper joint.

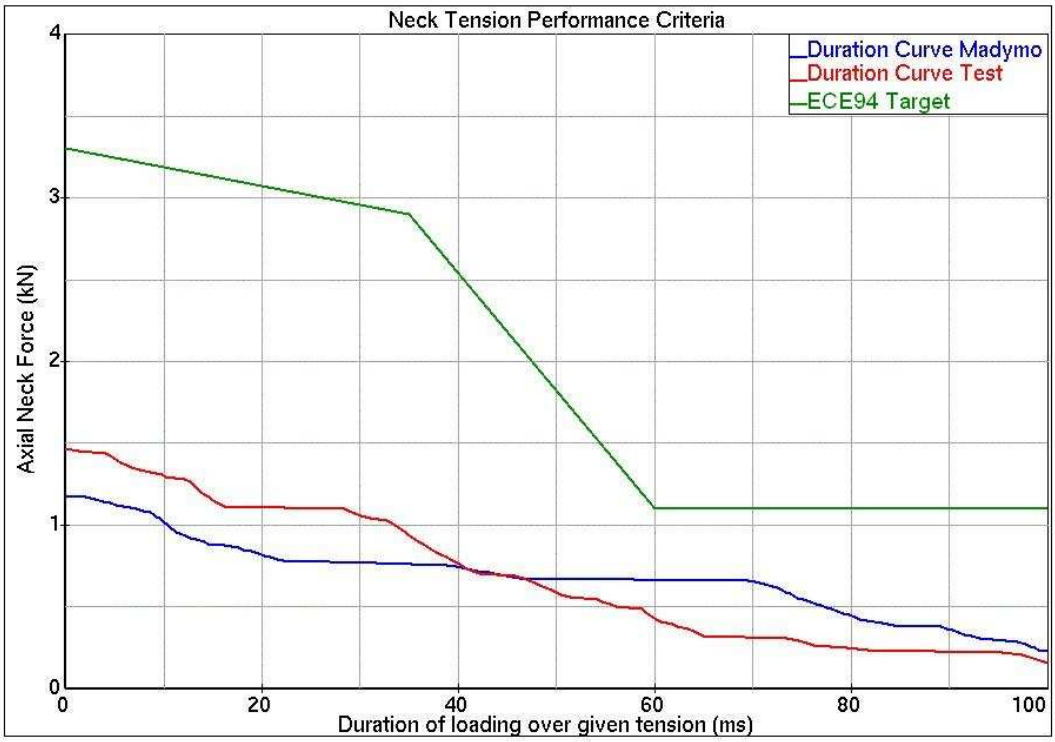

Figure 6.6. Neck tension performance comparison

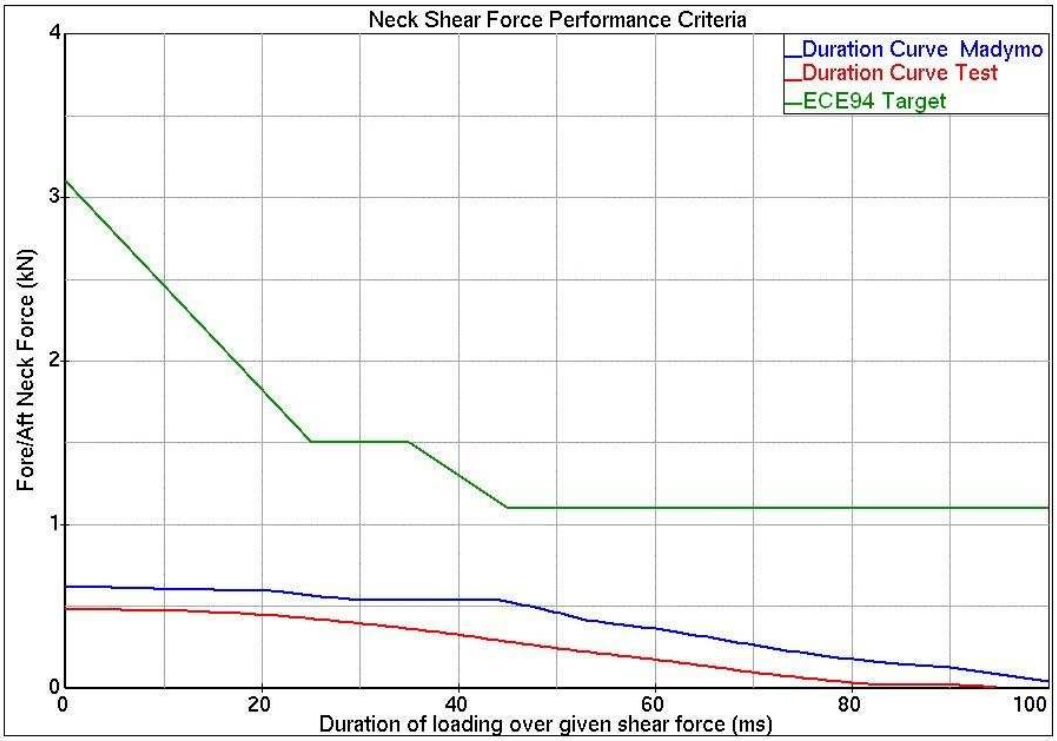

Figure 6.7. Neck shear performance comparison

Another injury parameter affected by the steering column ride down is the chest. The steering column had a softer ride down therefore at the steering wheel lower rim less force reacted to the chest motion. This resulted in lower chest compression and lower viscous criteria for the chest. (see values in Table 6.1)

There might be a couple of reasons for steering column's unexpected ride down. Test reports from the manufacturer states that steering column's ride down is sensitive to steering column height adjustment angle. Crash test is performed at the steering column design position in which the steering column shaft makes an angle of 27° with vehicle x-axis (ground plane). At this angle steering column can ride down 78.2 mm. However, test results show that when the column angle is adjusted to 31° (highest position) steering column can ride down only 36.4 mm. Another test, in which the steering column's ride down is started by applying the load 50 mm away in lateral direction from the steering column center, states that the column can ride down 50.8 mm. According to these results, any change in steering column alignment, even one or two degrees change, due to vehicle global motion or due to a contact between knee and steering column shroud will affect steering column ride down behavior and steering column will stop earlier than expected.

Such a case is not seen in sled tests because in sled test deceleration is in one direction and steering column angle is at the design position through the deceleration.

To validate that the difference comes from steering column's unexpected ride down, the steering column stroke at 107 ms is measured and this stroke is assigned to the model as the maximum distance that the steering column can travel. In that manner, it is guaranteed that the steering column ride down will stop at 107 ms. The results of the analysis is listed in Table 6.2. As shown in the table a good correlation is achieved between crash test and the Madymo model.

Table 6.2. Results after steering column's ride down is set to 60.2 mm

		Test	**Madymo**	**Madymo**
Steering column's ride down (mm)		-	78.2	60.2
Head performance criterion (HPC)		304	267	307
Neck axial force (maximum)	[kN]	1.47	1.18	1.39
Neck shear force (maximum)	[kN]	0.49	0.61	0.57
Thorax compression criterion ThCC	[mm]	35.2	30.6	34.2
Viscous criterion (V*C) for the thorax	[m/s]	0.20	0.14	0.17

Unlike the mismatches in head, neck and chest injury parameters, results from crash test and Madymo simulation for femur and tibia injury parameters are similar as shown in Figure 6.8 and Figure 6.9. This is expected as pelvis acceleration, pelvis and femur contact interactions with seat, femur instrument panel contact interactions, which determine the femur and tibia forces were previously correlated with sled test data. Therefore, a similar representation is achieved in these parameters. For femur forces, peak values measured for femur forces are similar. However, duration curves of femur show a 20 ms more compression force on the femurs. As what happened inside the vehicle during crash cannot be monitored, the reason of the increase will stay unknown. It can be concluded that femur unloading curve needs to be softer for an early separation from the instrument panel, or the intrusions during crash in Madymo model are higher compared to the crash test causing a long contact between the knee and the instrument panel.

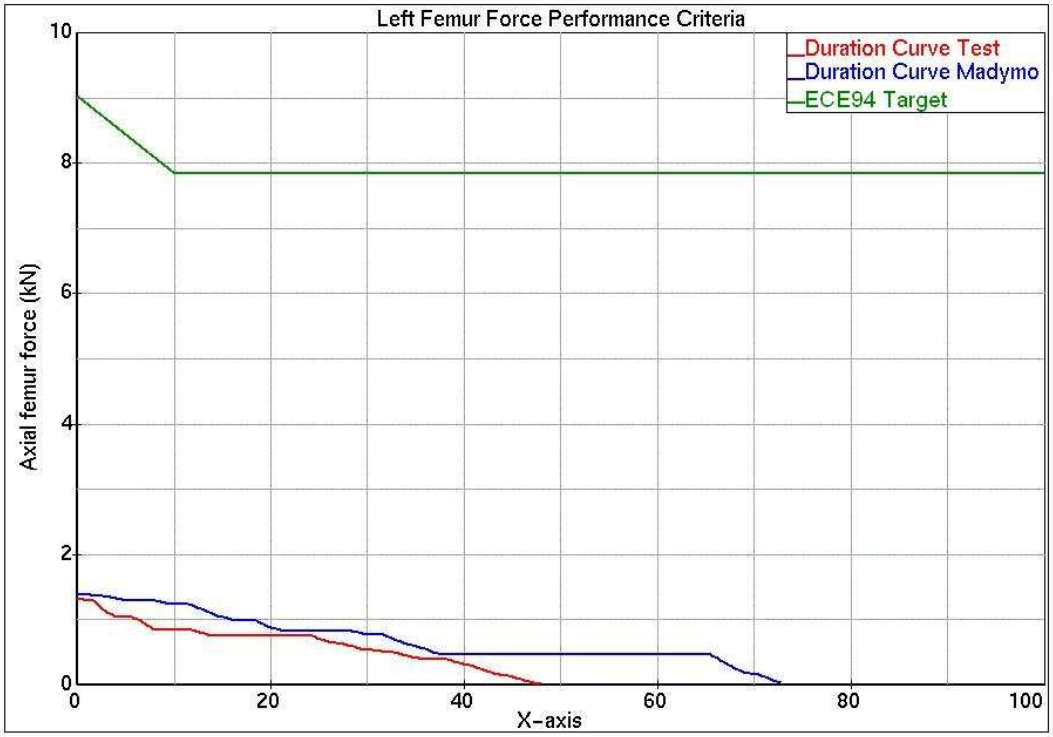

Figure 6.8. Left femur force performance criteria comparison

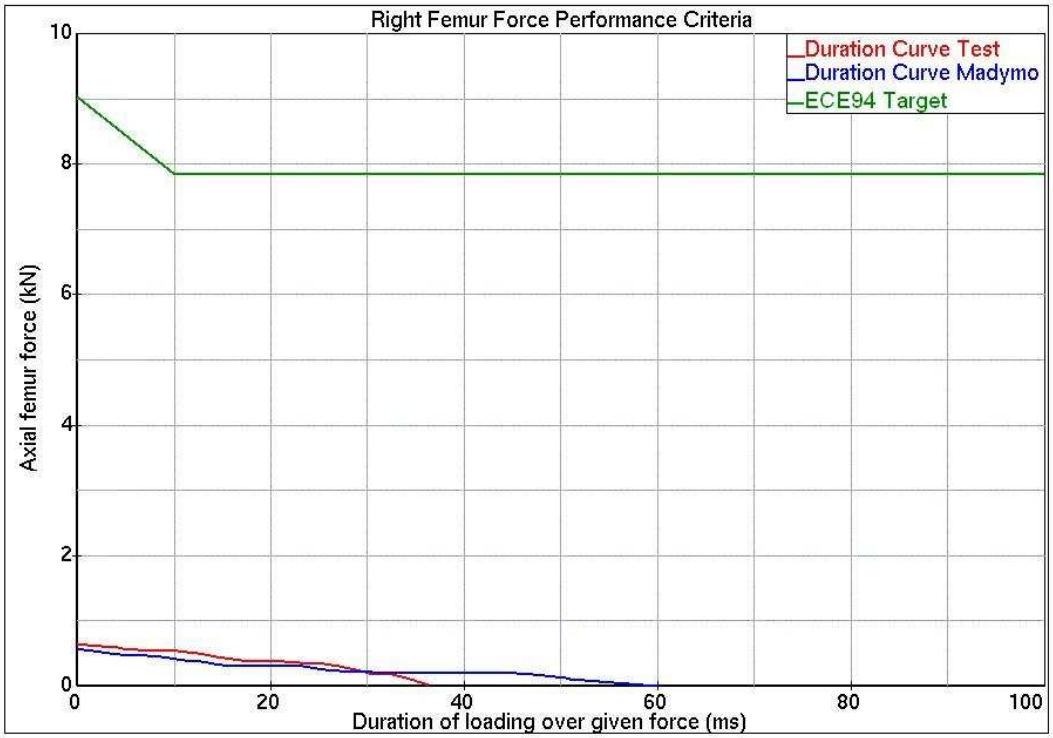

Figure 6.9. Right femur force performance criteria comparison

7. CONCLUSION

A Madymo model is constructed to determine dummy kinematics during crash. Parameters and functions used in Madymo model construction are derived from sled test and finite element analysis results. Sled test results are used to find the best force penetration functions for contact interactions and best safety belt parameters to be used in the Madymo model. Finite element analysis results are used to define vehicle global motion and intrusions inside the vehicle interior space. Results from Madymo model constructed are compared with actual crash test results.

In the above mentioned steps, calibration of sled test results with Madymo sled test simulation results can be skipped. Without a calibration between the sled test and the Madymo model, and with inputs from finite element model and with the generic data used in constructing a Madymo model, the model can be built and correlation can be done between the real crash test results and the Madymo simulation results. However, this is not favored because crash tests don't provide the necessary information needed for a correlation.

In the sled test, the calibration starts with the calibration of head acceleration values. The parameters affecting head acceleration are vehicle deceleration and shoulder belt force until head to airbag contact occurs, and after head to airbag contact occurs parameters from head to airbag and head to steering column contact interactions are added to these parameters. Dividing the dummy motion into intervals like these helps in dealing with less parameters to modify in correlating the results. It is easy to divide the motion into intervals in a sled test because in a sled test exact time for head to airbag contact and steering column's ride down can be monitored. This enables to find the best parameter to modify to match the results. For example, in the sled vehicle deceleration data is from the finite element model and this data is close to actual because it is already correlated. Therefore d-ring parameters are the only items to modify until head to airbag contact occurs to match head acceleration curves. If a good calibration can be done between the sled test results and Madymo model in this first interval, in the next interval these parameters are no more

modified. Instead the focus is on the airbag's and steering column's contact interaction parameters.

Apart from the interval based calibration mentioned in the above paragraph, sled test enables an item based correlation starting from dummy head and ending at dummy tibia. In a Madymo model dummy head motion is affected from the least number of parameters, while chest is affected by more parameters and pelvis even more. Compared to head motion, chest motion is affected by vehicle deceleration, d-ring parameters, airbag and steering column contact interactions, belt friction parameters, belt internal force characteristics and belt load limiting force curve. However, four of these parameters are already calibrated in the attempts to calibrate head motion and in chest motion there is less parameter to deal with. Similarly, calibration of parameters during the attempts to calibrate chest motion decreases the number of parameters to deal with in pelvis motion and so on. It is not easy to achieve a such a good understanding of what's going on in a crash test, because contact interactions and dummy motion can not be monitored clearly in a crash test. Also there are always additional parameters like vehicle motion, vehicle rotation and component intrusions, which increases the number of parameters affecting results. Sled tests give the chance to work in a more filtered environment from external disturbances.

Similarly, using finite elements results enables a better modeling of vehicle deformation and motion during crash. Vehicle motion may be represented correctly by using acceleration data recorded during the test, however there is no efficient alternative of including intrusions into the model except from using finite element analysis results. Therefore, apart from a well-calibrated sled test model, a good calibration between the finite element analysis results (post-crash displacements, vehicle pulses) and crash test needs to be achieved for a reliable and valid Madymo simulation.

Although a good representation of dummy motion is achieved between the sled test dummy and the Madymo dummy, and vehicle motion and deformations are calculated similar to the crash test; crash test results and Madymo simulation results may still be not similar. Apart from all the efforts to find the best parameters, the nature of the crash test may cause one item to behave unexpectedly and this item (like steering column's ride down) may emerge as a parameter affecting all results and changing the overall dummy

behavior. Except from steering column's unexpected ride down due to the change in boundary conditions functions derived for certain cases may not define the case that occurs during vehicle crash. For example, a function derived to define seat pelvis interaction in vertical direction may lead to a wrong representation in case the dummy pelvis motion is not vertical but with some degree to the seat cushion or a change in belt routing on the chest can lead to unexpected chest values.

Physical nature of a crash test is chaotic and includes many noise factors. Any small change in initial conditions or boundary conditions may change results unexpectedly. Therefore, a good understanding of what is happening during crash is essential. As it has been in this study, according to the crash scenario a second evaluation stage may be needed for a better calibration between crash test and Madymo model. However, the need for a second evaluation stage does not mean that sled test or finite element calibrations are not essential because early calibrations decrease the number of parameters and scenarios to deal with in later stages. In the existence of an unexpected scenario, it is easier to understand what is going on and to set the conditions for the new scenario.

Necessity for a second evaluation stage also means that there is no unique Madymo model that can represent every crash test under same conditions; however, this is not due to modeling capabilities of Madymo. Crash tests, because of their nature, do not always occur in the same sequence or do not always give the same results. Therefore, for every crash test a unique crash test scenario needs to be defined. Defining different crash scenarios for each test may result in the conclusion that, Madymo is not a useful tool in understanding crash tests, however, once calibrated with the crash test, Madymo models generate valuable information on dummy kinematics during crash and can be used safely to guide restraint system design.

REFERENCES

1. *Trafik Kazaları Özeti 2004*, http://www.kgm.gov.tr/kaza2k.asp, 2006

2. ECE94 Regulations, www.unece.org, 2006

3. Linzmaier L.C., J. R. Carvalho, M. Benar, D. Vilela P. Altamore, *Occupant Safety Design Approaches using Physical Testing and Numerical Simulation*, Society of Automotive Engineers, No. 2001-01-3921, 2001

4. Slaats P. M. A., W. Lee, V. Babu and K. R. Thomson, *Tools for Occupant Protection Analysis,* Society of Automotive Engineers, No. 2001-01-2725, 2001

5. Geigl B. C., H. Hoschopf, H. Steffan. and A. Moser, *Reconstruction of Occupant Kinematics and Kinetics for Real World Accidents, Internatiol Journal of Crashworthiness*, Vol. 8, No.1, pp. 17-27, 2003

6. Deshpande B. R., Gunasekar T. J., Gupta V., Jayaraman S. and Summers S. M., *Development of MADYMO Models of Passenger Vehicles for Simulating Side Impact Crashes*, Society of Automotive Engineers, No. 1999-01-2885, 1999

7. Deshpande B. R., Gunasekar T. J., Morris R., Parida S., Rashidy M., and Summers S. M, *Methodology Development for Simulating Full Frontal and Offset Frontal Impacts Using Full Vehicle MADYMO Models,* http://www.easi.com/papers, 2006

8. Hahm S., Won Y. and Kim D., *Frontal Crash Feasibility Study Using MADYMO 3D Frame Model*, Society of Automotive Engineers, No. 1999-01-0072, 1999

9. Grandfils T. and Ikels K., *Improvement of Occupant Restraint Systems using Enhanced Hybrid III Dummy Models in Madymo-3D*, http://www.easi.com/papers, 2006

10. Croft A. C., Herring P., Freeman M. D. and Haneline M. T., *The Neck Inhury Criterion: Future Considerations, Accident Analysis and Prevention,* No. 34, pp. 247-255, 2002

11. Steffan H., Geigl B. C. and Moser A., *A New Approach to Occupant Simulation Through the Coupling of PC-Crash and MADYMO,* Society of Automotive Engineers, No. 1999-01-0444, 1999

12. Zweep C.D., Kellendonk G. and Lemmen P., *Evaluation of Fleet Systems Model for Vehicle Compatibility, Internatiol Journal of Crashworthiness,* Vol. 10, No.5, pp. 483-494, 2005

13. Lupker H. A., Coo P. J. A. Nieboer J. J. and Wismans J., *Advances in MADYMO Crash Simulations,* Society of Automotive Engineers, No. 910879, 1991

14. *Madymo (v 5,4) Manuals and Applications,* TNO Road-Vehicles Research Institue, NL-Delft, 2003

15. Wismans J. and Hermans J. H. A., *MADYMO 3D Simulation of Hybrid III Dummy Sled Tests,* Society of Automotive Engineers, No. 880645, 1988

16. Cichos D., Vogel D., Otto M., Schaar O. and Zölsch S., *Crash Analysis Criteria Description,* Ford Motor Company Internal, 2005

17. *Madymo Front Occupant Modelling Procedures (v 1.0),* Ford Motor Company Internal, May, 2002

18. *Easi-Crash Mad v4.5 Training Manual,* Esi-Group, April, 2005

19. *Seat Belt Systems,* http://www.autoliv.com/Products/SeatBelts, 2006

20. Zellmer H., Kahler C. and Eickhoff B., *Optimized Pretensioning of the Belt System: A Rating Criterion and the Benefit in Consumer Tests,* Paper No. 05-0004, http://www-nrd.nhtsa.dot.gov/pdf/nrd-01/esv/esv19/05-0004-O.pdf, 2006

21. Kock H. O., *Seatbelt Systems: State of the Art and Future Trends,* http://www.autoliv.com/Appl_ALV/alvweb.nsf/Files/AutolivSeatbeltSystems/$file/AutolivSeatbeltSystems.pdf, 2006

22. *Frontal Airbags,* http://www.autoliv.com/Products/FrontalAirbags, 2006

23. *Hypermesh 7.0 Training Manual*, Altair, September, 2005

24. *M-Crash (v 2.0.1) Training Manual,* Mecalog SARL, June, 2002

25. *Radioss Theory Manual,* Mecalog SARL, February, 2005

26. Paas M., *Transformation of Sensor Acceleration Signals to Global Vehicle Motions,* Ford Motor Company Internal, April, 2005

27. Lankarani H. M. and Pereira M. F., *Treatment of Impact with Frictionin Planar Multibody Mechanical Systems,* Multibody System Dynamics, No.6, pp. 203-227, 2001

28. Craig K. J., Stander N. and Balasubramanyam S., *Worst Case Design in Head Impact Crashworthiness Optimization,* International Journal for Numerical Methods in Engineering, No. 57, pp. 795-817, 2003